Purdue University
Purdue e-Pubs

Joint Transportation Research Program | Civil Engineering

12-2011

Development of Load and Resistance Factor Design for Ultimate and Serviceability Limit States of Transportation Structure Foundations

Rodrigo Salgado
Purdue University, rodrigo@ecn.purdue.edu

Sang Inn Woo
Purdue University, woo4@purdue.edu

Dongwook Kim
Korea Institute of Construction Technology, dwkim@kict.re.kr

Recommended Citation
Salgado, R., S. Woo, and D. Kim. *Development of Load and Resistance Factor Design for Ultimate and Serviceability Limit States of Transportation Structure Foundations*. Publication FHWA/IN/JTRP-2011/03. Joint Transportation Research Program, Indiana Department of Transportation and Purdue University, West Lafayette, Indiana, 2011. doi: 10.5703/1288284314618

This document has been made available through Purdue e-Pubs, a service of the Purdue University Libraries. Please contact epubs@purdue.edu for additional information.

JOINT TRANSPORTATION RESEARCH PROGRAM

INDIANA DEPARTMENT OF TRANSPORTATION
AND PURDUE UNIVERSITY

DEVELOPMENT OF LOAD AND RESISTANCE FACTOR DESIGN FOR ULTIMATE AND SERVICEABILITY LIMIT STATES OF TRANSPORTATION STRUCTURE FOUNDATIONS

Rodrigo Salgado
Professor of Civil Engineering
Purdue University
Corresponding Author

Sang Inn Woo
Graduate Research Assistant
School of Civil Engineering
Purdue University

Dongwook Kim
Graduate Research Assistant
School of Civil Engineering
Purdue University

SPR-3108
Report Number: FHWA/IN/JTRP-2011/03
DOI: 10.5703/1288284314618

This page intentionally left blank.

RECOMMENDED CITATION

Salgado, R., S. I. Woo, and D. Kim. *Development of Load and Resistance Factor Design for Ultimate and Serviceability Limit States of Transportation Structure Foundations*. Publication FHWA/IN/JTRP-2011/03. Joint Transportation Research Program, Indiana Department of Transportation and Purdue University, West Lafayette, Indiana, 2011. doi: 10.5703/1288284314618

CORRESPONDING AUTHOR

Professor Rodrigo Salgado
School of Civil Engineering
Purdue University
(765) 494-5030
salgado@purdue.edu

ACKNOWLEDGMENTS

The work presented here is the fruit of considerable amount of work done by the authors and others who have worked on LRFD development at Purdue University. Discussions with Prof. Mônica Prezzi are appreciated. The material in chapter 4 draws upon work that Dipanjan Basu has assisted with; that assistance is appreciated. Some of the pile design methods for which resistance factors are proposed have not yet appeared in print, but are described in technical reports or are else detailed in the present report. The assistance of JTRP staff and, in particular, INDOT technical staff and the Study Advisory Committee members, is much appreciated.

JOINT TRANSPORTATION RESEARCH PROGRAM

The Joint Transportation Research Program serves as a vehicle for INDOT collaboration with higher education institutions and industry in Indiana to facilitate innovation that results in continuous improvement in the planning, design, construction, operation, management and economic efficiency of the Indiana transportation infrastructure.
https://engineering.purdue.edu/JTRP/index_html

Published reports of the Joint Transportation Research Program are available at: http://docs.lib.purdue.edu/jtrp/

NOTICE

The contents of this report reflect the views of the authors, who are responsible for the facts and the accuracy of the data presented herein. The contents do not necessarily reflect the official views and policies of the Indiana Department of Transportation or the Federal Highway Administration. The report does not constitute a standard, specification or regulation.

This page intentionally left blank.

TECHNICAL REPORT STANDARD TITLE PAGE

1. Report No.	2. Government Accession No.	3. Recipient's Catalog No.
FHWA/IN/JTRP-2011/03		

4. Title and Subtitle	5. Report Date
Development of Load and Resistance Factor Design for Ultimate and Serviceability Limit States of Transportation Structure Foundations	2011
	6. Performing Organization Code
7. Author(s)	8. Performing Organization Report No.
Rodrigo Salgado, San Inn Woo, Dongwook Kim	FHWA/IN/JTRP-2011/03
9. Performing Organization Name and Address	10. Work Unit No.
Joint Transportation Research Program Purdue University 550 Stadium Mall Drive West Lafayette, IN 47907-2051	
	11. Contract or Grant No. SPR-3108
12. Sponsoring Agency Name and Address	13. Type of Report and Period Covered
Indiana Department of Transportation State Office Building 100 North Senate Avenue Indianapolis, IN 46204	
	14. Sponsoring Agency Code

15. Supplementary Notes

Prepared in cooperation with the Indiana Department of Transportation and Federal Highway Administration.

16. Abstract

.

Most foundation solutions for transportation structures rely on deep foundations, often on pile foundations configured in a way most suitable to the problem at hand. Design of pile foundation solutions can best be pursued by clearly defining limit states and then configuring the piles in such a way as to prevent the attainment of these limit states. The present report develops methods for load and resistance factor design (LRFD) of piles, both nondisplacement and displacement piles, in sand and clay. With the exception of the method for design of displacement piles in sand, all the methods are based on rigorous theoretical mechanics solutions of the pile loading problem. In all cases, the uncertainty of the variables appearing in the problem and of the relationships linking these variables to the resistance calculated using these relationships are carefully assessed. Monte Carlo simulations using these relationships and the associated variabilities allow simulation of resistance minus load distributions and therefore probability of failure. The mean (or nominal) values of the variables can be adjusted so that the probability of failure can be made to match a target probability of failure. Since an infinite number of combinations of these means can be made to lead to the same target probability of failure, we have developed a way to determine the most likely ultimate limit state for a given probability of failure. Once the most likely ultimate limit state is determined, the values of loads and resistances for this limit state can be used, together with the values of the mean (or nominal) loads and resistances to calculate load and resistance factors. The last step in the process involves adjusting the resistance factors so that they are consistent with the load factors specified by AASHTO. Recommended resistance factors are then given together with the design methods for which they were developed.

17. Key Words	18. Distribution Statement
Piles; piling; pile resistance; pile design; load and resistance factor design; LRFD	No restrictions. This document is available to the public through the National Technical Information Service, Springfield, VA 22161

19. Security Classif. (of this report)	20. Security Classif. (of this page)	21. No. of Pages	22. Price
Unclassified	Unclassified		

Form DOT F 1700.7 (8-69)

This page intentionally left blank.

CONTENTS

LIST OF TABLES . . . iii

LIST OF FIGURES . . . iv

EXECUTIVE SUMMARY . . . 1

CHAPTER 1. INTRODUCTION . . . 1
1.1. Background . . . 1
1.2. Problem Statement . . . 2
1.3. Objectives and Organization . . . 2

CHAPTER 2. FOUNDATION DESIGN AS A PROBLEM OF DECISION MAKING UNDER UNCERTAINTY . . . 2
2.1. Introduction . . . 2
2.2. Decision under Uncertainty: probabilities, outcomes and the notion of value . . . 2
2.3. Foundation Design as an Exercise of Decision under Uncertainty: reliability analysis . . . 3
2.4. Reliability Analysis . . . 3
2.5. Review of Basic Probability Theory Concepts . . . 4
2.6. Assessment of the Uncertainty of Independent and Dependent Variables . . . 5
2.7. Uncertainties of models and transformations . . . 6
2.8. Target Probability of Failure and number of M-C runs . . . 6
2.9. First-Order Reliability Method (FORM) . . . 6
2.10. Monte Carlo Simulations . . . 7

CHAPTER 3. LRFD OF PILE FOUNDATIONS . . . 8
3.1. Introduction . . . 8
3.2. Live Load-Dead Load Ratio for Transportation Structures . . . 8
3.3. Location of the Most Probable Ultimate Limit State and Calculation of Load and Resistance Factors . 9
3.4. Distributions of Load and Resistance Factors . . . 9
3.5. Adjusted Load and Resistance Factors . . . 10
3.6. Mean Factor of Safety . . . 10

CHAPTER 4. RESISTANCE FACTORS FOR DRILLED SHAFTS IN SAND . . . 11
4.1. Introduction . . . 11
4.2. Unit Base and Shaft Resistance: Purdue Sand Method for Nondisplacement Piles . . . 11
4.3. Uncertainty Assessment of Design Variables and Model Uncertainty . . . 12
4.4. Analysis . . . 15
4.5. Results . . . 16
4.6. Conclusions . . . 23

CHAPTER 5. RESISTANCE FACTORS FOR DRILLED SHAFT IN CLAY . . . 26
5.1. Introduction . . . 26
5.2. Unit Base and Shaft Resistance: Purdue Clay Method for Nondisplacement Piles . . . 26
5.3. Uncertainty Assessment of Design Variables and Model Uncertainty . . . 27
5.4. Analysis . . . 29
5.5. Results . . . 31
5.6. Conclusions . . . 37

CHAPTER 6. RESISTANCE FACTORS OF DRIVEN PILES IN SAND . . . 39
6.1. Introduction . . . 39
6.2. Unit Base and Shaft Resistance: Purdue Sand Method for Driven Piles . . . 39
6.3. Uncertainty Assessment of Design Variables and Model Uncertainty . . . 40
6.4. Analysis . . . 41
6.5. Results . . . 43
6.6. Suggested values of Resistance Factors . . . 46

CHAPTER 7. RESISTANCE FACTORS OF DRIVEN PILES IN CLAY . . . 47
7.1. Introduction . . . 47

7.2. Unit Base and Shaft Resistance: Purdue Clay Method for Displacement Piles 47
7.3. Uncertainty Assessment of Design Variables and Model Uncertainty 48
7.4. Analysis 50
7.5. Results 50
7.6. Conclusions 59

CHAPTER 8. SUMMARY AND CONCLUSIONS 59
8.1. General 59
8.2. Drilled Shafts in Sand 59
8.3. Drilled Shafts in Clay 60
8.4. Driven Piles in Sand 60
8.5. Driven Piles in Clay 60

REFERENCES 60

LIST OF TABLES

Table	Page
Table 4.1 Resistance factors for different drilled shafts and adjusted with $(\mathrm{LF})_{\mathrm{DL}}^{\mathrm{code}} = 1.25$ and $(\mathrm{LF})_{\mathrm{LL}}^{\mathrm{code}} = 1.75$ when $q_{c,\mathrm{mean}}(z)$ is given as input	22
Table 4.2 Summary of Purdue Sand Method for NonDisplacement Piles: design equations, variable and model uncertainties, load and resistance factors	23
Table 4.3 Resistance factors for different drilled shafts and adjusted with $(\mathrm{LF})_{\mathrm{DL}}^{\mathrm{code}} = 1.25$ and $(\mathrm{LF})_{\mathrm{LL}}^{\mathrm{code}} = 1.75$ when $N_{60,\mathrm{mean}}(z)$ is given as input	26
Table 5.1 Resistance factors for different drilled shafts and adjusted with $(\mathrm{LF})_{\mathrm{DL}}^{\mathrm{code}} = 1.25$ and $(\mathrm{LF})_{\mathrm{LL}}^{\mathrm{code}} = 1.75$ when $q_{c,\mathrm{mean}}(z)$ is given as input	35
Table 5.2 Resistance factors for different drilled shafts and adjusted with $(\mathrm{LF})_{\mathrm{DL}}^{\mathrm{code}} = 1.25$ and $(\mathrm{LF})_{\mathrm{LL}}^{\mathrm{code}} = 1.75$ when $s_{u,\mathrm{mean}}$ from UC tests is given as input	39
Table 6.1 Percentage of increase/decrease of $(RF)_b$ and $(RF)_s$ when (LL)/(DL) =1 changes to 0.25 or 2 for $p_{f,\mathrm{target}} = 10^{-3}$	47
Table 6.2 Percentage of increase/decrease of $(RF)_b$ and $(RF)_s$ when (LL)/(DL) =1 changes to 0.25 or 2 for $p_{f,\mathrm{target}} = 10^{-4}$	47
Table 6.3 Resistance factors calculated for different combinations of $Q_{b,ult}{}^{(\mathrm{n})}/\ Q_{sL}{}^{(\mathrm{n})}$, (LL)/(DL), and $p_{f,\mathrm{target}}$ adjusted with the AASHTO load factors [$(\mathrm{LF})_{\mathrm{DL}}^{\mathrm{code}} = 1.25$ and $(\mathrm{LF})_{\mathrm{LL}}^{\mathrm{code}} = 1.75$]	48
Table 7.1 Resistance factors for different driven piles and adjusted with $(\mathrm{LF})_{\mathrm{DL}}^{\mathrm{code}} = 1.25$ and $(\mathrm{LF})_{\mathrm{LL}}^{\mathrm{code}} = 1.75$ when $q_{c,\mathrm{mean}}(z)$ is given as input	56
Table 7.2 Resistance factors for different driven piles and adjusted with $(\mathrm{LF})_{\mathrm{DL}}^{\mathrm{code}} = 1.25$ and $(\mathrm{LF})_{\mathrm{LL}}^{\mathrm{code}} = 1.75$ when $s_{u,\mathrm{mean}}$ from UC test is given as input	59

LIST OF FIGURES

Figure	Page
Figure 1.1 Sources of pile resistance.	2
Figure 1.2 Typical load-settlement response of pile.	2
Figure 2.1 Mean and nominal values of a parameter x.	6
Figure 2.2 Scatter of a variable X around its mean for constant COV.	6
Figure 2.3 Geometrical illustration of reliability index β in two-dimensional space	7
Figure 4.1 Flow chart of Monte-Carlo simulations	17
Figure 4.2 Details of soil profiles: (a) (1)–(2), (b) (3)–(5) and (c) (6)	18
Figure 4.3 Optimal resistance and load factors versus critical state friction angle ϕ_c when $q_{c,\mathrm{mean}}(z)$ is given as input	19
Figure 4.4 Optimal resistance and load factors versus coefficient K_0 of earth pressure at rest when $q_{c,\mathrm{mean}}(z)$ is given as input	19
Figure 4.5 Optimal resistance and load factors for different soil profiles when $q_{c,\mathrm{mean}}(z)$ is given as input	19
Figure 4.6 Optimal resistance and load factors for different drilled shaft dimensions when $q_{c,\mathrm{mean}}(z)$ is given as input	19
Figure 4.7 Optimal resistance and load factor versus live load to dead load ratio when $q_{c,\mathrm{mean}}(z)$ is given as input	20
Figure 4.8. Effect of target probability of failure on resistance and load factors and on the corresponding mean factor of safety: (a) mean factor of safety and (b) optimal resistance and load factors versus target probability of failure when $q_{c,\mathrm{mean}}(z)$ is given as input	20
Figure 4.9 Plots of (a) optimal load and resistance factors and (b) code-adjusted resistance factors versus live load to dead load ratio when $q_{c,\mathrm{mean}}(z)$ is given as input	21
Figure 4.10 Optimal resistance and load factors versus critical state friction angle ϕ_c for drilled shaft A and (a) COV(N_{60}) = 0.3 and (b) COV(N_{60}) = 0.5 when $N_{60,\mathrm{mean}}(z)$ is given as input	24
Figure 4.11 Optimal resistance and load factors versus coefficient K_0 of earth pressure at rest for drilled shaft B and (a) COV(N_{60}) = 0.3 and (b) COV(N_{60}) = 0.5 when $N_{60,\mathrm{mean}}(z)$ is given as input	24
Figure 4.12 Optimal load and resistance factors versus diameter to length ratio for (a) LL/DL = 2.0 and (b) LL/DL = 0.25 when $N_{60,\mathrm{mean}}(z)$ is given as input	25
Figure 4.13 Optimal resistance and load factor versus live load to dead load ratio for (a) drilled shaft A and (b) drilled shaft B when $N_{60,\mathrm{mean}}(z)$ is given as input	25
Figure 4.14 Mean factor of safety versus target probability of failure for (a) drilled shaft A and (b) drilled shaft B when $N_{60,\mathrm{mean}}(z)$ is given as input.	26
Figure 4.15 Optimal resistance and load factors versus target probability of failure for (a) drilled shaft A and (b) drilled shaft B = 0.5 when $N_{60,\mathrm{mean}}(z)$ is given as input	26
Figure 4.16 Optimal and code-adjusted resistance factors versus live load to dead load ratio for (a) drilled shaft A and (b) drilled shaft B when $N_{60,\mathrm{mean}}(z)$ is given as input	27
Figure 5.1 Limit unit base resistance of circular foundation versus depth (Salgado et al. 2004)	28
Figure 5.2 Flow chart of Monte-Carlo simulations	31
Figure 5.3 Details of soil profile	32
Figure 5.4 Optimal load and resistance factors versus $\phi_{c,\mathrm{mean}}$ - $\phi_{r,\mathrm{min,mean}}$ for (a) drilled shaft A and (b) drilled shaft C when $q_{c,\mathrm{mean}}(z)$ is given as input	32
Figure 5.5 Optimal load and resistance factors versus diameter to length ratio for (a) LL/DL = 0.25 and (b) LL/DL = 2.0 when $q_{c,\mathrm{mean}}(z)$ is given as input	33
Figure 5.6 Optimal load and resistance factors versus live load to dead load ratio for (a) drilled shaft A and (b) drilled shaft C when $q_{c,\mathrm{mean}}(z)$ is given as input	34
Figure 5.7 Mean factor of safety versus target probability of failure for (a) drilled shaft A and (b) drilled shaft C when $q_{c,\mathrm{mean}}(z)$ is given as input	34
Figure 5.8 Optimal resistance and load factors versus target probability of failure for drilled shaft A and (a) LL/DL = 0.25 and (b) LL/DL = 2.0 when $q_{c,\mathrm{mean}}(z)$ is given as input	35

Figure 5.9 Optimal and code-adjusted resistance factors versus live load to dead load ratio for (a) drilled shaft A and (b) drilled shaft C when $q_{c,\text{mean}}(z)$ is given as input 35

Figure 5.10 Optimal load and resistance factors versus $\phi_{c,\text{mean}}$ - $\phi_{r,\text{min,mean}}$ for (a) drilled shaft A and (b) drilled shaft C when $s_{u,\text{mean}}$ from UC testing is given as input 36

Figure 5.11 Optimal load and resistance factors versus diameter to length ratio for (a) LL/DL = 0.25 and (b) LL/DL = 2.0 when $s_{u,\text{mean}}$ from UC testing is given as input 36

Figure 5.12 Optimal load and resistance factors versus live load to dead load ratio for (a) drilled shaft A and (b) drilled shaft C when $s_{u,\text{mean}}$ from UC testing is given as input 37

Figure 5.13 Mean factor of safety versus target probability of failure for (a) drilled shaft A and (b) drilled shaft C when $s_{u,\text{mean}}$ from UC testing is given as input 37

Figure 5.14 Optimal resistance and load factors versus target probability of failure for drilled shaft A and (a) LL/DL = 0.25 and (b) LL/DL = 2.0 when $s_{u,\text{mean}}$ from UC testing is given as input 38

Figure 5.15 Optimal and code-adjusted resistance factors versus live load to dead load ratio for (a) drilled shaft A and (b) drilled shaft C when $s_{u,\text{mean}}$ from UC tests is given as input 39

Figure 6.1. Relationship between $q_{b,ult}$ / q_{bL} and D_R 40

Figure 6.2. Relationship between q_{sL} / q_{bL} and D_R 41

Figure 6.3. Bias factor, COV, and distribution of $q_{b,ult,meas.}/q_{b,ult.pred.}$ 42

Figure 6.4. Bias factor, COV, and distribution of $q_{sL,meas.}/q_{sL.pred.}$ 42

Figure 6.5. Procedure of calculations of optimal factors 43

Figure 6.6. Description of pile and soil profiles: profiles (1) and (2) 44

Figure 6.7. Description of pile and soil profiles: profiles (3) – (5) 44

Figure 6.8. Description of pile and soil profile: profiles (6) 44

Figure 6.9. Optimal resistance and load factors versus ϕ_c 45

Figure 6.10. Optimal resistance and load factors versus K_0 45

Figure 6.11. Optimal resistance and load factors versus B_p for L_p = 10m 45

Figure 6.12. Optimal resistance and load factors versus B_p for L_p = 30m 45

Figure 6.13. Optimal resistance and load factors versus (LL)/(DL) 45

Figure 6.14. Optimal resistance and load factors versus p_f for soil profile (1). 46

Figure 6.15. Optimal resistance and load factors for different profiles [profile (1) – (6)] 46

Figure 6.16. $(RF)_b$ and $(RF)_s$ versus $Q_{b,ult}^{(n)}/ Q_{sL}^{(n)}$ for all the profiles (1) – (6) for $p_f = 10^{-3}$ 46

Figure 6.17. $(RF)_b$ and $(RF)_s$ versus $Q_{b,ult}^{(n)}/ Q_{sL}^{(n)}$ for profiles (1) – (6) for $p_f = 10^{-4}$. 47

Figure 6.18. $(FS)_{\text{mean}}$ calculated using equation (3.13) compared with typical ASD FS value of 3.0 for $p_f = 10^{-3}$ and 10^{-4}. 48

Figure 7.1 Limit unit base resistance of circular foundation versus depth (Salgado et al. 2004) 49

Figure 7.2 Comparison of α values predicted by the proposed equations with those calculated following the API RP-2A criterion and obtained from the field data reported by Sempel and Rigden (1984) (P. Basu et al 2010) 50

Figure 7.3 Flow chart of Monte-Carlo simulations 52

Figure 7.4 Details of soil profile 52

Figure 7.5 Optimal load and resistance factors versus $\phi_{c,\text{mean}}$ - $\phi_{r,\text{min,mean}}$ for (a) driven pile A and (b) driven pile C when $q_{c,\text{mean}}(z)$ is given as input 53

Figure 7.6 Optimal load and resistance factors versus diameter to length ratio for (a) LL/DL = 0.25 and (b) LL/DL = 2.0 when $q_{c,\text{mean}}(z)$ is given as input 54

Figure 7.7 Optimal load and resistance factors versus live load to dead load ratio for (a) driven pile A and (b) driven pile C when $q_{c,\text{mean}}(z)$ is given as input 54

Figure 7.8 Mean factor of safety versus target probability of failure for (a) driven pile A and (b) driven pile C when $q_{c,\text{mean}}(z)$ is given as input 55

Figure 7.9 Optimal resistance and load factors versus target probability of failure for driven pile A and (a) LL/DL = 0.25 and (b) LL/DL = 2.0 when $q_{c,\mathrm{mean}}(z)$ is given as input 55

Figure 7.10 Optimal and code-adjusted resistance factors versus live load to dead load ratio for (a) driven pile A and (b) driven pile C when $q_{c,\mathrm{mean}}(z)$ is given as input 56

Figure 7.11 Optimal load and resistance factors versus $\phi_{c,\mathrm{mean}}$ - $\phi_{r,\mathrm{min,mean}}$ for (a) driven pile A and (b) driven pile C when $s_{u,\mathrm{mean}}$ from UC testing is given as input 57

Figure 7.12 Optimal load and resistance factors versus diameter to length ratio for (a) LL/DL = 0.25 and (b) LL/DL = 2.0 when $s_{u,\mathrm{mean}}$ from UC testing is given as input 57

Figure 7.13 Optimal load and resistance factors versus live load to dead load ratio for (a) driven pile A and (b) driven pile C when $s_{u,\mathrm{mean}}$ from UC testing is given as input 58

Figure 7.14 Mean factor of safety versus target probability of failure for (a) driven pile A and (b) driven pile C when $s_{u,\mathrm{mean}}$ from UC testing is given as input 58

Figure 7.15 Optimal resistance and load factors versus target probability of failure for driven pile A and (a) LL/DL = 0.25 and (b) LL/DL = 2.0 when $s_{u,\mathrm{mean}}$ from UC testing is given as input 59

Figure 7.16 Optimal and code-adjusted resistance factors versus live load to dead load ratio for (a) driven pile A and (b) driven pile C when $s_{u,\mathrm{mean}}$ from UC test is given as input 59

EXECUTIVE SUMMARY

DEVELOPMENT OF LOAD AND RESISTANCE FACTOR DESIGN FOR ULTIMATE AND SERVICEABILITY LIMIT STATES OF TRANSPORTATION STRUCTURE FOUNDATIONS

Introduction

Pile foundations are used in most foundation solutions for transportation structures. Design of pile foundation solutions can best be pursued by clearly defining limit states and then configuring the piles in such a way as to prevent the attainment of these limit states. There are three approaches to do this; in order of complexity, they are: working stress design (WSD), load and resistance factor design (LRFD), and reliability-based design (RBD). All three approaches account in some way for the fact that foundation engineering problems are not deterministic, and most, if not all, variables in the problem are random or have a random component. In this report, we develop LRFD methodology for ultimate limit states related to the application of axial load on single piles. Both displacement and nondisplacement piles are considered; likewise, sands and clays are the two soil types we have considered.

We have developed our LRFD design methods using reliability analysis and the specific technique of Monte Carlo simulations. The principles that we have adhered to in doing so are:

(1) Recognize that resistance factors are inseparable from the design method for which they are developed and that "one size fits all" does not work with LRFD.
(2) Perform careful, detailed, specific evaluation of the uncertainties in variables and relationships entering the design calculations. With respect to these evaluations, "one size fits all" does not work either. Attempts to find universal coefficients of variation for a given soil property, regardless of the method used to estimate it, for example, negates the benefits of LRFD.
(3) Use to the maximum extent possible theories that are both realistic and rigorous, for it will be easier and more logical to account for variability of the theoretical method and its variables if this requirement is met.
(4) Probabilities of failure must balance the need for safety with the impracticality or cost of attempting to reduce them too far.

We have taken load factors as given by AASHTO. This means that resistance factors calculated in the course of the reliability analyses are then adjusted to match the specified load factors. The methods of design we have determined resistance factors for have been developed and refined both in the course of the current research and in previous research at Purdue University.

Findings

The approach we have followed to develop ultimate limit state design check methods has proven to be effective. Resistances calculated using design equations compare well with experiments performed under controlled conditions and better-quality field experiments. Calculations of equivalent factors of safety also show that the resistance factors arrived at appear reasonable for the probabilities of failure assumed in calculations. For example, for foundations based on one drilled shaft supporting one column, where redundancies resulting for use of pile groups are not a factor, a probability of failure between one pile in one thousand and one pile in ten thousand should be targeted. Equivalent factors of safety resulting from this level of risk appear reasonable in light of the experience accumulated over the years with WSD and the use of rigorous methods for all but one case in this report: that of piles driven in sand, where reliance on empirical considerations is still necessary.

The final result of the research done and reported here is a set of design equation or inequalities with accompanying resistance factors for use with AASHTO load factors for single nondisplacement (bored) or displacement (driven) piles installed in sand or clay.

Implementation

Implementation of this research requires that the design methods be used in projects in which enough testing during and after pile installation is done so that any required adjustments or questions may be addressed in further research. This testing must include not only dynamic but also static pile load tests. Every effort to use instrumented piles in the static tests should be made. High-quality characterization of the soil before pile design and installation should also be done.

CHAPTER 1. INTRODUCTION

1.1. Background

Routine transportation structures are founded more commonly on piles, including drilled shafts, than on other types of foundations, and design of pile foundations is the focus of the present report. Pile foundations have been used in construction for thousands of years as an economical means of transmitting the loads from superstructures to the underlying soil or rock strata. Piles support the load applied from the superstructure Q_t through basically two sources: 1) friction between the pile shaft and the surrounding soil and 2) compressive resistance of the soil below the pile base. The frictional resistance offered by the soil surrounding the pile is called shaft resistance Q_s, and the compressive resistance offered by the soil at the base is referred to as base resistance Q_b (Figure 1.1).

As the applied load at the pile head is increased, pile settlement increases until eventually the pile plunges into the ground when the shaft and base resistances reach their limit values. During this loading process, there is high localization of shearing within a thin layer of soil around the pile shaft. As the thickness of this layer (shear zone) is very small, only a small amount of axial displacement of the pile is sufficient for full mobilization of the limit shaft capacity (Q_{sL}). In contrast to the shaft resistance mobilization mechanism, mobilization of the base resistance involves substantial amount of soil compression and requires large pile settlements. In fact, it is almost impossible for the plunging load or limit load Q_L of piles routinely used in practice to be reached with conventional load testing equipment unless the soil profile is very weak. Therefore, ultimate load (Q_{ult}) criteria have been traditionally used to define the capacity of a pile. In the case of the 10% - relative - settlement criterion, Q_{ult} corresponds to the load for which the pile head displacement is 10% of the pile diameter; this is an example of an ultimate load criterion that is widely used in practice. The base resistance Q_b at a pile displacement of 10% of the pile diameter is denoted ultimate

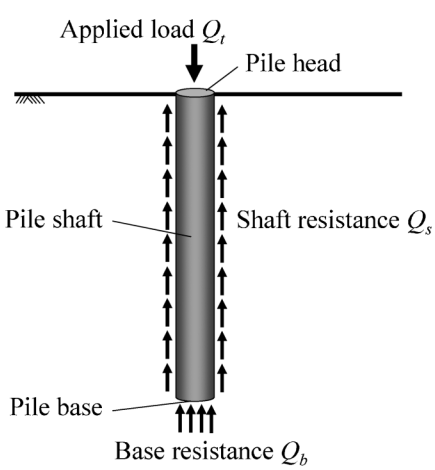

Figure 1.1 Sources of pile resistance.

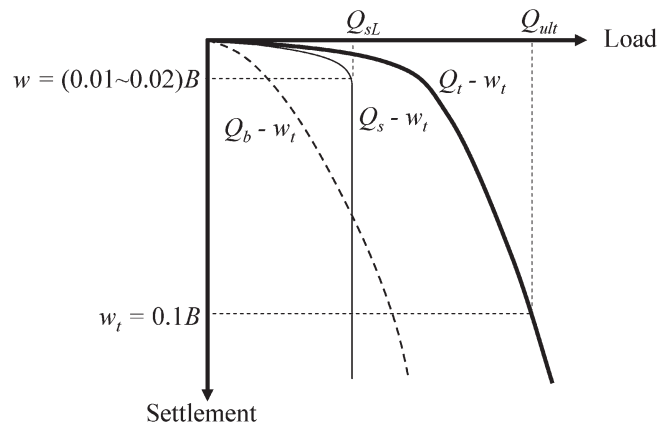

Figure 1.2 Typical load-settlement response of pile.

base resistance $Q_{b,ult}$. Figure 1.2 illustrates these concepts.

The ultimate total resistance Q_{ult} of a drilled shaft is the summation of the ultimate base resistance $Q_{b,\mathrm{ult}}$ and limit shaft resistance $Q_{s\mathrm{L}}$ (Salgado 2008). The ultimate base and limit shaft resistances are expressed as:

$$Q_{b,\mathrm{ult}} = q_{b,\mathrm{ult}} A_b \tag{1.1}$$

$$Q_{s\mathrm{L}} = \sum_i q_{s\mathrm{L},i} A_{s,i} \tag{1.2}$$

where $q_{b,\mathrm{ult}}$ is the ultimate unit base resistance and A_b ($= \pi B_b^2/4$) is the area of the pile base (B_b = pile base diameter); $q_{s\mathrm{L},i}$ is the limit unit shaft resistance along the segment of the shaft intersecting the ith sub-layer; H_i = thickness of ith sub-layer; $A_{s,i}$ ($= \pi B_s H_i$) is the corresponding shaft surface area (B_s = pile shaft diameter). The division into soil sub-layers along the pile shaft generally follows the natural stratification as established through the field investigation, with individual soil layers being further subdivided into thinner sub-layers to reflect trends of penetration resistance (SPT blow counts or cone resistance) within a layer and to increase the accuracy of the computations.

Design of a pile for axial loading consists of determining the geometry of the pile and the location of its base in a soil profile so that it will neither plunge through the soil nor settle excessively under that load. Traditionally, that was accomplished by calculating the pile resistance Q_{ult} (see Figure 1.2) and dividing it by a factor of safety FS, an approach known as working stress design (WSD) because the allowable load so calculated is then compared with the working load (the applied load). This factor of safety was typically made large enough to prevent serviceability problems as well.

In recent years, AASHTO and FHWA have started to transition geotechnical design away from WSD to Load and Resistance Factor Design (LRFD). In LRFD, instead of using a single safety factor, engineers use factors to reduce resistances and increase loads. The total reduced resistance is compared with the total

increased load and, if found sufficient, the design is safe. The appeal of this method is the possibility of separately accounting for the uncertainties of loads and resistances and imposing more discipline and rigor in how geotechnical engineers define quantities and determine values for them. It also forces engineers to think about the methods of analysis that they use and the uncertainties particular to that method. The research carried out and reported in this report adheres strictly to these principles and differs from most research done on the subject so far. As appropriate, these differences are pointed out in the body of the report.

1.2. Problem Statement

In the LRFD framework, the capacity (total resistance) and demand (applied loads) are related as:

$$(\mathrm{RF})R^{(\mathrm{n})} \geq \sum (\mathrm{LF})_i L_i^{(\mathrm{n})} \tag{1.3}$$

where (RF) = resistance factor, $R^{(\mathrm{n})}$ is the nominal (or characteristic) resistance, $(\mathrm{LF})_i$ = load factor corresponding to the ith nominal (or characteristic) load $L_i^{(\mathrm{n})}$, and the superscript (n) represents nominal loads and resistances. The deterministic loads and resistances estimated by design engineers based on procedures prescribed by codes, manuals and books or on experience are called the nominal loads and resistances, respectively

For pile problems, we have two sources of resistances: base resistance and shaft resistance. Base and shaft resistances of piles are calculated separately, and the mechanisms by which these resistances develop are quite different. The loading that develops along the pile shaft closely approximates simple shear loading and, at an ultimate limit state, corresponds to critical state values of shear stress. The loading around the base is much more complex, with mean stress increasing at almost every point around the base and shear stresses developing to different degrees and at different rates depending on the point. Consequently, the two capacity equations are subjected to different sets of uncertainties. We define an ultimate limit state of a pile as any state for which the sum of all loads applied at the pile head reaches the ultimate capacity Q_{ult} of the pile, which is the sum of ultimate base resistance $Q_{b,ult}$ and limit shaft resistance $Q_{s\mathrm{L}}$. This is reflected in inequality (1.3), which we consider to be more appropriate for our analysis. In this research, inequality (1.3) is used as the LRFD criterion, which, for applied dead and live loads, can be rewritten as:

$$(\mathrm{RF})_b Q_{b,\mathrm{ult}}^{(\mathrm{n})} + (\mathrm{RF})_s Q_{sL}^{(\mathrm{n})} \geq (\mathrm{LF})_{\mathrm{DL}} (\mathrm{DL})^{(\mathrm{n})} + (\mathrm{LF})_{\mathrm{LL}} (\mathrm{LL})^{(\mathrm{n})} \tag{1.4}$$

where $Q^{(\mathrm{n})}{}_{b,ult}$ and $Q^{(\mathrm{n})}{}_{sL}$ are the nominal values of $Q_{b,ult}$ and Q_{sL}, $(\mathrm{DL})^{(\mathrm{n})}$ = nominal dead load, $(\mathrm{LL})^{(\mathrm{n})}$ = nominal live load, $(\mathrm{RF})_b$ = base resistance factor, $(\mathrm{RF})_s$ = shaft resistance factor, $(\mathrm{LF})_{\mathrm{DL}}$ = dead load factor and $(\mathrm{LF})_{\mathrm{LL}}$ = live load factor.

The problem addressed by this research can be posed through the following questions:

(1) What is the best way of developing the resistance factors and defining resistance for piles?
(2) What are those factors and resistances for piles in the classical cases of nondisplacement and displacement piles (see Chapter 12 of Salgado 2008 for detailed discussion of pile types) installed in sand and clay?

1.3. Objectives and Organization

In Chapter 2, we describe the design process in a probabilistic context and connect that discussion with reliability analysis and LRFD. In Chapter 3, we expand on the discussion of LRFD and how reliability analysis can be used to establish factor and other key quantities in LRFD along with pile designs in general in the context of LRFD of piles. In Chapters 4, 5, 6, and 7 we shows how we have developed the LRFD framework for nondisplacement piles in sand, nondisplacement piles in clay, displacement piles in sand and displacement piles in clay. Chapter 8 contains a summary of main finding and values of various quantities to use in design.

CHAPTER 2. FOUNDATION DESIGN AS A PROBLEM OF DECISION MAKING UNDER UNCERTAINTY

2.1. Introduction

Although the uncertainties in most routine activities tend to be small over extended periods of time, giving a false impression of a largely deterministic world, life is in fact largely uncertain, and so is engineering activity. The risks associated with the uncertainty involved in decisions made at design time are often masked by relatively gently varying variables, by alleviating factors not modeled because of imperfect knowledge of underlying physical processes or by the underappreciated dependence of phenomena on time. So every engineering decision is made in the context of a cloud of uncertainty, irrespectively of the degree to which the designer is aware of this uncertainty.

Decision under uncertainty if often discussed in the context of games of chance. In the next section, we start the discussion with a game example and then connect it to engineering design decisions. We then illustrate how well known methods from probability theory, notably reliability analysis, can be used to frame engineering design decision making, and finally show how LRFD can be considered a "pre-cooked" reliability analysis-based design.

2.2. Decision under Uncertainty: probabilities, outcomes and the notion of value

When evaluating the prospects for making a bet, which is essence a decision between two options,

making or not making the bet, an intelligent individual would go through the following steps:

1) Identify all the possible outcomes (e.g., a number from 1 to 6 for a single throw of a dice);
2) Assess the probability of each outcome (1/6 in a game of dice);
3) Assess the gains and losses proposed in the bet (in the example of the game of dice, only play against a naïve player, who being unaware of the 1/6 probability of any of the outcomes in a game of dice, would potentially make a bet offering opportunities for gain);
4) Calculate the expected value of the bet (in essence, the summation of the products of each outcome probability by its value or gain);
5) If the expected value of making the bet is greater than that of not making it, make it; otherwise, pass. An example of a game of dice worth playing might be against someone who would be willing to bet a large amount of money on "six" based on an incorrect assessment of the probability of six coming up.

An obvious component of this type of decision is the notion of value, which is not uniquely related to monetary value. For example, playing Russian Roulette would not appear very compelling to a sane person, no matter the amounts of money involved. For a government organization like INDOT or FHWA, value should be assigned to safety, environment preservation, sustainability and other such goals not easily expressed in monetary terms because they are not typically traded in private markets.

A complication not present in games of chance but very much a part of many other activities, including engineering, is the difficulty of assessing the probabilities of different outcomes. So engineering decision making depends very much on the subjective assessment of (a) value and (b) probability of each outcome.

2.3. Foundation Design as an Exercise of Decision under Uncertainty: reliability analysis

Barring construction blunders or defective quality assurance/control of construction, which cannot be taken into account at design time, foundation design has, in general terms, two possible outcomes: satisfactory foundation performance or unsatisfactory foundation performance. Design outcomes defined in this manner are only useful if what would be considered satisfactory and the characterization of performance are specifically defined. The concept of a limit state is helpful in clearly defining both concepts. A limit state is a marginally undesirable outcome, defining the limit between acceptable and unacceptable performance, defined specifically with respect to a measurable variable associated with the response of the foundation to loads or other actions during the life of the structure. The most common geotechnical limit states for a pile are:

(a) The pile or pile group experiences a settlement expected to cause architectural problems or other serviceability problems (for example, a "rough ride" in a bridge or overpass application);
(b1) The pile or pile group experiences a settlement expected to cause damage (such as open cracking or partial or complete collapse) to a supported structure.
(b2) The pile or pile group plunges into the ground.

Limit state (a) (LS II in the terminology used by Salgado 2008) is known as a serviceability limit state because it impairs the structure's functionality but not its integrity and safety. Limit states (b) (LSIA-1 and LSIB in the terminology in Salgado 2008) are known as ultimate limit states. Ultimate limit states (ULSs) are associated with danger or loss of safety. A designer's main goal should be to properly identify all of the outcomes associated with ULSs and minimize the probability of their occurrence to a level that is acceptable according to the owner of the structure or as prescribed by an agency through specifications or codes of practice. In order to do this in the context of a decision made under uncertainty, an engineer may use reliability analysis.

In reliability analysis, all the variables defining the foundation design problem, variables related to the foundation element, the soil and the loadings on the foundation element, are treated as random variables. These random variables appear in a limit state equation (of the type load = resistance or demand = capacity) which separates states in which the minimum requirements for the foundation defined according to the limit state equation are not met from those in which they are and the foundation therefore performs adequately. Since the variables are random variables, each described by a probability density function, and an equation exists that clearly and specifically defines what constitutes a limit state, it is possible to calculate the probability that the foundation is in an acceptable state. If that probability is subtracted from 1, we have the probability that the foundation has reached or exceeded a limit state, which is often referred to as the probability of failure.

2.4. Reliability Analysis

Reliability analysis of an engineering problem consists in obtaining the reliability index or probability of failure of a given design. More generally, it involves determining the design leading to a required maximum probability of failure or minimum reliability index.

The engineering problem of interest for us is that of a pile subjected to axial loading (dead or live), which it resists through development of shaft and base resistance. The shaft and base resistance depend on variables related to the soil, pile-soil interface and pile. All of these variables (soil variables, pile variables and interface variables on the resistance side and live and dead loads on the loading side), which are random and have PDFs associated with them, define a multivariate space. In this space, the limit state equation is defined as a "surface" (hypersurface, with hyper meaning a term typically used in the context of 3D space is being used

in the context of multivariate space) with dimension one less than the number of space dimensions. The surface separates states that violate the limit state criterion from those that do not.

A "point" can be defined in this multivariate space whose coordinates are the means of all variables involved in the problem. If the point lies on the limit state "surface", it is a limit state. If it is on the acceptable side of the "surface" then it is not a limit state; however, since the variables defining the problem are all random, the mean "point" is at the center of a hypercloud of uncertainty, and if this uncertainty cloud advances too deeply into the "unacceptable" side of the limit state hypersurface, the risk of having the design produce an unacceptable outcome may become too high. This hypercloud of uncertainty may be defined in terms of hypersurfaces around the mean hyperpoint, each surface corresponding to a certain level of uncertainty (described, for example, through the standard deviations of all the variables).

2.5. Review of Basic Probability Theory Concepts

A probability density function (PDF) represents a probability distribution of a particular random variable x. For the random variable x, the PDF $p_x(x)$ is a nonnegative function whose integral from $-\infty$ to $+\infty$ is equal to one:

$$\int_{-\infty}^{\infty} p_x(x)dx = 1 \tag{2.1}$$

The idea behind that is that integrating from $-\infty$ to $+\infty$ spans the entire range of possible outcomes for x, and therefore the probability of that must be 1.

The cumulative distribution function (CDF) of x', denoted as $P_x(x')$, is an integral of $p_x(x)$ from $-\infty$ to x':

$$P_x(x') = \int_{-\infty}^{x'} p_x(x)dx \tag{2.2}$$

When a population (with size = n) of a certain random variable x exists, the mean μ_x and variance V_x of the population of x are:

$$\mu_x = \frac{\sum_{i=1}^{n} x_i}{n} \tag{2.3}$$

$$V_x = \frac{\sum_{i=1}^{n} (x_i - \mu_x)^2}{n} \tag{2.4}$$

The standard deviation σ_x of the population of x is the positive square root of its variance and is a measure of intensity of scatter about its mean μ_x:

$$\sigma_x = \sqrt{V_x} = \sqrt{\frac{\sum_{i=1}^{n} (x_i - \mu_x)^2}{n}} \tag{2.5}$$

The estimation of mean and standard deviation of a certain property x for a population with size greater than n is possible from a sample that consists of "n" measurements (x_1, x_2, $\cdots$, x_n) of x. These estimated mean and standard deviation of the population are called the sample mean and sample standard deviation, and are denoted by $\bar{x}$ and s_x, respectively. The expressions for the sample mean and sample standard deviation are:

$$\bar{x} = \frac{\sum_{i=1}^{n} x_i}{n} \tag{2.6}$$

$$s_x = \sqrt{\frac{\sum_{i=1}^{n} (x_i - \bar{x})^2}{(n-1)}} \tag{2.7}$$

The covariance of random variables x and y is a measure of the strength of correlation between x and y. The covariance of x and y is defined by:

$$\mathrm{COV}(x,y) = E\left[(x-\mu_x)(y-\mu_y)\right] \tag{2.8}$$

The covariance has positive sign when x and y are positively correlated and vice versa. When x and y are highly positively or negatively correlated, the absolute value of the covariance is large. If x and y are independent of each other, the covariance is equal to zero. The covariance between two identical random variables is equal to the variance of the variable. For discrete random variables x and y (i =1, 2, $\cdots$, n), the covariance can be expressed as:

$$\mathrm{COV}(x,y) = \frac{\sum_{i=1}^{n} (x_i - \mu_x)(y_i - \mu_y)}{n} \tag{2.9}$$

The correlation coefficient $\rho(x,y)$ of random variables x and y is equal to covariance divided by the standard deviation of these two random variables:

$$\rho(x,y) = \frac{\mathrm{COV}(x,y)}{\sigma_x \sigma_y} \tag{2.10}$$

By this normalization, the strength of correlation between x and y can be expressed as a dimensionless number that is independent of the units of x and y. The correlation coefficient varies from -1 to 1. The correlation coefficient value is equal to 1 (-1), if x and y have a perfect positive (negative) linear relationship.

If a certain variable Y is a linear combination of n random variables X_1, X_2, $\cdots$, X_n , as in

$$Y = \sum_{i=1}^{n} a_i X_i \tag{2.11}$$

The mean of Y is

$$\begin{aligned} E[Y] &= E\left[\sum_{i=1}^{n} a_i X_i\right] \\ &= a_1 E[X_1] + a_2 E[X_2] + \cdots + a_n E[X_n] \\ &= a_1\mu_1 + a_2\mu_2 + \cdots + a_n\mu_n \end{aligned} \tag{2.12}$$

When $X_1, X_2, \cdots, X_n$ are mutually independent, the variance of Y is

$$\begin{aligned} V[Y] &= V\left[\sum_{i=1}^{n} a_i X_i\right] \\ &= a_1^2 V[X_1] + a_2^2 V[X_2] + \cdots + a_n^2 V[X_n] \end{aligned} \tag{2.13}$$

It follows that the standard deviation of Y ($X_1, X_2, \cdots, X_n$ being mutually independent) is

$$\sigma_Y = \sqrt{V[Y]} = \sqrt{a_1^2\sigma_{X_1}^2 + a_2^2\sigma_{X_2}^2 + \cdots + a_n^2\sigma_{X_n}^2} \tag{2.14}$$

The mean (or expected) value of a continuous random variable x whose probability distribution function is $p_x(x)$ can be expressed as:

$$\mu_x = E[x] = \int_a^b x\, p_X(x)dx \tag{2.15}$$

where a and b are the lower and upper bound values of the PDF, respectively.

The mean of discrete values of x whose discrete probability distribution is $p_x(x_i)$ can be expressed as:

$$\mu_x = E[x] = \sum_{i=1}^{n} x_i \cdot p_X(x_i) \tag{2.16}$$

where n is the number of x observations (or measurements).

As shown in Figure 2.1, the nominal value of a variable may not be equal to its mean value. In other words, the nominal value could be either greater than or less than the mean value. The nominal value as a deterministic value that does not have any uncertainty defined in some specific way. To account for the relationship between the nominal value and the mean value, the bias factor (the ratio of mean value to nominal value) is introduced:

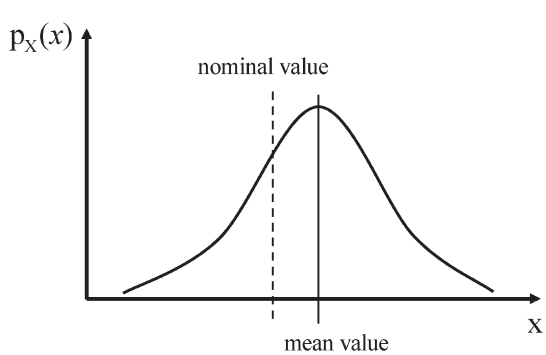

Figure 2.1 Mean and nominal values of a parameter x.

$$\text{bias factor} = \frac{\mu_x}{x_{\text{nominal}}} \tag{2.17}$$

where μ_x and x_{nominal} are the mean and nominal values of a variable x, respectively.

If the bias factor of a variable x is a known value, the mean value of x can be directly calculated by multiplying the bias factor by the nominal value.

2.6. Assessment of the Uncertainty of Independent and Dependent Variables

The uncertainties associated with the design variables are quantified by treating each of these variables as a random variable with an associated probability density function (PDF). One measure of variable uncertainty is the sample coefficient of variation (COV). The COV of a random variable x is defined as the ratio of its (estimated) standard deviation to its (estimated) mean:

$$\text{COV} = \frac{s_x}{\bar{x}} \tag{2.18}$$

The COV is a measure of the relative scatter of values of a variable around its mean. The basic idea behind this quantity is that the absolute measure of scatter around the mean should be proportional to the mean. The uncertainties that we consider in our analyses are the uncertainties in (a) soil variables, (b) design equations (model uncertainties), (c) applied loads and (d) pile dimensions. In the work reported here, for each variable, we assume the PDF as either a normal or lognormal distribution and estimate its mean (expected value) and COV (see Figure 2.2).

Biases often arise in the estimation of the design variables (material properties, loads and resistances) making the nominal values calculated by the designers different from the corresponding mean values. In such cases, the mean and nominal values are related though bias factors, as expressed by equation (2.17).

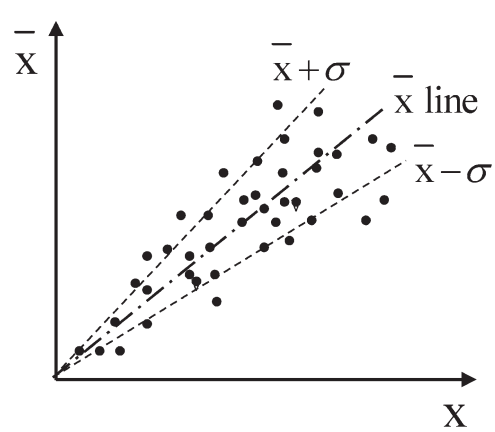

Figure 2.2 Scatter of a variable X around its mean for constant COV.

2.7. Uncertainties of models and transformations

Model and transformation uncertainties arise because the mathematical models (equations) we use are not perfect representation of a process but approximations of the actual behavior based on a set of assumptions.

If a function $y = f(x_1, x_2, \ldots, x_n)$ represents a mathematical relationship between y and component variables $x_1, x_2, \ldots, x_n$ of function f, then the model or transformation uncertainty associated with the function f appears as a difference between realizations (or measurements) y_i and $f(x_{1,i}, x_{2,i}, \ldots, x_{n,i})$. The difference between y_i and $f(x_{1,i}, x_{2,i}, \ldots, x_{n,i})$ can be expressed through the following ratio:

$$w_i = \frac{y_i}{f(x_{1,i}, x_{2,i}, \cdots, x_{n,i})} \tag{2.19}$$

Scatter around w_i values is caused by random fluctuations of $(x_1, x_2, \ldots, x_n)$ and y_i, generally arising because of imperfections in f as a true representation of the relationship between y and $x_1, x_2, \ldots, x_n$. The bias of the model or transformation f is the average value of w_i:

$$\bar{w} = \frac{\sum_{i=1}^{n} w_i}{n} \tag{2.20}$$

Since only the information about sample space is generally known, the estimate of standard deviation s_w of w is considered as the standard deviation of the model or transformation. Calculation of model or transformation standard deviation is possible using the following equation:

$$s_w = \sqrt{\frac{\sum_{i=1}^{n} (w_i - \bar{w})^2}{(n-1)}} \tag{2.21}$$

It follows that the COV of $y = f(x_1, x_2, \ldots, x_n)$ is:

$$\mathrm{COV} = \frac{s_w}{\bar{w}} \tag{2.22}$$

2.8. Target Probability of Failure and number of M-C runs

For most structural designs, a target p_f of approximately 10^{-3} (corresponding to a target reliability index of 3) is often assumed (Foye 2005, Ellingwood et al. 1982). However, depending on the importance of a structure and the relative cost of safety measures, different target reliability indices may be set (JCSS 2000). Moreover, particular components of a structure, e.g., steel connections, may require a target reliability index greater than 3 (Fisher et al. 1978). As an example of the significance of this number in the context of our work, a target probability of failure of 10^{-3} for drilled shafts implies that one in every one thousand piles may fail. Under typical conditions, this incidence of failure may be too high. A target $p_f = 10^{-4}$, corresponding to a failure rate of one in every ten thousand drilled shafts, is perhaps more realistic. Accordingly, we considered two values of target p_f, 10^{-3} and 10^{-4}, in our calculations and developed resistance factors for both these target probabilities of failure.

2.9. First-Order Reliability Method (FORM)

The concept of the reliability index β was introduced by Cornell (1969) and Hasofer and Lind (1974). To apply the reliability index concept to limit state analysis, we need to have a well-defined limit state equation, a mean (or expected) value, a bias factor, and a standard deviation (or COV) for each random variable used in the analysis.

As discussed earlier, if we have n random variables in the ultimate limit state (ULS) equation, the ULS equation defines a limit state hypersurface in n-dimensional hyperspace; likewise, a hyperpoint whose coordinates are the mean values of the n random variables can also be defined in the n-dimension hyperspace. Geometrically, the reliability index β is the ratio of the closest distance between the hyperpoint defined by the mean values of the n variables and the limit state hypersurface to the standard deviation of the joint probability density function for the n variables.

For example, if we have only two variables (x and y) in the ULS equation, the limit state hypersurface is represented by a line (Figure 2.3) and the mean hyperpoint or state is represented by a point (μ_x, μ_y) defined by the mean values of the two variables. It is possible to calculate the standard deviation of the joint probability density function by assessing the uncertainties associated with load and resistance. The closest distance between (μ_x, μ_y) and the failure surface also follows from the figure. The reliability index β is then calculated as the ratio of this distance to the standard deviation of the joint probability density function.

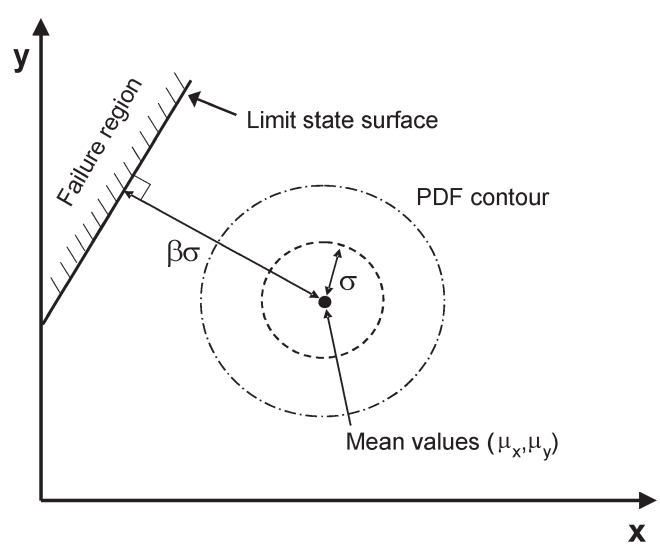

Figure 2.3 Geometrical illustration of reliability index β in two-dimensional space

The reliability index β can be calculated from (Low and Tang 1997):

$$\beta = \min \sqrt{(\mathbf{x}_{LS} - \mathbf{m})^{\mathbf{T}} \mathbf{C}^{-1} (\mathbf{x}_{LS} - \mathbf{m})} \qquad (2.23)$$

where $\mathbf{m}$ is the vector or hyperpoint whose components are the mean values of the random variables x_i, $\mathbf{x_{LS}}$ is a vector or hyperpoint consisting of values of the random variables x_i that satisfy the limit state equation, and $\mathbf{C}$ is the covariance matrix. For n random variables x_i (i=1, 2,$\cdots$, n) and the corresponding ULS equation [M(x_1, x_2, $\cdots$, x_n) = 0], the reliability index β is calculated as the minimum distance between the hyperpoint corresponding to the mean values of these n variables and the ULS hypersurface defined by the limit state equation. The state corresponding to β is a hyperpoint along a contour around the mean hyperpoint $\mathbf{m}$ corresponding to β standard deviations that is closest to the ULS hypersurface.

The covariance matrix $\mathbf{C}$ is:

$$\mathbf{C} = \begin{bmatrix} \mathrm{COV}(x_1,x_1) & \mathrm{COV}(x_1,x_2) & \cdots & \mathrm{COV}(x_1,x_n) \\ \mathrm{COV}(x_2,x_1) & \mathrm{COV}(x_2,x_2) & \cdots & \mathrm{COV}(x_2,x_n) \\ \vdots & \vdots & \ddots & \vdots \\ \mathrm{COV}(x_n,x_1) & \mathrm{COV}(x_n,x_2) & \cdots & \mathrm{COV}(x_n,x_n) \end{bmatrix} \qquad (2.24)$$

where COV(x_i, x_j) is called the covariance between x_i and x_j.

2.10. Monte Carlo Simulations

Monte Carlo simulation is the repetitive process of generating a very large number of values of a random variable according to that variable's mean and standard deviation (or other parameters that define the uncertainty in the variable) in order to reproduce the probability distribution of the variable. If a function exists of random variables, by generating PDFs for each variable and calculating the corresponding values of the function, it is also possible to produce a PDF for the function. The advantage of this method is its simplicity, but the method is computationally intensive.

To illustrate the process of a Monte Carlo simulation, consider a function G of direct input parameters (x_i; i = 1, $\cdots$, n) and derived input parameters (y_j; j = 1, $\cdots$, m), which are functions of some random variables z_i:

$$\mathrm{G} = f(x_1, \cdots, x_n; y_1, \cdots, y_m) \qquad (2.25)$$

For each direct input parameter x_i, we can generate random numbers following its assumed PDF. For the derived input parameters, we need to account for the uncertainties associated with the transformations from z_i to y_i in order to generate the random y_i numbers. The final value of y_j is then taken into the function G. This process is used for each derived variable.

Suppose we have a random variable x with PDF $p_x(x)$ and a transformation of x to y is given by y = $f(x)$. Random values of x can be generated based on:

$$\int_{-\infty}^{x'} p_x(x)dx = \xi \qquad (2.26)$$

where x' is the generated random number reflecting $p_x(x)$, and ξ is a variable following a uniform distribution between 0 and 1.

Because ξ represents a Cumulative Distribution Function (CDF) of x', it ranges between 0 and 1. To generate a large number of x′ values, a large number of ξ values are randomly generated from a uniform distribution between 0 and 1, and x' values are back-calculated by inputting the generated ξ values to (2.26). The distribution of the generated values of x' will then follow the original PDF $p_x(x)$.

For each value of x' from the large set generated as described, the prediction for the corresponding y value is made using the transformation y = $f(x)$, and the uncertainty of this transformation is added to the predicted y value. By repeating this process for all the generated x' values, we obtain the PDF of y, which is denoted by $p_y(y)$.

The reliability analyses performed in this study rely on rigorous Monte Carlo simulations. The Monte Carlo simulations produce the probability of failure and the most probable ultimate limit state values of resistances and loads more accurately than FORM if the simulations are properly done (Bailey et al., 1996, Cawlfield and Wu, 1993, Menching 1992, and Jang et al., 1994).

The number n_{total} of M-C runs required to ensure that a target probability of failure p_f is achieved can be estimated as (Fenton and Griffiths 2008):

$$n_{\mathrm{total}} = p_f\left(1 - p_f\right)\left(\frac{z_\alpha}{e}\right)^2 \qquad (2.26)$$

where e is the maximum error in p_f estimated with a confidence interval of α (expressed either as a percentage or a fraction) and z_α is the number of standard deviations of the standard normal variate Z (with mean $\bar{z} = 0$ and standard deviation σ_z = 1) such that the probability $P[\bar{z} - z_\alpha\sigma_z < Z < \bar{z} + z_\alpha\sigma_z] = P[-z_\alpha < Z < z_\alpha]$ (i.e., the area under the standard normal curve extending symmetrically about the zero mean to a distance of $\pm$ z_α) equals α. The values of z_α are calculated from an inverse error function and are readily available. For example, for 90% confidence, α = 0.9, for which z_α can be calculated as 1.645. The above equation is obtained with the assumption that each M-C run is a Bernoulli trial.

Using equation (2.26), we estimated the required number of M-C runs n_{total} to be equal to 270,332 for a target p_f = 10^{-3} with 90% confidence (α = 0.9; z_α = 1.645) that the maximum relative error in the estimation of p_f is 10% (i.e., e = 0.0001). We chose n_{total} = 271,000; thus, the number n_f of failures corresponding to p_f = 10^{-3} is 271. For the target p_f = 10^{-4}, n_{total}

required to maintain the error in p_f within the stringent bound of 10%, with 90% confidence, is prohibitively large. Consequently, we chose $n_{\text{total}} = 1{,}000{,}000$, which ensured, with 90% confidence, that the maximum relative error in the estimation of p_f is 16.5%. For practical purposes, the relative error of 16.5% is perfectly acceptable for the low probability-of-failure case, where only one out of ten thousand piles is expected to reach the limit state. For $n_{\text{total}} = 1{,}000{,}000$, $n_f = 1{,}000$ corresponds to the target $p_f = 10^{-4}$.

The target probability of failure, however, cannot generally be achieved by performing only one set of M-C simulations. For a given soil profile and drilled shaft geometry, the assumed mean values of $(\text{DL})^{(\text{mean})}$ and $(\text{LL})^{(\text{mean})}$ (actually the (LL) / (DL) ratio) may not exactly produce $n_f = 271$ or 1,000; n_f may be greater or less than the corresponding target value. If the first set of M-C simulations produces a pf greater than target p_f (i.e., $n_f > 271$ or 1,000), then we reduce the applied mean loads $(\text{DL})^{(\text{mean})}$ and $(\text{LL})^{(\text{mean})}$ and again perform a set of M-C simulations. On the other hand, if the first set of M-C simulations produces a p_f less than the target p_f (i.e., $n_f < 271$ or 1,000), we increase the applied mean loads. We continue performing successive sets of M-C simulations with adjustments in the mean values of loads until the target p_f is reached. In numerical calculations, a small window of $0.9 \times 10^{-\theta} < p_f < 1.1 \times 10^{-\theta}$ (with $\theta = 3$ or 4) was used as the termination criterion in place of the exact value of $p_f = 10^{-\theta}$.

CHAPTER 3. LRFD OF PILE FOUNDATIONS

3.1. Introduction

The Federal Highway Administration (FHWA) has mandated the use of load and resistance factor design (LRFD) for foundations of all bridge structures. This mandate may have started a trend in the US of change from the traditional Working (or Allowable) Stress Design (WSD or ASD) to LRFD of foundations and geotechnical structures. This is a natural trend because LRFD is conceptually superior to WSD. In LRFD, the uncertainties associated with the design variables and methodologies can be systematically allocated to factors - the resistance and load factors - that are associated separately with the resistances and applied loads. In contrast, WSD relies on ad hoc use of one factor - the factor of safety - that attempts to single-handedly account for all the uncertainties. LRFD is appropriate for geotechnical designs because the variabilities and uncertainties associated with natural systems, the ground in this case, are much greater than those associated with well controlled engineered systems (Lacasse and Nadim 1996). Consequently, the development of LRFD methods for various geotechnical problems (e.g., design of foundations, slopes and retaining structures) has been an active field of research since the last decade.

Early efforts toward establishing LRFD codes for geotechnical designs in the US were not sufficiently rigorous; the specifications were calibrated based on a combination of simplistic reliability analysis, fitting to WSD and engineering judgment (Paikowsky 2004). The lack of rigor followed from the reliance of traditional geotechnical design approaches on ad hoc judgment and empirical methods and from the difficulty in quantifying uncertainties associated with geotechnical designs. A large number of research studies on reliability analysis or LRFD of piles have relied on calibrations with respect to field pile load tests to obtain target reliability indices or resistance factors (Yoon and O'Neil 1996, Yoon et al. 2008). Most of these research studies have been done for driven piles (Titi et al. 2004, Kwak et al. 2007), although studies on drilled shafts (or bored piles) also exist. Ochiai et al. (1994) proposed a reliability based design method for bored piles based on an in situ test-based design equation by considering the spatial variation of standard penetration test (SPT) results. Honjo et al. (2002) used a conditional first-order, second-moment approach to obtain resistance factors of cast-in-situ concrete piles in Japan. Misra and Roberts (2006), (2009) and Misra et al. (2007) developed a reliability analysis for drilled shafts based on an elasto-plastic pile shaft-soil interaction model by using Monte-Carlo (M-C) analysis. Zhang et al. (2005) introduced a bias factor in order to account for the differences in the failure criteria used for design of bored piles. McVay et al. (2003), based on load tests of drilled shafts in Florida limestone, assessed the reliability of drilled shafts as a function of cost. Yang et al. (2008) calibrated, based on data from O-cell tests, the side resistance factors for drilled shafts in weak rock.

In this chapter, we discuss the procedure that we have followed at Purdue University to develop an LRFD framework for piles that satisfies our four requirements:

(1) use of current design methods, based on scientifically sound analyses;
(2) no reliance on calibration against WSD;
(3) careful accounting of uncertainties of each variable and relationship;
(4) use of reliability analysis with a suitable probability of failure.

3.2. Live Load-Dead Load Ratio for Transportation Structures

An appropriate range of live-to-dead load (LL)/(DL) must be examined for pile analysis problems. Hansell and Viest (1971) reported that the live-to-dead load is a function of dynamic allowance IM (a factor converting dynamic load effects into an equivalent static load effect; $IM = 0.33$; AASHTO, 2007) and bridge span length (L) (in meters) of a bridge, and proposed the following equation for the estimation of (LL)/(DL):

$$(\text{LL})/(\text{DL}) = \frac{1}{0.0433(1+IM)L} \tag{3.1}$$

In this report, we assumed three different ratios (0.25, 1, and 2) of (LL)/(DL) for the calculations of resistance factors. From equation (3.1), the (LL)/(DL) values of 0.25 and 2.0 correspond to the span lengths of 70m and 8.5m, respectively.

3.3. Location of the Most Probable Ultimate Limit State and Calculation of Load and Resistance Factors

The ultimate limit state is reached when capacity C equals demand D. Thus, in the PDF of C − D, the origin of the (C − D) axis represents the limit state. For each set of M-C simulations, we located the limit state by capturing the minimum of the random |C − D| values subject to the condition that $|C - D| < \varepsilon$ where ε is a pre-assigned tolerable error in the loads (typically, for applied loads in the range of 1,000 kN or greater, ε = 50 kN was assumed). For the final set of M-C simulations, which satisfies the condition of $p_f \approx 10^{-\theta}$ (θ = 3 or 4 in this report), we identify the particular M-C run for which |C − D| is the minimum (the numerical equivalent of C = D); the values of shaft and base resistances and DL and LL that produce the minimum |C − D| are the ultimate limit state resistances.

For a given pile and given soil properties, these ultimate limit state resistances and loads are not unique values, varying simulation to simulation. This results from the fact that we are determining the ULS on the basis of having C − D = 0 but this equality can be achieved by multiple combinations of the random variables defining the problem even while satisfying the requirement that $p = p_f$. To overcome this nonuniqueness limitation, we must find the most probable ultimate limit state values of resistances ($Q_{b,\mathrm{ult}}^{(\mathrm{LS})}$ and $Q_{s\mathrm{L}}^{(\mathrm{LS})}$) and loads ($(\mathrm{DL})^{(\mathrm{LS})}$ and $(\mathrm{LL})^{(\mathrm{LS})}$), where the superscript (LS) denotes the most probable ultimate limit state. In this study, we generated 200 cases of ultimate limit states by running 200 M-C simulations and stored 200 sets of ultimate limit state values of $Q_{b,ult}$, Q_{sL}, DL, and LL resulting from the 200 M-C runs. For the 200 sets of ultimate limit state values of $Q_{b,ult}$, Q_{sL}, DL, and LL, we have a multi-dimensional probability density function (PDF) of $Q_{b,ult}$, Q_{sL}, DL, and LL. For the multi-dimensional PDF, the equiprobable lines can be represented through the following equation:

$$(\mathbf{x}-\mathbf{m})^{\mathbf{T}}\mathbf{C}^{-1}(\mathbf{x}-\mathbf{m}) = d^2 \tag{3.2}$$

where d represents the distance from the mean point to the equiprobable line in standard normal space; this distance is expressed as a multiple of the standard deviation of the multi-dimensional PDF.

We define the most probable ultimate limit state as the point of tangency between the ultimate limit state hypersurface and the equiprobable hypersurface with the minimum d. The values of $Q_{b,ult}$, Q_{sL}, DL, and LL at the most probable ultimate limit state are $Q_{b,\mathrm{ult}}^{(\mathrm{LS})}$, $Q_{s\mathrm{L}}^{(\mathrm{LS})}$, $(\mathrm{DL})^{(\mathrm{LS})}$, and $(\mathrm{LL})^{(\mathrm{LS})}$, respectively.

Generally, the most probable ultimate limit state values ($Q_{b,\mathrm{ult}}^{(\mathrm{LS})}$, $Q_{s\mathrm{L}}^{(\mathrm{LS})}$, $(\mathrm{DL})^{(\mathrm{LS})}$, and $(\mathrm{LL})^{(\mathrm{LS})}$) determined following the procedure above are very close to the averages of the 200 ultimate limit state values of $Q_{b,ult}$, Q_{sL}, DL, and LL. Therefore, taking averages of a large number of ultimate limit state values of $Q_{b,ult}$, Q_{sL}, DL, and LL from M-C simulations can be a sufficiently good approximation to $Q_{b,\mathrm{ult}}^{(\mathrm{LS})}$, $Q_{s\mathrm{L}}^{(\mathrm{LS})}$, $(\mathrm{DL})^{(\mathrm{LS})}$, and $(\mathrm{LL})^{(\mathrm{LS})}$.

At the limit state:

$$Q_{b,\mathrm{ult}}^{(\mathrm{LS})} + Q_{s\mathrm{L}}^{(\mathrm{LS})} = (\mathrm{DL})^{(\mathrm{LS})} + (\mathrm{LL})^{(\mathrm{LS})} \tag{3.3}$$

This equation can be rewritten as:

$$\frac{Q_{b,\mathrm{ult}}^{(\mathrm{LS})}}{Q_{b,\mathrm{ult}}^{(\mathrm{n})}} Q_{b,\mathrm{ult}}^{(\mathrm{n})} + \frac{Q_{s\mathrm{L}}^{(\mathrm{LS})}}{Q_{s\mathrm{L}}^{(\mathrm{n})}} Q_{s\mathrm{L}}^{(\mathrm{n})} = \frac{(\mathrm{DL})^{(\mathrm{LS})}}{(\mathrm{DL})^{(\mathrm{n})}} (\mathrm{DL})^{(\mathrm{n})} + \frac{(\mathrm{LL})^{(\mathrm{LS})}}{(\mathrm{LL})^{(\mathrm{n})}} (\mathrm{LL})^{(\mathrm{n})} \tag{3.4}$$

Defining:

$$(\mathrm{RF})_b = Q_{b,\mathrm{ult}}^{(\mathrm{LS})} \Big/ Q_{b,\mathrm{ult}}^{(\mathrm{n})} \tag{3.5}$$

$$(\mathrm{RF})_s = Q_{s\mathrm{L}}^{(\mathrm{LS})} \Big/ Q_{s\mathrm{L}}^{(\mathrm{n})} \tag{3.6}$$

$$(\mathrm{LF})_{\mathrm{DL}} = (\mathrm{DL})^{(\mathrm{LS})} \Big/ (\mathrm{DL})^{(\mathrm{n})} \tag{3.7}$$

$$(\mathrm{LF})_{\mathrm{LL}} = (\mathrm{LL})^{(\mathrm{LS})} \Big/ (\mathrm{DL})^{(\mathrm{n})} \tag{3.8}$$

equation (3.4) can be rewritten as:

$$(\mathrm{RF})_b Q_{b,\mathrm{ult}}^{(\mathrm{n})} + (\mathrm{RF})_s Q_{s\mathrm{L}}^{(\mathrm{n})} = (\mathrm{LF})_{\mathrm{DL}} (\mathrm{DL})^{(\mathrm{n})} + (\mathrm{LF})_{\mathrm{LL}} (\mathrm{LL})^{(\mathrm{n})} \tag{3.9}$$

For any set of M-C simulations, we calculate the nominal loads $(\mathrm{DL})^{(\mathrm{n})}$ and $(\mathrm{LL})^{(\mathrm{n})}$ from the corresponding mean loads (used in the M-C simulations) by dividing the mean loads by the corresponding bias factors (dead load bias factor = 1.05; live load bias factor = 1.0 or 1.15). Using the limit-state and nominal values, we calculate the resistance and load factors using equations (3.5)−(3.8).

Equation (3.9) still represents the limit state. In design, the equality sign in equation (3.9) is replaced by "≥" [inequality (1.3)], indicating that the sum of the factored resistances must be no less than the sum of the factored loads.

3.4. Distributions of Load and Resistance Factors

It is evident from equation (3.9) that multiple combinations of resistance and load factors producing

the same limit state are possible because there are four variables — $(RF)_b$, $(RF)_s$, $(LF)_{DL}$ and $(LF)_{LL}$ — that can mutually adjust to satisfy one equation. In other words, for a given problem (i.e., for a given soil profile and pile geometry), multiple values of limit state loads and resistances are possible. Thus, instead of obtaining unique values of the resistance and load factors for a given problem, we generate their distributions (histograms) by repeating the calculations described above in their entirety (i.e., running multiple sets of M-C simulations until the target p_f is reached, and then identifying the limit states and calculating the resistance and load factors from the final set of M-C simulations) 200 times. The choice of 200 iterations was made by trial and error; 200 was found to be the minimum number of iterations that produced nearly identical (repeatable) distributions of the load and resistance factors with consistent means and standard deviations.

For design, however, representative values (i.e., actual numbers that will be used in design calculations), and not distributions, of load and resistance factors are required. As discussed earlier, the mean values of the distributions are good approximations to what the representative values should be. In order to verify that this is indeed the case, we tracked the 200 iterations to identify those runs in which both the resistance factors were 0.05SD (SD = standard deviation) less than their respective mean values and, at the same time, both the load factors were 0.05SD greater than their respective mean values. In all the problems analyzed in this report, there was no simultaneous occurrence of both the resistance factors less than their respective mean values by 0.05SD and of both the load factors greater than their respective mean values by 0.05SD. In addition, comparisons with the more rigorous approach to identification of the most probable ULS described earlier have proven satisfactory. Consequently, we considered it appropriate to identify the mean (expected) values of the resistance and load factors calculated using our procedure as the representative values of the resistance and load factors that can be used in design (and, in theoretical terms, as very good approximations to the values corresponding to the most probable ULS).

3.5. Adjusted Load and Resistance Factors

The resistance and load factors obtained using the method described in the previous section are optimal factors that satisfy the limit state condition, equation (3.9). Ideally, the optimal factors would be used in design. However, most pile designs are done with factored loads calculated by structural engineers using load factors prescribed in codes. The optimal resistance factors are not compatible with the code-prescribed load factors because their combination does not satisfy the limit state equation (3.9). Consequently, the optimal resistance factors are adjusted to make them compatible with the load factors prescribed in the codes. This is done by using adjusted resistance factors $(RF)^{code}$ calculated using (Foye et al. 2006b):

$$(RF)^{code} = (RF)^{opt} \min\left\{\frac{(LF)^{code}_{DL}}{(RF)^{opt}_{DL}}, \frac{(LF)^{code}_{LL}}{(RF)^{opt}_{LL}}\right\} \quad (3.10)$$

where $(RF)^{opt}$ = optimal resistance factor (for either shaft or base resistance) as obtained from the analysis described above; $(LF)^{code}_{DL}$, $(LF)^{code}_{LL}$ = dead and live load factors prescribed in code; $(LF)^{opt}_{DL}$, $(LF)^{opt}_{LL}$ = optimal dead and live load factors (obtained from analysis described above); and $\min\{\cdot,\cdot\}$ = minimum of the two arguments within {}. In design, $(RF)^{code}$ should be used with code-specified load factors. However, if designs can be done with optimal load factors, then $(RF)^{opt}$ should be used instead. In this study, we used the AASHTO (2007) recommended load factors, $(LF)^{code}_{DL}$ = 1.25 and $(LF)^{code}_{LL}$ = 1.75, to obtain the adjusted resistance factors $(RF)^{code}_b$ and $(RF)^{code}_s$.

3.6. Mean Factor of Safety

In order to feel comfortable with the LRFD framework, some designers like to estimate the "factor of safety" of their designs so that they can link their designs performed using the LRFD method with the WSD framework. Although the traditional factor of safety of the WSD method is not defined in the LRFD framework, a "mean" factor of safety $(FS)_{mean}$ can be defined as the ratio $C^{(mean)}/D^{(mean)}$ of the mean capacity and demand. Defining the total load and total resistance factors in terms of the mean total resistance and mean total applied load as

$$\begin{aligned}(RF)_{total} &= \left(Q^{(LS)}_{b,ult} + Q^{(LS)}_{sL}\right) \Big/ \left(Q^{(mean)}_{b,ult} + Q^{(mean)}_{sL}\right) \\ &= C^{(LS)} \big/ C^{(mean)}\end{aligned} \quad (3.11)$$

$$\begin{aligned}(LF)_{total} &= \left(DL^{(LS)} + LL^{(LS)}\right) \big/ \left(DL^{(mean)} + LL^{(mean)}\right) \\ &= D^{(LS)} \big/ D^{(mean)}\end{aligned} \quad (3.12)$$

and recognizing that $Q^{(LS)}_{b,ult} + Q^{(LS)}_{sL} = DL^{(LS)} + LL^{(LS)}$, the mean factor of safety can be expressed as:

$$(FS)_{mean} = \frac{(LF)_{total}}{(RF)_{total}} \quad (3.13)$$

We calculated the mean total resistance $C^{(mean)} = Q^{(mean)}_{b,ult} + Q^{(mean)}_{sL}$ by averaging the sum of the random values of $Q_{b,ult}$ and Q_{sL} generated in the course of the M-C simulations. The remaining quantities required to calculate $(FS)_{mean}$ — limit state resistances and mean and limit state loads — are already available as a consequence of the M-C simulations discussed previously. Equation Chapter (Next) Section 1

CHAPTER 4. RESISTANCE FACTORS FOR DRILLED SHAFTS IN SAND

4.1. Introduction

In this chapter, we determine the resistance factors for drilled shafts in sand for a soil variable-based design method. A systematic probabilistic analysis is performed in which the uncertainties (probability density functions) associated with each of the soil variables and design equations are quantified. The individual uncertainties are then combined using Monte-Carlo (M-C) simulations based on a target acceptable risk (i.e., target probability of failure) to identify the limit state; and the load and resistance factors are obtained by dividing the limit-state values of loads and resistances by the corresponding nominal values.

The major difference between the present study and prior studies on LRFD of drilled shafts is that, in this research, the resistance factors are developed by quantifying individually the uncertainties of all the basic soil variables appearing in the mechanistic design equations and not by calibrating the final resistances obtained from the design equations against pile load test data. Calibrations with load tests cannot identify and discriminate between the different sources of uncertainties associated with the problem. Our approach is possible because the design equations used in this study were developed from rigorous analyses of non-displacement piles (Lee and Salgado 1999, Loukidis and Salgado 2008, Salgado and Prezzi 2007, Salgado 2008) that realistically simulate the load-transfer mechanisms along the pile shaft and at the pile base.

4.2. Unit Base and Shaft Resistance: Purdue Sand Method for Nondisplacement Piles

The unit shaft resistance $q_{s\mathrm{L}}$ in sand is often determined using the β method, according to which:

$$q_{s\mathrm{L}} = (K \tan \delta)\sigma_v' = \beta \sigma_v' \tag{4.1}$$

where σ_v' is the *in situ* vertical effective stress at the depth at which $q_{s\mathrm{L}}$ is calculated, K is a coefficient and δ is the friction angle mobilized along the pile-soil interface. Several researchers have outlined different procedures for estimating β (Reese et al. 1976, Stas and Kulhawy 1984, O'Neill and Reese 1999). However, these methods are mostly empirical and do not always give reliable estimates of β and are not valid for all sand types (O'Neill and Hassan 1994, Loukidis et al. 2008). Recently, Loukidis and Salgado (2008) performed finite element analysis coupled with an advanced constitutive model to investigate the mechanics of load transfer at the interface of non-displacement piles in sands. Based on their analysis, Loukidis and Salgado (2008) proposed the following equation for K:

$$K = \frac{K_0}{e^{0.2\sqrt{K_0 - 0.4}}} C_1 e^{\frac{D_R}{100}\left[1.3 - 0.2 \ln\left(\frac{\sigma_v'}{p_A}\right)\right]} \tag{4.2}$$

where D_R is the relative density of sand expressed as a percentage, and p_A is a reference stress (100 kPa). The above equation mechanistically captures the dependence of K on the relative density and overburden pressure (i.e., depth) and reliably predicts K for angular and rounded sands. Loukidis and Salgado (2008) found that the coefficient C_1 is equal to 0.71 for angular sands (based on results for Toyoura sand, which is angular) and is equal to 0.63 for rounded sands (based on results for Ottawa sand) and suggested a value of $C_1 = 0.7$ to be used in calculations for clean sands in general. Loukidis and Salgado (2008) also found that the angle δ is approximately equal to the triaxial-compression critical-state friction angle ϕ_c; thus, $\delta = \phi_c$ can be assumed in calculations without any significant error.

The ultimate unit base resistance $q_{b,\mathrm{ult}}$ is related to the limit bearing capacity and is consequently affected by both friction and dilatancy (Salgado 2008). Thus, $q_{b,\mathrm{ult}}$ is a function of D_R and ϕ_c (see, for example, Bolton 1986). Based on load tests, some researchers have expressed $q_{b,\mathrm{ult}}$ as ad hoc fractions of cone penetration resistance q_c (e.g., Ghionna et al. 1994) on the basis that the cone penetration test (CPT) can be viewed as a scaled-down pile load test, so that q_c is approximately equal to the limit unit base resistance $q_{b\mathrm{L}}$ (which corresponds to the limiting value of the unit base load at which the soil mass surrounding the pile can no longer generate additional resistance, leading to plunging of the pile). However, the $q_{b,\mathrm{ult}}/q_{b\mathrm{L}}$ (or $q_{b,\mathrm{ult}}/q_c$) values proposed by these researchers vary over a somewhat wide range (Salgado 2008) and do not mechanistically relate to the fundamental soil variables associated with the problem. Lee and Salgado (1999) performed nonlinear finite element analysis and used plate load tests in calibration chambers to find that $q_{b,\mathrm{ult}}/q_{b\mathrm{L}}$ depends primarily on D_R. Based on this analysis, Salgado (2008) proposed an analytical expression for $q_{b,\mathrm{ult}}$ corresponding to 10% relative settlement (i.e., an expression of unit base resistance q_b when pile head settlement equals 10% of pile diameter):

$$q_{b,\mathrm{ult}} = q_{b,10\%} = 0.23 e^{-0.0066 D_R} q_{b\mathrm{L}} \tag{4.3}$$

where the limit unit base capacity $q_{b\mathrm{L}}$ ($= q_c$) can be expressed, based on rigorous cavity expansion analysis (Salgado and Randolph 2001, Salgado and Prezzi 2007), in terms of the fundamental soil variables as:

$$\frac{q_{b\mathrm{L}}}{p_A} = 1.64 e^{0.1041\phi_c + (0.0264 - 0.0002\phi_c)D_R} \left(\frac{\sigma_h'}{p_A}\right)^{0.841 - 0.0047 D_R} \tag{4.4}$$

where $\sigma_h' = K_0 \sigma_v'$ is the *in situ* effective horizontal stress and K_0 is the coefficient of earth pressure at rest. Equations (4.1)–(4.4) mechanistically relate the ultimate pile resistance to the fundamental soil variables and are based on rigorous analyses. They form the basis for what we will call the Purdue Sand Method for Nondisplacement Piles (PSM-NP).

For the calculations of $q_{b\mathrm{L}}$ and $q_{b,10\%}$, appropriate ϕ_c, D_R and σ_h' values must be used that are representatives of the zone below the pile base within

which the resistance to downward movement of the pile develops. At the limit condition (i.e., when the pile is about to plunge), a plastic zone forms immediately below the pile base. On the other hand, the zone of influence for the condition corresponding to 10% relative settlement is somewhat wider and deeper for sand because there has not been localization of strains due to plasticity. As far as we know, there has been no study that conclusively outlines the exact extent of the zone of influence below the pile base under either working or limit conditions. We considered it appropriate to use the values of ϕ_c, D_R and σ_h' corresponding to a depth of $B_b/2$ below the pile base (B_b = pile base diameter) for calculating q_{bL} and $q_{b,10\%}$. For the cases studied here, in which density is either constant or increases from the pile base down, this is conservative even in the event that a large influence depth would be in effect.

Equations (4.1)–(4.4) for calculating shaft and base capacities was based on the fact that these equations have been obtained from rigorous analyses that mechanistically relate the pile capacities to the fundamental soil variables; additionally, these equations have been compared against specific, high-quality experimental data. Such a fundamental approach automatically allows a systematic consideration of the uncertainties in the soil variables and in the design equations to calculate the uncertainties associated with the pile capacity.

4.3. Uncertainty Assessment of Design Variables and Model Uncertainty

4.3.1. Uncertainties in Soil Variables

The soil variables required for pile capacity calculations in this analysis are ϕ_c, D_R, K_0 and soil unit weight γ (required to calculate the in situ stresses). K_0 is difficult to estimate in the field, and not much information (e.g., PDF or COV) is available regarding its variability. However, if a deposit is known to be normally consolidated, for example, then K_0 falls within a relatively narrow range of roughly 0.4–0.5, depending on the relative density of the deposit. Accordingly, we assumed K_0 to be deterministic with its value in the 0.4–0.5 range and indirectly accounted for the variation of K_0 by performing analyses with three fixed (deterministic) values: K_0 = 0.4, 0.45 and 0.5. The remaining variables are treated probabilistically. This excludes overconsolidated deposits from the cases we have considered; however, because the equations for base and shaft resistance calculation work very similarly for both NC and OC sand, the resulting resistance factors should not differ much.

Based on experimental observations, Bolton (1986) reported a $\pm 1^\circ$ band encompassing all measurements of critical-state friction angle ϕ_c. Thus, the maximum error in the estimation of ϕ_c at a particular site is expected to be $\pm 1^\circ$. Assuming that ϕ_c follows a normal distribution (Foye 2005), the spread of 2° results in a standard deviation of 0.33° for ϕ_c. Because ϕ_c of different types of sand lie typically within the 28°–36° range (Salgado 2008), the maximum and minimum values of COV of ϕ_c that can be expected at a particular site are 0.33°/28° = 0.012 and 0.33°/36° = 0.009. Kim (2008) estimated the COV of ϕ_c to be in the 0.0081–0.0172 range based on the experimental studies by Verdugo and Ishihara (1996) and Negussey et al. (1987). In this study, we conservatively assume the COV of ϕ_c to be equal to 0.02, which is slightly greater than the maximum value reported in the literature. We also assume that ϕ_c follows a normal distribution.

The variability of soil unit weight has been studied by many researchers. Baecher and Christian (2003) reported, based on studies by Lee et al. (1983), Lacasse and Nadim (1996) and Lumb (1974), that the COV of unit weight does not exceed 0.1. Kim (2008) corroborates the finding based on studies by Phoon and Kulhawy (1999), White et al. (2005) and Hammit (1966). In our research, we assumed that γ follows a normal distribution with a COV = 0.1.

The estimation of relative density depends on the correct estimation of the *in situ* void ratio e, and the maximum and minimum void ratios $e_{\max}$ and $e_{\min}$. Baecher and Christian (2003) reported, based on a study by Phoon and Kulhawy (1999), that the COV of D_R varies between 0.1 and 0.4. However, such a wide variation seems unlikely for a particular site and may have resulted from clubbing of data applicable for a wide range of D_R (30%–70%). It is likely that the variability will be greater for lower values of D_R and will decrease as D_R increases. A more reliable and practical method of calculating D_R is from CPT results as proposed by Salgado (2008), which is a result of rigorous cavity expansion analysis (Salgado and Prezzi 2007):

$$D_R(\%) = \frac{\ln\left(\frac{q_c}{p_A}\right) - 0.4947 - 0.1041\phi_c - 0.841n\left(\frac{\sigma'_h}{p_A}\right)}{0.0264 - 0.0002\phi_c - 0.0047\ln\left(\frac{\sigma'_h}{p_A}\right)} = f(q_c, \phi_c, \sigma') \quad (4.5)$$

In this research, instead of treating D_R as a fundamental variable, we assume cone resistance q_c for a soil profile as the starting point, with the implication that CPT results are available for the site and calculate the PDF of D_R from the PDF of q_c and from the PDF of the relationship between q_c and D_R (i.e., the $q_c \rightarrow D_R$ model uncertainty) given by equation (4.5). According to FHWA (2001), the COV of q_c is 0.07. Foye (2005) found that the COV of q_c is 0.08 and that q_c follows a normal distribution. It is possible that both values overestimate the amount of uncertainty related strictly to the performance of a CPT and reflect some of the soil variability as well. In this research, we assumed that q_c follows a normal distribution with COV = 0.08. The model uncertainty associated with equation (4.5) is estimated following a procedure explained next.

If CPT results are not available but SPT results are, we can alternatively use the SPT results in the calculation of relative density using equation (4.6) based on the work by Meyerhof (1957) and Skempton (1986).

$$\frac{D_R}{100\%} = \sqrt{\frac{N_{60}}{A + BC(\sigma'_v/p_A)}} \tag{4.6}$$

where N_{60} is corrected (standard) SPT blow count, σ_v' is the *in situ* effective vertical stress, p_A is the reference stress (=100 kPa), A and B are correlation coefficients ($27 \leq A \leq 46$ and $B \approx 27$), and $C = (1 + 2K_0) / (1+2K_{0,NC})$. In this case, we assume standard SPT blow count N_{60} as the starting point and calculate the PDF of D_R from the PDF of N_{60} and from the model uncertainties of equation (4.6). According to Kulhawy and Trautmann (1996), the COV of N in sand ranges from 0.14 to 1.00 but indicated that it should be closer to the lower limit of this range. Akbas and Kulhawy (2009) reported that the COV of N_{60} can be calculated as between 0.23 and 0.56. Moreover, they assumed the probability distribution of N as lognormal. Spry et al. (1988) and Phoon and Kulhawy (1999) argue that most soil properties can be modeled as lognormal random variables, and doing so has the advantage that negative N values (which are indeed impossible) are not admissible in a lognormal distribution. In this research, we assumed that N_{60} follows a lognormal distribution with COV of 0.3 (for optimistic) and 0.5 (for pessimistic conditions).

4.3.2. Model Uncertainties

The model uncertainty in the $q_c \rightarrow D_R$ relationship was investigated by Foye (2005) using results of twenty-five well-controlled calibration chamber tests (Salgado 1993). Based on the study by Foye (2005), we estimated the mean of the normalized error of D_R [$W^* = (D_{R,\text{measured}} - D_{R,\text{calculated}})/D_{R,\text{calculated}}$] to be about -0.03 (i.e., $E(W^*) = -0.03$), which implies that D_R is over-predicted by 3% using equation (4.5). Thus, there is a bias present in equation (4.5), because of which the values of D_R to be used in the M-C calculations should be obtained by multiplying the nominal D_R values calculated from equation (4.5) by 0.97 (i.e., the bias factor $= M_{DR}^{\text{bias}} = 1 + E(W^*) = 0.97$). Foye (2005) calculated the standard deviation S_{DR} ($= S_Y$) of D_R to be equal to 10%, (i.e., 0.1 if relative density is expressed as a fraction) with q_c ($= X$) as a deterministic variable (i.e., $\sigma_f = S_f = 0$ was used in the calculations). When $S_f = 0$, S_M is equal to $S_{DR}/\left(M_{DR}^{\text{bias}} E(f_{DR})\right) = S_{DR}/0.97E(f_{DR})$. Foye (2005) also observed that the normalized error follows a normal distribution.

The incorporation of the $q_c \rightarrow D_R$ model error in the M-C simulations was done by introducing a bias factor M_{DR}^{bias} and a new random variable M_{DR} representing the $q_c \rightarrow D_R$ model uncertainty and by rewriting equation (4.5) as:

In the M-C simulations, M_{DR} is treated as a random variable that follows a normal distribution with a mean $E(M_{DR}) = 1.0$ and standard deviation $S_{MDR} = S_{DR}/0.97E(f_{DR}) = 10\%/0.97E(f_{DR})$ (or, $S_{MDR} = 0.1/0.97E(f_{DR})$ if relative density is expressed as a fraction).

When we use the SPT results to estimate the capacity of a pile, we should consider the model uncertainty related to the $N_{60} \rightarrow D_R$ relationship. Equation (4.6) already implies a level of uncertainty in the $N_{60} \rightarrow D_R$ relationship since the correlation coefficient A is expressed as a range. The upper and lower bound values of A are 27 and 46, respectively, with a range for A of 19. We can estimate the standard deviation for a variable that has upper and lower bound values and follows a normal distribution using the 6σ method (Withiam et al. 1997, Foye et al. 2006):

$$\sigma = \frac{\text{Range}}{6} \tag{4.8}$$

where σ is the standard deviation. In this study, we assumed that the mean value of A is 36.5, and, assuming that A follows a normal distribution, the standard deviation of A is 3.17, which is equal to the range divided by 6.0.

The model uncertainty associated with q_{sL} arises in the estimation of β through the use of equation (4.2). In order to estimate the uncertainty in equation (4.2), results of eight centrifuge tests by Fioravante (2002) and Colombi (2005) were used. The centrifuge tests were performed with a sand with $\phi_c = 32.3°$ for two relative densities ($D_R = 66\%$ and 90%) and with $K_0 = 0.45$. In order to compare the results from equation (4.2), which is valid for field conditions, with the centrifuge test results, the scale effects associated with the ratio of the pile diameter to the thickness of the shear band that forms around the shaft should be incorporated. Therefore, the finite element analysis of Loukidis and Salgado (2008) that was used to obtain equation (4.2) for field conditions was redone to simulate the conditions prevailing in the centrifuge tests, and an equation of K for the centrifuge-test conditions was developed following exactly the same procedure as was done for the case of equation (4.2):

$$K = 0.88K_0 e^{\frac{D_R}{100}\left[1.95 - 0.48\ln\left(\frac{\sigma'_v}{P_A}\right)\right]} \tag{4.9}$$

The above equation was used to estimate β for the centrifuge tests and the normalized error [$W^* = (\beta_{\text{measured}} - \beta_{\text{calculated}})/\beta_{\text{calculated}}$] between the measured and estimated β values was calculated. For the tests corresponding to $D_R = 66\%$, the mean of the normalized error, $E(W^*)$, was obtained as -0.08, while, for the tests corresponding to $D_R = 90\%$, the mean was 0.01. Thus, the model over-predicted β by 8% for $D_R = 66\%$ and under predicted β by 1% for $D_R = 90\%$. Because the bias was opposite for the two relative densities and because the data available from the centrifuge tests were limited, we decided that no model bias for β will be considered in our analysis (i.e., bias factor $= M_\beta^{\text{bias}} =$

1). The standard deviation of the normalized error S_{W*} for D_R = 66% and D_R = 90% were found to be 0.215 and 0.216, respectively. So, in order to incorporate the $q_{s\mathrm{L}}$-model uncertainty in our analysis, we introduce a new variable M_β that follows a normal distribution with expectation $E(M_\beta) = 1.0$ and standard deviation $S_{M\beta} = S_{W*}/M_\beta^{\mathrm{bias}} = 0.2$. The equation used to calculate $q_{s\mathrm{L}}$ in the Monte-Carlo simulations is:

$$q_{s\mathrm{L}} = M_\beta \frac{0.7K_0}{e^{0.2\sqrt{K_0-0.4}}} e^{\frac{D_R}{100}\left[1.3-0.2\ln\left(\frac{\sigma'_v}{p_A}\right)\right]} \sigma'_v \tan\phi_c \tag{4.10}$$

The model uncertainty associated with unit base resistance (equations (4.3) and (4.4)) was estimated from twenty one well-controlled "deep" plate load tests performed within a calibration chamber (Lee and Salgado 1999). The same procedure used earlier for calculating the normalized error was followed. However, before the estimation of the model uncertainty, we investigate whether the tests performed in the calibration chamber have any chamber boundary effect. Lee and Salgado (1999) simulated, using their finite element model, the pile base response for real field conditions and for calibration chamber test conditions. They assumed identical values of sand relative densities and stress states at the pile base for the field and the calibration chamber. They considered two extreme boundary conditions for the lateral walls of the calibration chamber: constant horizontal stress and zero horizontal displacement. The simulated field values of $q_{b,10\%}$ were greater than the corresponding simulated calibration chamber values by about 9% for the constant-horizontal-stress boundary condition of the calibration chamber, while an opposite result, with field values less than calibration chamber values by about 4%, was observed for the zero-horizontal-displacement boundary condition of the calibration chamber. We calculated the normalized error between the $q_{b,10\%}$ values simulated for the field ($q_{b,10\%,\mathrm{field}}$) and calibration chamber tests ($q_{b,10\%,\mathrm{plate}}$), and found that the mean and standard deviation of the normalized error $[(q_{b,10\%,\mathrm{field}} - q_{b,10\%,\mathrm{plate}})/q_{b,10\%,\mathrm{field}}]$, considering both constant horizontal stress and zero horizontal displacement conditions is 0.025 and 0.09. In the field, neither constant stress nor zero displacement conditions exist; rather, a condition between these two extremes prevails. Thus, the small overall bias of 2.5% will very likely not exist. Consequently, we considered it appropriate to neglect the boundary effects in our analysis.

The plate load tests in the calibration chamber were done for two relative densities: D_R = 50% and D_R = 90%. We found that, for D_R = 50%, the mean of the normalized error between measured and predicted unit base resistance $[W^* = (q_{b,10\%,\mathrm{measured}} - q_{b,10\%,\mathrm{calculated}})/q_{b,10\%,\mathrm{calculated}}]$ is −0.03 (i.e., $E(W^*) = -0.03$) while, for D_R = 90%, the mean $E(W^*)$ is 0.16. Thus, the model over-predicts $q_{b,10\%}$ by 3% for D_R = 50% and under predicts $q_{b,10\%}$ by 16% for D_R = 90%. Consequently, the calculated nominal $q_{b,10\%}$ values from equations (4.3) and (4.4) must be multiplied by 0.97 for D_R = 50% (i.e., bias factor = $M_{qb}^{\mathrm{bias}} = 1 + E(W^*) = 0.97$) and by 1.16 for D_R = 90% (i.e., bias factor = $M_{qb}^{\mathrm{bias}} = 1 + E(W^*) = 1.16$) before they are used in the M-C simulations. Since no reliable data were available for other values of D_R, we assumed a linear interpolation of the bias factor for values of D_R intermediate between 50% and 90%. Also, we assumed that the bias factor is equal to 0.97 for $D_R \leq 50\%$ and is equal to 1.16 for $D_R \geq 90\%$. The standard deviation of the normalized error S_{W*} was found to be equal to 0.15 and 0.08 for D_R = 50% and 90%, respectively. A large standard deviation of 0.15 occurred for D_R = 50% because, in the calibration chamber test, relative densities at these levels are not as reproducible or uniform as those for denser samples. Additionally, in the specific case of these tests, samples with D_R between 49.1% and 60.2% were grouped for the comparisons. For real field conditions, the standard deviation is expected to be less. This is corroborated by the standard deviation value 0.08 for the tests corresponding to D_R = 90%, which are known to be more uniform and are more reproducible (witnessed by test samples having relative densities that fall in the much narrower 90.6–92.8% range). Therefore, we assumed a standard deviation of 0.1 in our calculations.

In order to incorporate the model uncertainty of $q_{b,10\%}$ in calculations, we introduced a bias factor M_{qb}^{bias} in the equation of $q_{b,10\%}$ with M_{qb}^{bias} equal to 0.97 for $D_R \leq 50\%$, equal to 1.16 for $D_R \geq 90\%$ and equal to a linearly interpolated value between 0.97 and 1.16 for $50\% < D_R < 90\%$. We also introduced a new random variable M_{qb}, with $E(M_{qb}) = 1$ and S_{Mqb} equal to 0.1 based on the preceding discussion. M_{qb} is assumed to follow a normal distribution. The modified equation of $q_{b,10\%}$ used in the Monte-Carlo simulation is given by:

$$q_{b,10\%} = M_{qb}^{\mathrm{bias}} M_{qb} 0.38\, p_A e^{-0.0066D_R} e^{0.1041\phi_c + (0.0264-0.0002\phi_c)D_R} \left(\frac{\sigma'_h}{p_A}\right)^{0.841-0.0047D_R} \tag{4.11}$$

4.3.3. Uncertainties in Applied Loads

According to Ellingwood and Tekie (1999), dead load can be described by a normal distribution with a bias factor of 1.05 and COV equal to 0.1. According to Nowak (1994) and FHWA (2001), the bias factor and COV for dead load are in the range 1.03−1.05 and 0.08−0.1, respectively, depending on the type of structural components. In this analysis, we assumed, that dead load follows a normal distribution with a bias factor = 1.05 and COV = 0.1.

Live load is generally described using a lognormal distribution (Foye et al. 2006a). According to FHWA (2001), live load has a bias factor of 1.1–1.2 and a COV of 0.18. According to Ellingwood and Tekie (1999), however, live load is represented by a Type 1

distribution of largest values with a bias factor = 1.0 and COV = 0.25. We plotted the PDFs of the Type 1 extreme value distribution and the lognormal distribution for identical values of bias factor and COV, and found that the PDFs of both distributions are nearly identical for the range of live load values encountered in practice for piles. This finding is indirectly corroborated by Ghosn and Moses (1998), who separately calculated reliability indices for highway bridge structures with live loads following a lognormal distribution and a Type 1 extreme value distribution, and found that the results of both calculations were sufficiently close. Consequently, we decided to use the widely-used lognormal distribution to describe live loads. For most of the problems analyzed in this research, we conservatively chose a COV = 0.25 and the corresponding bias factor = 1.0, as recommended by Ellingwood and Tekie (1999). For a few selected problems, however, we performed analysis also for live load COV = 0.18 and bias factor = 1.15, as recommended by FHWA (2001), and compared the results.

4.3.4. Uncertainties in Pile Dimensions

Drilled shafts are constructed by removing soil from the ground by drilling and filling the resulting cylindrical void with concrete and reinforcement. The construction process is controlled; so the as-built diameter of the drilled shaft varies little. As far as we know, there is no systematic study available regarding the variability of the drilled shaft diameter. Based on experience and typical construction tolerances, we assume that the drilled shaft diameter B_p ($= B_s = B_b$) follows a normal distribution with a COV = 0.02.

Typically, drilling is done to refusal or to a minimal embedment into the bearing layer noticeable by a substantial change in drilling resistance. Thus, the lengths of drilled shafts do not vary considerably, and any variation that may occur, if still greater than the minimum length specified by the designer, results in lengths slightly greater than the design lengths. Therefore, in our analysis, we assume that the pile length L_p is deterministic (equal to the design length) because any additional length (due to variability in the depth to the bearing layer, for example) will work towards a conservative design.

4.4. Analysis

Monte-Carlo (M-C) simulations were performed to obtain the probability distributions of the capacity ($Q_{b,\mathrm{ult}} + Q_{s\mathrm{L}}$), the demand (DL + LL) and their difference. We assumed in our analysis that the capacity and the demand are statistically independent. We also assumed that all the random variables — soil properties, loads and the variables representing model uncertainties — are uncorrelated.

We start with a soil profile with known (or assumed) mean values of ϕ_c, γ and K_0 (K_0 is deterministic, so the mean value is the constant deterministic value) and with an assumed mean trend of CPT profile $q_c(z)$ or SPT profile $N_{60}(z)$, where z is the depth. We also assume a mean value of applied dead load $(\mathrm{DL})^{(\mathrm{mean})}$ and a (LL)/(DL) ratio (which gives the mean live load $(\mathrm{LL})^{(\mathrm{mean})}$). Then, we consider a drilled shaft with an assumed length and an assumed mean diameter embedded in the soil profile. With the mean soil profile, applied loads and pile dimensions established, we start the first run of the M-C simulations (Figure 4.1). We start with shaft capacity calculations at depth $z = 0$ m and move down along the pile shaft. First, a random value of q_c or N_{60} is generated for a particular depth along with random values of ϕ_c and γ. Then random values of M_{DR} in equation (4.7) or A in equation (4.6) is generated to calculate a random value of D_R. Subsequently, random realizations of M_β and D_R, are generated to calculate a random value of limit unit shaft resistance for that depth. This shaft capacity calculation is repeated for different depths along the pile shaft with new random values of q_c or N_{60} (typically, soil sub-layers of 1-m thickness with different mean q_c or N_{60} were assumed), D_R and the other variables. The calculated shaft capacities at the different depths are summed over the entire pile length to obtain the random value of the total shaft resistance $Q_{s\mathrm{L}}$. Then, as we reach the pile base, a random value of the base resistance $Q_{b,\mathrm{ult}}$ is calculated using the random values of soil variables at $z = L_p + B_p/2$, a random value of B_p, a random value of M_{qb} and the appropriate value of the bias factor M_{qb}^{bias}. Equations (4.10), (4.11) were used to obtain these random values of $Q_{b,\mathrm{ult}}$ and $Q_{s\mathrm{L}}$. After calculating the random $Q_{b,\mathrm{ult}}$ and $Q_{s\mathrm{L}}$, random values of (DL) and (LL) are generated and the difference $(Q_{b,\mathrm{ult}} + Q_{s\mathrm{L}}) - (\mathrm{DL} + \mathrm{LL})$ between the random values of capacity $\mathrm{C} = Q_{b,\mathrm{ult}} + Q_{s\mathrm{L}}$ and demand $\mathrm{D} = (\mathrm{DL} + \mathrm{LL})$ is calculated. The above set of calculations completes one run of the M-C simulations.

The above set of calculations (corresponding to one M-C run) was repeated n_{total} times; the value of n_{total} depends on the target probability of failure $p_{f,\mathrm{T}}$, as discussed later. We will call this repeated n_{total} number of calculations one set of M-C simulations. Each set of M-C simulations generated the probability distributions (or histograms) of the capacity and demand. The number of runs n_f for which $(Q_{b,\mathrm{ult}} + Q_{s\mathrm{L}}) - (\mathrm{DL} + \mathrm{LL})$ was less than zero (i.e., the number of times for which demand exceeded capacity) was noted. The ratio n_f / n_{total} approximates the probability of failure p_f. Theoretically, for a continuous probability distribution of C − D, the area under the PDF curve on the negative side of the C − D axis gives p_f.

If the calculated p_f does not fall in the range $p_{f,\mathrm{T}}$ $\pm 10\%$, DL and LL are adjusted until it does. After that, we locate the ultimate limit state values of the base and shaft capacities and dead and live loads corresponding to the Monte-Carlo run for which |C − D| is the minimum (or C−D ≈0). The nominal values of resistances and loads are calculated separately. Optimum factors of base and shaft resistances and

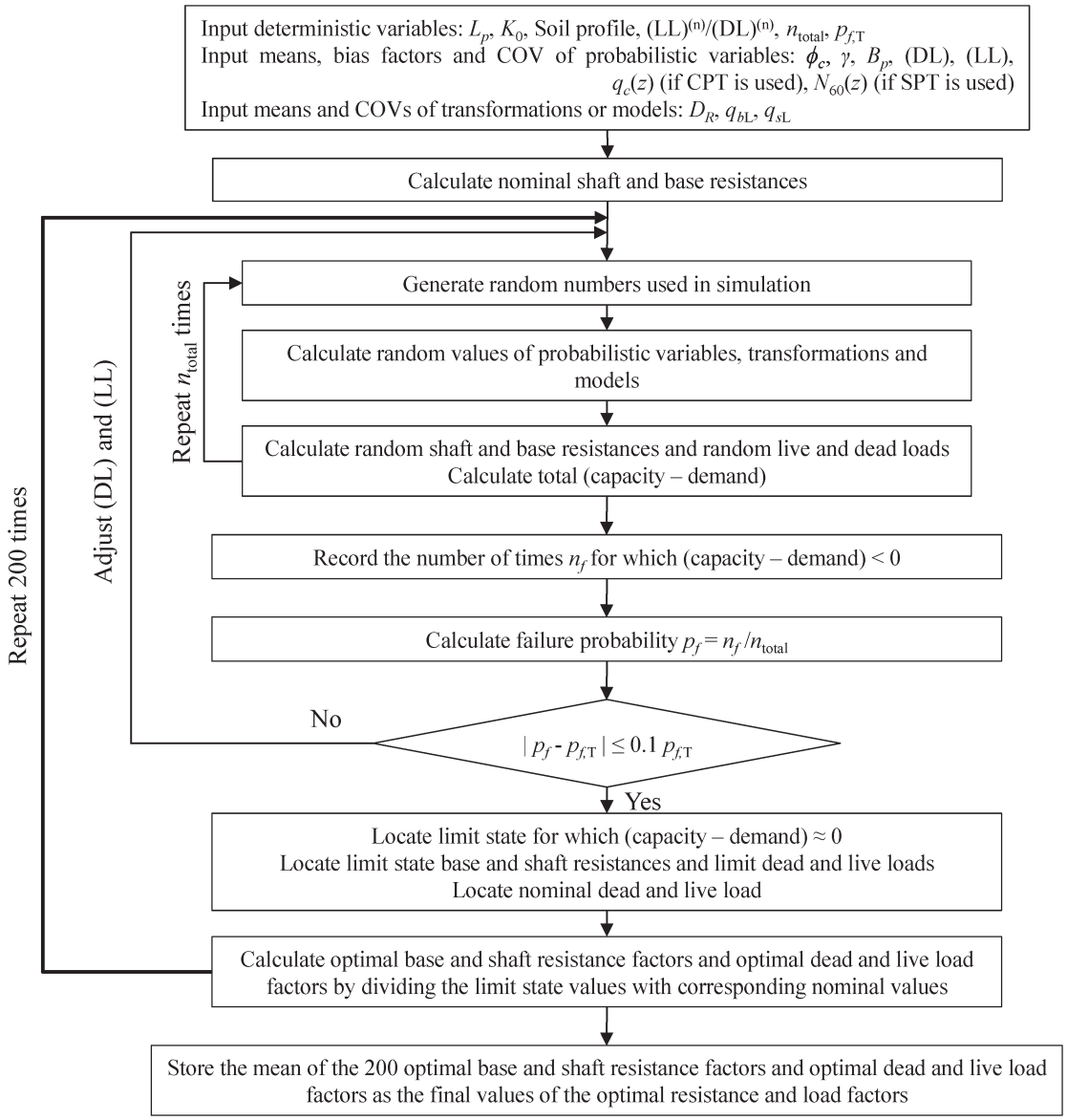

Figure 4.1 Flow chart of Monte-Carlo simulations

dead and live loads are calculated by dividing the ultimate limit state values by the corresponding nominal values.

As explained in Chapter 3, because of the non-uniqueness of the ultimate limit state, the calculations of optimum factors are repeated 200 times and their average values (means of the 200 optimal base and shaft resistance factors and dead and live load factors) are proposed as the final values of the optimal resistance and load factors.

4.5. Results

The primary goal of this research is to present resistance factors that can be used in design of drilled shafts in normally consolidated sand deposits. However, in addition to presenting the design resistance factors, we investigate how the optimal resistance and load factors change with different field conditions and variables. We consider a range of soil profiles, pile dimensions and live to dead load ratios that may occur in real field conditions.

The soil profiles (Figure 4.2) considered in this research consist of: (1) a homogeneous, completely dry[§] deposit of sandy soil with a mean relative density $D_{R,\text{mean}}$ = 70%; (2) the same homogeneous sand deposit described in (1) (i.e., with $D_{R,\text{mean}}$ = 70%) with a water table located at the ground surface; (3) a

[§]Soil above the water table is referred to as "dry". Soil is assumed to be dry for the purposes of calculating unit weights and effective stresses. As capillary rise in sand is limited to distances of the order of one meter and suction does not materially affect results, this assumption has negligible impact on the results.

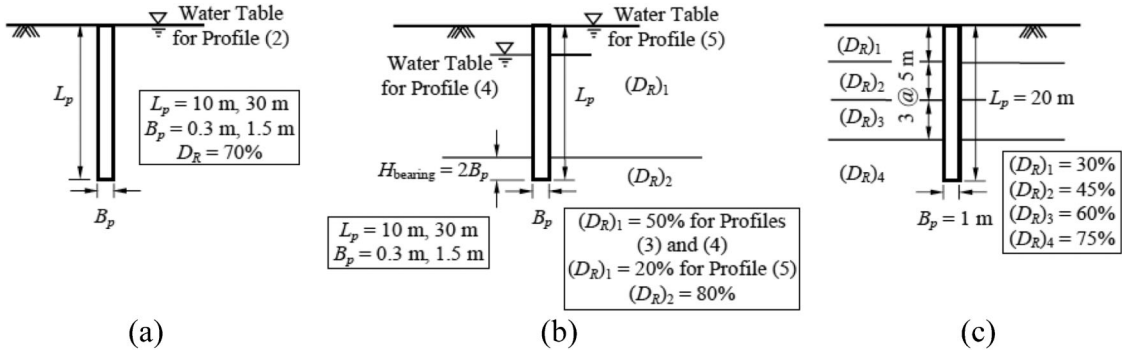

Figure 4.2 Details of soil profiles: (a) (1)–(2), (b) (3)–(5) and (c) (6)

completely dry sand deposit with a loose layer ($D_{R,\text{mean}}$ = 50%) overlying a strong bearing layer ($D_{R,\text{mean}}$ = 80%) that extends to great depth; (4) a two-layer system, as in (3) — with $D_{R,\text{mean}}$ = 50% for the top layer and $D_{R,\text{mean}}$ = 80% for the underlying layer — with a water table located at a depth of 2 m below the ground surface (the soil above the water table is assumed to be completely dry); (5) a two-layer system with the top layer consisting of extremely loose sand having $D_{R,\text{mean}}$ = 20% and the bearing layer consisting of dense sand having $D_{R,\text{mean}}$ = 80% and with a water table located at the ground surface; and (6) a four-layer, completely dry deposit consisting of a loose top layer with $D_{R,\text{mean}}$ = 30% spanning 0−5 m down from the ground surface, a second layer with $D_{R,\text{mean}}$ = 45% spanning 5−10 m below the ground surface, a third layer with $D_{R,\text{mean}}$ = 60% spanning 10−15 m below the ground surface and a bearing layer with $D_{R,\text{mean}}$ = 75% that lies below the third layer and extends down to great depth. The thicknesses of the soil layers in profiles (3)−(6) were assumed to be deterministic variables. In deciding the thicknesses of the top layers of the two-layer profiles (3), (4) and (5), we assumed that the depth of pile embedment H_{bearing} in the bearing layer is two times the mean pile diameter $B_{p,\text{mean}}$ (Figure 4.2). As will be discussed later, for analyses with CPT results, we considered soil profiles (1) through (6), whereas only soil profile (1) was assumed in the analyses starting from SPT results.

For these deposits, we considered three different sand types with mean critical-state friction angle $\phi_{c,\text{mean}}$ = 30°, 33° and 36° and, for each type, we assume three different values of K_0: 0.4, 0.45 and 0.5. The mean values of sand unit weight γ_{mean} [= $(G_s + Se_{\text{mean}}) / (1+e_{\text{mean}})$] ($G_s$ = specific gravity of sand solid particles = 2.62, S = degree of saturation) was calculated using the mean values of void ratio e_{mean}. The mean void ratio e_{mean} was obtained from the mean relative density $D_{R,\text{mean}}$ using the equation $e_{\text{mean}} = e_{\max} - (D_{R,\text{mean}} / 100)(e_{\max} - e_{\min})$ where $e_{\max}$ (=0.9) and $e_{\min}$ (= 0.45) are the maximum and minimum void ratios. Note that, in the Monte-Carlo analyses, mean q_c profiles $q_{c,\text{mean}}(z)$ (i.e., $q_{c,\text{mean}}$ versus depth curves) were given as inputs that produced the mean relative densities $D_{R,\text{mean}}$ mentioned in the previous paragraph using equation (4.7). The $q_{c,\text{mean}}(z)$ curves were initially back calculated from pre-assumed values of $D_{R,\text{mean}}$, γ_{mean}, $\phi_{c,\text{mean}}$ and K_0 using the inverse of equation (4.7), and then given as input to the Monte-Carlo analysis code.

The slenderness ratio (L_p/B_p), and diameter and length of drilled shafts that we considered in this research ranged from values that would be considered very low to values considered high for real field conditions. We studied the responses of four drilled shafts with (A) mean diameter $B_{p,\text{mean}}$ = 0.3 m and length L_p = 10 m, (B) $B_{p,\text{mean}}$ = 1.5 m and L_p = 10 m, (C) $B_{p,\text{mean}}$ = 0.3 m and L_p = 30 m and (D) $B_{p,\text{mean}}$ = 1.5 m and L_p = 30 m for the profiles (1)−(5). For profile (6), we considered a fifth drilled shaft E with $B_{p,\text{mean}}$ = 1.0 m and L_p = 20 m. For analyses for the CPT, we considered drilled shafts A to E, whereas for analyses for the SPT we considered drilled shaft A, B and additional drilled shafts with mean diameter $B_{p,\text{mean}}$ = 0.9 m and length L_p = 10 m.

The proportion of live and dead loads acting on a bridge structure depends on the span length (Hansell and Viest 1971). Titi et al. (2004) tabulated the (LL)/(DL) ratios recommended by AASHTO and FHWA for design of bridge structures; the recommended values vary over a wide range of 0.28−1.92. Accordingly, we considered (LL)/(DL) = 0.25, 1.0 and 2.0 in our analysis.

4.5.1. Results for CPT-Based Design

In this section, we describe how the optimal resistance and load factors change with different field conditions when the CPT is used in site investigation. Subsequently, we will compare the optimal resistance factors with the code-adjusted resistance factors. We also propose design values of code-adjusted resistance factors for use with CPT data as input.

In our study we found that the optimal load and resistance factors are independent of both ϕ_c and K_0 for all practical purposes. Figure 4.3 and Figure 4.4 show the plots of the resistance and load factors as functions of $\phi_{c,\text{mean}}$ and K_0, respectively, for a drilled shaft D installed in soil profile (1) with (LL)/(DL) = 0.25 and target $p_f = 10^{-3}$. The minor variations in the resistance and load factors observed in Figure 4.3 and Figure 4.4 were typical of all the other drilled shafts and soil profiles; the fluctuations were rather random without

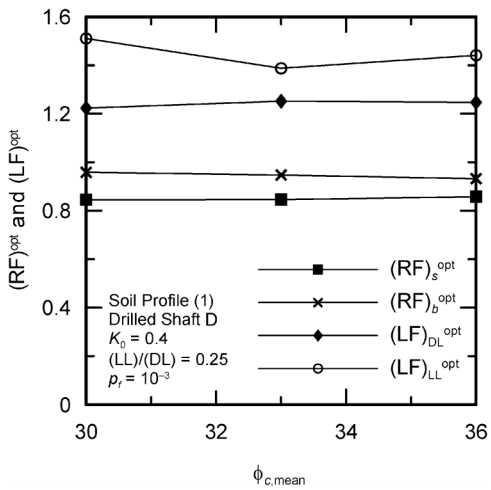

Figure 4.3 Optimal resistance and load factors versus critical state friction angle ϕ_c when $q_{c,\text{mean}}(z)$ is given as input

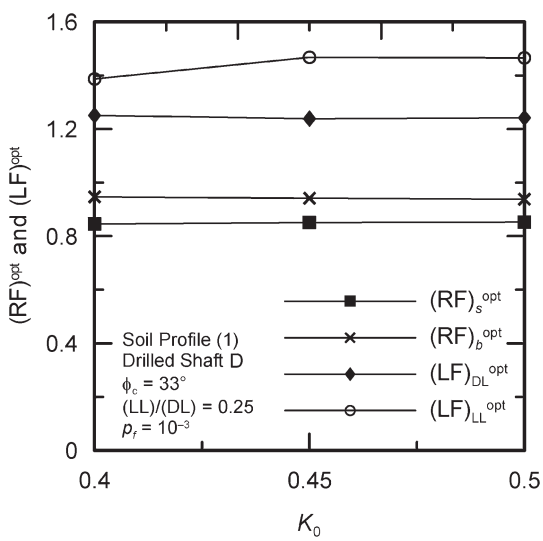

Figure 4.4 Optimal resistance and load factors versus coefficient K_0 of earth pressure at rest when $q_{c,\text{mean}}(z)$ is given as input

any particular trend. The presence of water table also affects the resistance and load factors only minimally. This is evident from a comparison of the results of soil profiles (1) and (2) and of (3) and (4) in Figure 4.5, in which the optimal resistance and load factors of drilled shaft B are plotted for the soil profiles (1) through (5) and for (LL)/(DL) = 1.0 and target $p_f = 10^{-3}$. Figure 4.5 clearly shows that the changes in the resistance and load factors are negligible from one soil profile to the other for all practical purposes. This invariance of the factors with soil profiles was also observed for the other drilled shafts and for other values of (LL)/(DL) and p_f. The invariance exists not only for soil profiles but also for pile dimensions as is evident from Figure 4.6, which shows the optimal resistance and load factors for drilled shafts A−D installed in soil profile (3) and for (LL)/(DL) = 1.0 and $p_f = 10^{-4}$. The trends observed in Figure 4.6, are

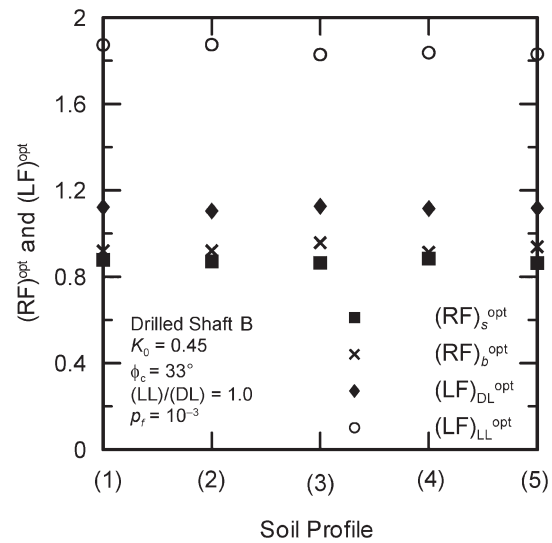

Figure 4.5 Optimal resistance and load factors for different soil profiles when $q_{c,\text{mean}}(z)$ is given as input

typical of all the other cases. This independence of the resulting factors from the soil profile is the main reason why we did not repeat all the analyses for the SPT, relying instead on the results for profile (1) to produce the required results.

Although soil properties and profiles and pile dimensions have practically no effect on the resistance and load factors, the (LL)/(DL) ratio has a non-negligible effect on the live load factor. As Figure 4.7 shows, the optimal resistance factors slightly increase and the optimal dead load factor slightly decreases with increase in (LL)/(DL) ratio; however, the increase in the optimal live load factor with increase in (LL)/(DL) ratio is significant. Figure 4.7 was plotted for drilled shaft D installed in soil profile (1) for different values of (LL)/

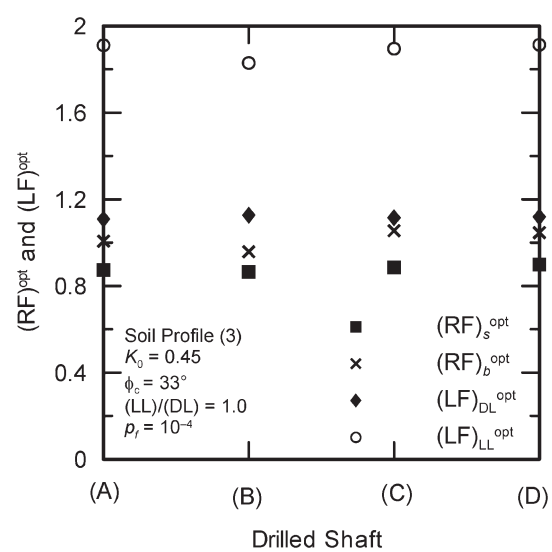

Figure 4.6 Optimal resistance and load factors for different drilled shaft dimensions when $q_{c,\text{mean}}(z)$ is given as input

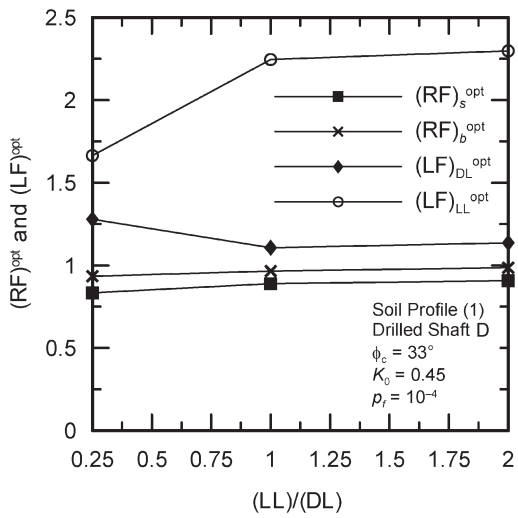

Figure 4.7 Optimal resistance and load factor versus live load to dead load ratio when $q_{c,\text{mean}}(z)$ is given as input

(DL) and $p_f = 10^{-4}$; the trend was consistent for all the other cases.

Figure 4.7 indicates indirectly that the LL/DL ratio affects the mean factor of safety $(\text{FS})_{\text{mean}}$ due to a significant change in the live load factor. This is corroborated by Figure 4.8(a), in which $(\text{FS})_{\text{mean}}$ for drilled shaft A installed in soil profile (3) is plotted against p_f for different values of (LL)/(DL). Figure 4.8(a) also shows that $(\text{FS})_{\text{mean}}$ increases with decreasing p_f. Also, the greater the (LL)/(DL) ratio, the higher the $(\text{FS})_{\text{mean}}$ is. This shows that $(\text{FS})_{\text{mean}}$ is not a true indicator of the reliability of a design; for the same mean factor of safety, the probabilities of failure are different for different proportions of applied live load. From another viewpoint, for the same probability of failure, a higher factor of safety is required to account for the higher uncertainty levels of live loads if (LL)/(DL) increases. The $(\text{FS})_{\text{mean}}$ plots are almost identical for all the different cases studied in this research.

The effect of target p_f on the optimal resistance and load factors are shown in Figure 4.8(b) for the same drilled shaft and soil profile of Figure 4.8(a) and for (LL)/(DL) = 1.0. It is evident, that the change in $(\text{FS})_{\text{mean}}$ due to change in p_f is strongly influenced by the live load. Similar trends were observed for the other drilled shafts and soil profiles. In order to study the effect of p_f, additional M-C simulations with target $p_f = 10^{-2}$ and 10^{-1} were done.

Since live load has the most effect on our reliability study, we considered it necessary to investigate how much change would occur in the values of resistance factors if, instead of our choice of live load COV = 0.25 and bias factor = 1.0 (Ellingwood and Tekie 1999), we use the live load COV = 0.18 and bias factor = 1.15 recommended by FHWA (2001). For this purpose, we ran M-C simulations for the different drilled shafts installed in soil profile (1). Figure 4.9(a) shows the optimal resistance and load factors for both sets of live load COV and bias factor plotted as a function of (LL)/(DL) ratio for drilled

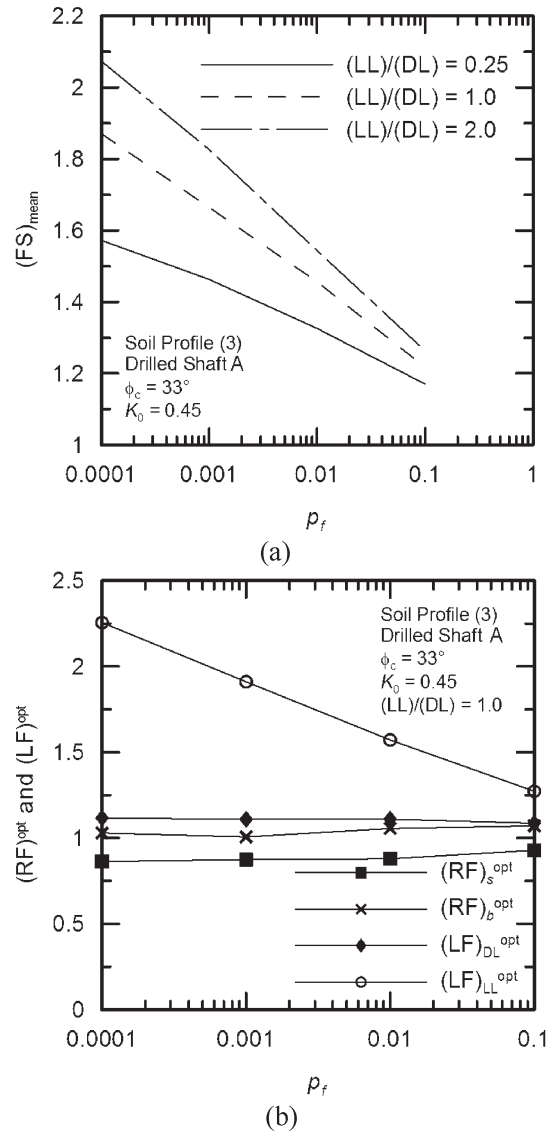

Figure 4.8. Effect of target probability of failure on resistance and load factors and on the corresponding mean factor of safety: (a) mean factor of safety and (b) optimal resistance and load factors versus target probability of failure when $q_{c,\text{mean}}(z)$ is given as input

shaft D and for $p_f = 10^{-4}$. Figure 4.9(b) shows the optimal and code-adjusted resistance factors for the same case. The figures, typical of all the drilled shafts, show that the resistance factors obtained by using both sets of live load COV and bias factor are nearly identical. The set by Ellingwood and Tekie (1999) produced slightly conservative code-adjusted resistance factors on the average; hence, we used this set in our calculations. Figure 4.9(b) also shows that the adjusted resistance factors do not vary much with (LL)/(DL) ratio. At the same time, we found that the adjusted factors, similarly to the optimal factors, do not change much across soil profiles or across drilled shafts.

Since the code-adjusted resistance factors do not vary significantly for the different drilled shafts, we con-

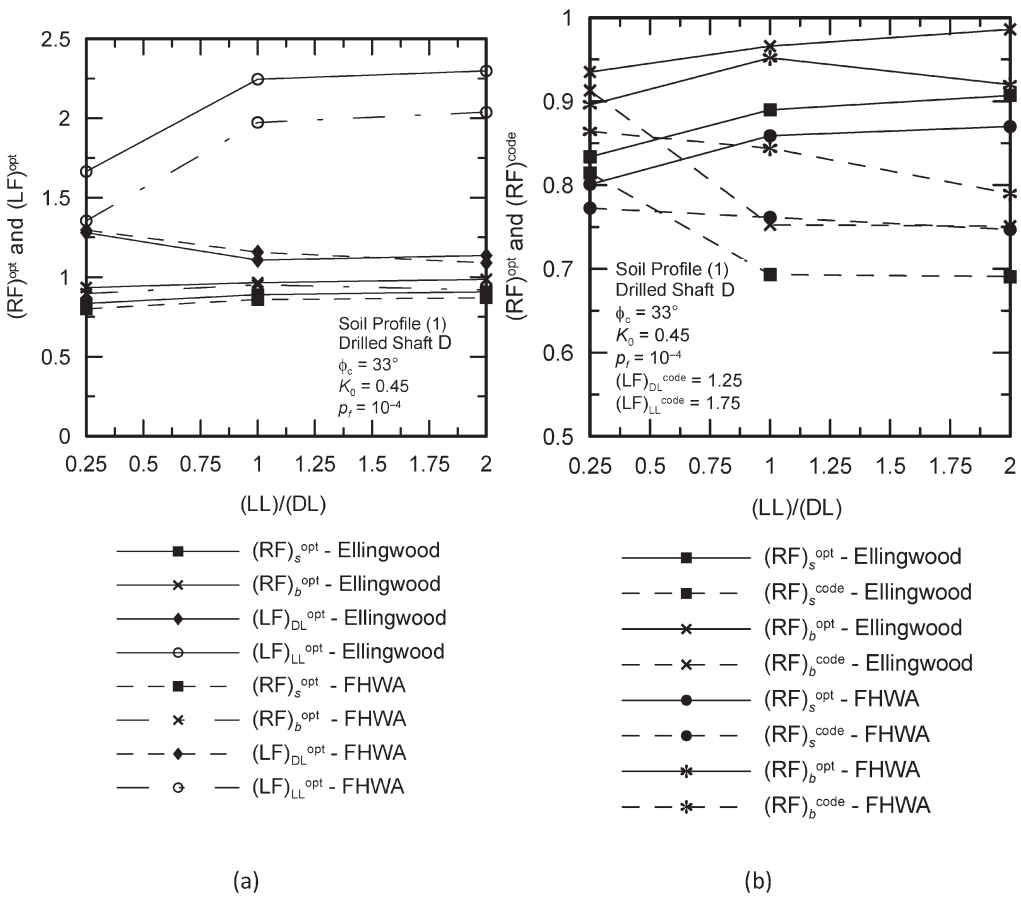

Figure 4.9 Plots of (a) optimal load and resistance factors and (b) code-adjusted resistance factors versus live load to dead load ratio when $q_{c,\text{mean}}(z)$ is given as input

solidate the results of the adjusted resistance factors over all the drilled shafts for a particular soil profile. We calculate the mean, standard deviation (SD), maximum and minimum of the resistance factors obtained for the different drilled shafts installed in a particular soil profile. We report these statistics for the different profiles in Table 4.1. We present the data separately for $p_f = 10^{-3}$ and 10^{-4}. Based on Table 4.1, we calculated the code-adjusted resistance factor with 99% confidence in order to produce reasonable and conservative resistance factors. The resulting values are: $(\text{RF})_b^{\text{code}} = 0.79$ and $(\text{RF})_s^{\text{code}} = 0.74$ for $p_f = 10^{-3}$ and $(\text{RF})_b^{\text{code}} = 0.63$ and $(\text{RF})_s^{\text{code}} = 0.57$ for $p_f = 10^{-4}$. Table 4.2 summarizes the PSM-NP design methodology; it contains the design equations, the different soil variables with their uncertainties and the resistance and load factors.

4.5.2. Results for SPT-Based Design

In this section, we describe how the optimal resistance and load factors change with different field conditions when the SPT is used in site investigation. Subsequently, we will compare the optimal resistance factors with the code-adjusted resistance factors. We also propose design values of code-adjusted resistance factors for use with SPT data as input.

Similarly to the analyses for the CPT, we found that the optimal load and resistance factors are independent of both ϕ_c and K_0 for all practical purposes when SPT results are used. Figure 4.10(a) and (b) show the plots of the resistance and load factors as functions of $\phi_{c,\text{mean}}$ for a drilled shaft A with (LL)/(DL) = 0.25 and target $p_f = 10^{-3}$ when COV(N_{60}) = 0.3 and COV(N_{60}) = 0.5, respectively. Figure 4.11 (a) and (b) show the plots of the resistance and load factors with respect to K_0 for a drilled shaft B with (LL)/(DL) = 2.0 and target $p_f = 10^{-3}$. The minor variations in the resistance and load factors observed in Figure 4.10 and Figure 4.11 were typical of all the other drilled shafts and soil profiles; the fluctuations were rather random without any particular trend. Figure 4.10 and Figure 4.11 show that the changes in the resistance and load factors are negligible from one soil profile to the other for all practical purposes.

Figure 4.12(a) and (b) shows the optimal resistance and load factors with respect to diameter to length ratio (B_p / L_p) when COV(N_{60}) = 0.3 and COV(N_{60}) = 0.5, respectively, for (LL)/(DL) = 2.0, $\phi_c = 30°$, $K_0 = 0.4$, and $p_f = 10^{-3}$. In the figures, the optimal shaft

TABLE 4.1

Resistance factors for different drilled shafts and adjusted with $(LF)_{DL}^{code} = 1.25$ and $(LF)_{LL}^{code} = 1.75$ when $q_{c,mean}(z)$ is given as input

Probability of Failure	Statistics	Soil Profile (1) $(RF)_b^{code}$	(1) $(RF)_s^{code}$	(2) $(RF)_b^{code}$	(2) $(RF)_s^{code}$	(3) $(RF)_b^{code}$	(3) $(RF)_s^{code}$	(4) $(RF)_b^{code}$	(4) $(RF)_s^{code}$	(5) $(RF)_b^{code}$	(5) $(RF)_s^{code}$	(6) $(RF)_b^{code}$	(6) $(RF)_s^{code}$
10^{-3}	Mean	0.928	0.816	0.924	0.813	0.950	0.823	0.948	0.823	0.939	0.827	0.917	0.833
	SD	0.054	0.025	0.057	0.026	0.051	0.024	0.061	0.024	0.052	0.026	0.038	0.040
	Maximum	1.017	0.859	1.051	0.867	1.069	0.872	1.073	0.866	1.043	0.873	0.954	0.879
	Minimum	0.853	0.771	0.847	0.772	0.869	0.789	0.861	0.786	0.880	0.798	0.878	0.805
10^{-4}	Mean	0.818	0.720	0.811	0.717	0.848	0.728	0.838	0.730	0.831	0.731	0.819	0.739
	SD	0.083	0.059	0.079	0.052	0.090	0.062	0.086	0.054	0.088	0.060	0.061	0.072
	Maximum	0.957	0.823	0.954	0.799	1.015	0.831	0.998	0.818	1.000	0.840	0.889	0.822
	Minimum	0.714	0.658	0.719	0.660	0.743	0.670	0.729	0.670	0.724	0.668	0.775	0.693

resistance factor and dead load factor are almost constant with respect to the relative depth, whereas the optimal base resistance factor and live load factor slightly decrease with increase of relative depth. However, for practical purposes, these variations can be considered negligible. The trends observed in Figure 4.12, are typical of all the other cases.

Although soil properties and profiles and pile dimensions have practically no effect on the resistance and load factors, the (LL)/(DL) ratio has a non-negligible effect on the live load factor. As Figure 4.13 (a) and (b) show, the optimal resistance factors slightly increase and the optimal dead load factor slightly decreases with increase in (LL)/(DL) ratio; however, the increase in the optimal live load factor with increase in (LL)/(DL) ratio is significant. This trend was consistent for all the other cases. Figure 4.13 (a) was plotted for drilled shaft A with respect to (LL)/(DL) when $p_f = 10^{-3}$; when COV(N_{60}) = 0.3, $\phi_c = 30°$, $K_0 = 0.4$, and $p_f = 10^{-3}$. Figure 4.13 (b) was plotted for drilled shaft B with respect to (LL)/(DL) when $p_f = 10^{-3}$; COV(N_{60}) = 0.5, $\phi_c = 30°$, $K_0 = 0.4$, and $p_f = 10^{-3}$.

Figure 4.13 indicates indirectly that (LL)/(DL) affects the mean factor of safety $(FS)_{mean}$ due to a significant change in the live load factor. This is corroborated by Figure 4.14 (a) in which $(FS)_{mean}$ for drilled shaft A is plotted against p_f for different values of (LL)/(DL) when COV(N_{60}) = 0.3, $\phi_c = 30°$, and $K_0 = 0.4$. Figure 4.14 (b), in which $(FS)_{mean}$ for drilled shaft B is plotted against p_f for different values of (LL)/(DL) when COV(N_{60}) = 0.5, $\phi_c = 30°$, and $K_0 = 0.4$, also shows the effect of (LL)/(DL) to the mean factor of safety due to a significant change in the live load factor. Figure 4.14 (a) and (b) also show that $(FS)_{mean}$ increases with decreasing p_f. Also, the greater the (LL)/(DL) ratio, the higher the $(FS)_{mean}$ is. This shows that $(FS)_{mean}$ is not a true indicator of the reliability of a design; for the same mean factor of safety, the probabilities of failure are different for different proportions of applied live load. From another viewpoint, for the same probability of failure, a higher factor of safety is required to account for the higher uncertainty levels of live loads if (LL)/(DL) increases. The $(FS)_{mean}$ plots are almost identical for all the different cases studied in this research.

The effect of target p_f on the optimal resistance and load factors are shown in Figure 4.15 (a) and (b) for the same conditions of Figure 4.14 (a) and (b), respectively. It is evident, that the change in $(FS)_{mean}$ due to change in p_f is strongly influenced by the live load. Similar trends were observed for the other drilled shafts and soil profiles. In order to study the effect of p_f, additional M-C simulations with target $p_f = 10^{-2}$ were done.

Figure 4.16(a) and (b) show the optimal and code-adjusted resistance factors for a drilled shaft A and a drilled shaft B, respectively when $p_f = 10^{-3}$ The code-adjusted resistance factors were obtained from the optimal resistance factors by using equation (3.10). For both drilled shafts, the code-adjusted resistance factors are slightly more conservative than the optimal

TABLE 4.2

Summary of Purdue Sand Method for NonDisplacement Piles: design equations, variable and model uncertainties, load and resistance factors

Quantity of Interest	Design Equation	Variables	Quantification	Remarks
Unit Shaft Resistance	q_{sL} $= M_\beta \frac{0.7K_0}{e^{0.2\sqrt{K_0-0.4}}} e^{\frac{D_R}{100}\left[1.3-0.2\ln\left(\frac{\sigma'_v}{p_A}\right)\right]} \tan\delta\sigma'_v$ Using during M-C Simulations	K_0	0.4–0.5	Deterministic
		Γ	COV = 0.1	$\Gamma = \Gamma_w\,(G_s + Se)\,/\,(1+e)$ $e = e_{\max} - (D_R\,/\,100)(e_{\max} - e_{\min})$
		D_R (%)	Through $q_c \rightarrow D_R$ Model Uncertainty Variable M_{DR}: $E(M_{DR}) = 0.97$, $S_{MDR} = S_{DR}\,/\,E(f_{DR}) = 10\%\,/\,E(f_{DR})$; q_c: COV = 0.08; ϕ_c: COV = 0.02.	$D_R(\%) = \frac{\ln\left(\frac{q_c}{p_A}\right) - 0.4947 - 0.1041\phi_c - 0.841n\left(\frac{\sigma'_h}{p_A}\right)}{0.0264 - 0.0002\phi_c - 0.0047\ln\left(\frac{\sigma'_h}{p_A}\right)}$
Unit Base Resistance	$q_{b,10\%}$ $= 0.38 p_A e^{-0.0066D_R} e^{0.1041\phi_c + (0.0264-0.0002\phi_c)D_R} \left(\frac{\sigma'_h}{p_A}\right)^{0.841-0.0047D_R}$ Using during M-C Simulations	M_β	$E(M_\beta) = 1.0$, $S_{M\beta} = 0.2$	q_{sL} - Model Uncertainty Variable
		K_0	See Above	—
		Γ	See Above	—
		D_R (%)	See Above	—
		ϕ_c	COV = 0.02	Typical Range: 30°–36°
		M_{qb}	$E(M_{qb}) = 0.97$ for $D_R \leq 50\%$ $E(M_{qb}) = 1.16$ for $D_R \geq 90\%$ $E(M_{qb})$ = linearly interpolated value between 0.97 and 1.16 for $50\% < D_R < 90\%$; $S_{Mqb} = 0.1$	$q_{b,10\%}$ - Model Uncertainty Variable
Shaft and Base Resistances	$Q^{(n)}_{b,\text{ult}} = q_{b,\text{ult}} A_b$ $Q^{(n)}_{sL} = \sum_i q_{sL,i} A_{s,i}$	B_p	COV = 0.02	Pile Diameter: $A_b = \pi B_p^2\,/\,4$ $A_{s,i} = \pi B_p H_i$ H_i = thickness of ith layer
LRFD	$(RF)_b Q^{(n)}_{b,\text{ult}} + (RF)_s Q^{(n)}_{sL} = (LF)_{DL}(DL)^{(n)} + (LF)_{LL}(LL)^{(n)}$	$(RF)_b$	0.85 for $p_f = 10^{-3}$ 0.70 for $p_f = 10^{-3}$	Calculated from Present Study
		$(RF)_s$	0.75 for $p_f = 10^{-3}$ 0.65 for $p_f = 10^{-3}$	Calculated from Present Study
		$(LF)_{DL}$	1.25	AASHTO (2007) Recommended
		$(LF)_{LL}$	1.75	AASHTO (2007) Recommended

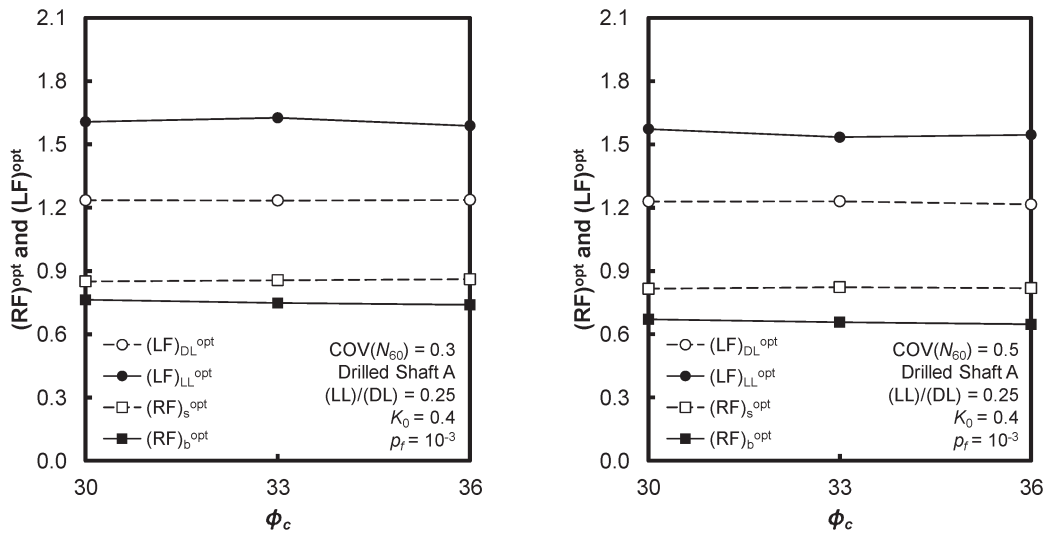

(a) (b)

Figure 4.10 Optimal resistance and load factors versus critical state friction angle ϕ_c for drilled shaft A and (a) COV(N_{60}) = 0.3 and (b) COV(N_{60}) = 0.5 when $N_{60,\text{mean}}(z)$ is given as input

resistance factors. Moreover, the code-adjusted resistance factors do not vary as much as the optimal resistance factors with (LL)/(DL) ratio.

Since the code-adjusted resistance factors do not vary significantly for the different drilled shafts, we consolidate the results of the adjusted resistance factors over all the drilled shafts for a particular soil profile. We calculate the mean, standard deviation (SD), maximum and minimum of the resistance factors obtained for the different drilled shafts installed in a particular soil profile. We report these statistics for the different profiles in Table 4.3. We present the data separately for $p_f = 10^{-3}$ and 10^{-4}. Based on Table 4.3, we calculated the code-adjusted resistance factor with 99% confidence to suggest reasonable and conservative resistance factors: $(\text{RF})_b^{\text{code}} = 0.45$ and $(\text{RF})_s^{\text{code}} = 0.59$ for $p_f = 10^{-3}$ and $(\text{RF})_b^{\text{code}} = 0.37$ and $(\text{RF})_s^{\text{code}} = 0.52$ for $p_f = 10^{-4}$ when COV(N_{60}) = 0.3; $(\text{RF})_b^{\text{code}} = 0.38$ and $(\text{RF})_s^{\text{code}} = 0.58$ for $p_f = 10^{-3}$ and $(\text{RF})_b^{\text{code}} = 0.33$ and $(\text{RF})_s^{\text{code}} = 0.49$ for $p_f = 10^{-4}$ when COV(N_{60}) = 0.5

4.6. Conclusions

We performed a systematic probabilistic analysis to develop the resistance factors for drilled shafts in normally consolidated sand for a soil variable-based

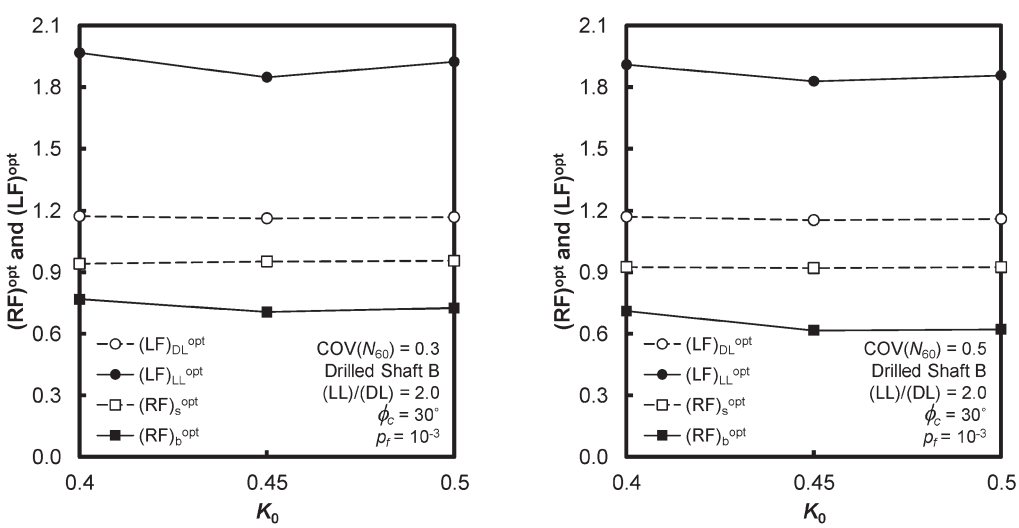

(a) (b)

Figure 4.11 Optimal resistance and load factors versus coefficient K_0 of earth pressure at rest for drilled shaft B and (a) COV(N_{60}) = 0.3 and (b) COV(N_{60}) = 0.5 when $N_{60,\text{mean}}(z)$ is given as input

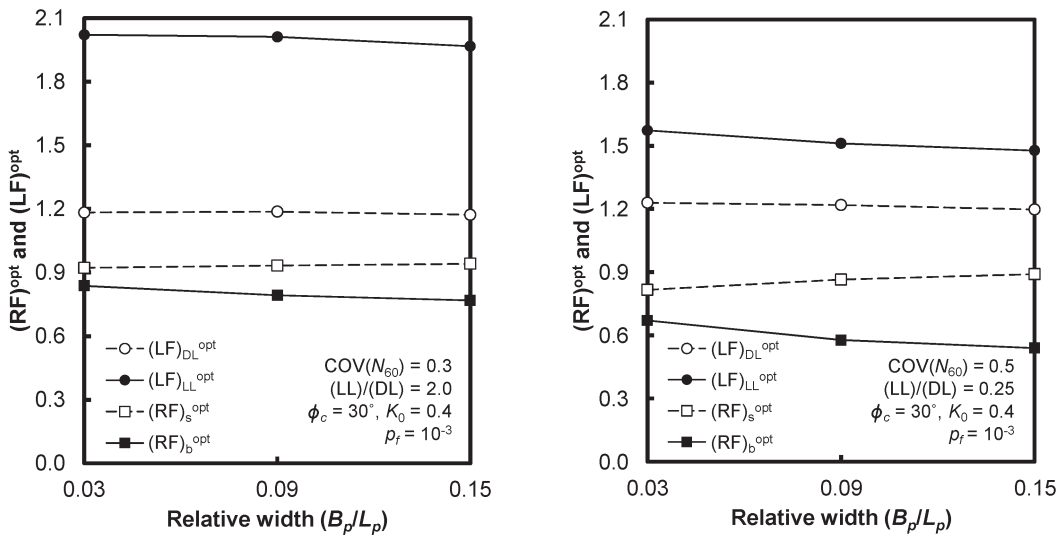

(a) (b)

Figure 4.12 Optimal load and resistance factors versus diameter to length ratio for (a) LL/DL = 2.0 and (b) LL/DL = 0.25 when $N_{60,\text{mean}}(z)$ is given as input

design method. The analysis involved identification of a robust design method, the Purdue Sand method for Nondisplacement Piles, quantification of the uncertainties (probability distributions) associated with the design variables and the design equations and subsequent performance of Monte-Carlo simulations to generate the probability distributions of the pile capacities and applied loads. The limit state loads and shaft and base capacities can be identified from these distributions based on a target probability of failure. From the calculated limit state and nominal values of shaft and base capacities and dead and live loads, the optimal resistance and load factors are obtained. The optimal resistance factors are then adjusted to make them compatible with the dead and live load factors recommended by AASHTO (2007).

In the course of the study, performed for six different soil profiles with different soil properties and for five different dimensions of drilled shafts, we found that the resistance and load factors did not vary to any significant extent between the different soil profiles and drilled shafts considered. The ratio of live to dead load was identified as the only variable that affected the results; however, it affected mostly the live load factor, with minimal effect on the resistance and dead load factors. The mean factor of safety was found,

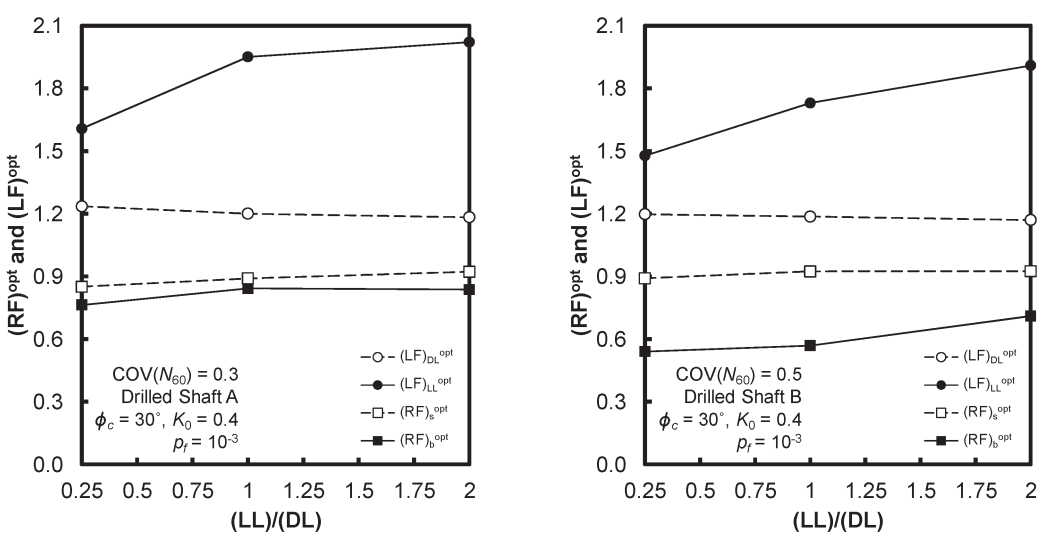

(a) (b)

Figure 4.13 Optimal resistance and load factor versus live load to dead load ratio for (a) drilled shaft A and (b) drilled shaft B when $N_{60,\text{mean}}(z)$ is given as input

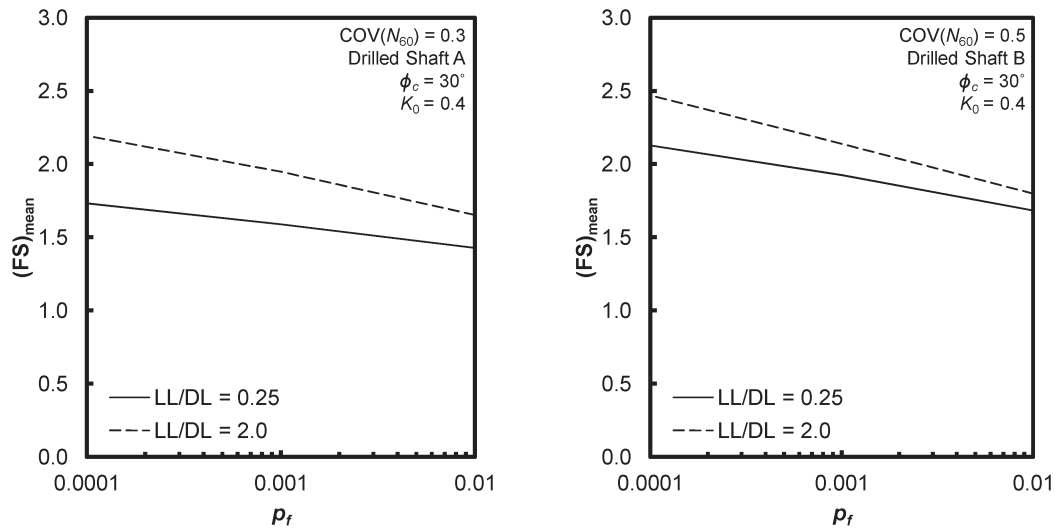

(a) (b)

Figure 4.14 Mean factor of safety versus target probability of failure for (a) drilled shaft A and (b) drilled shaft B when $N_{60,mean}(z)$ is given as input.

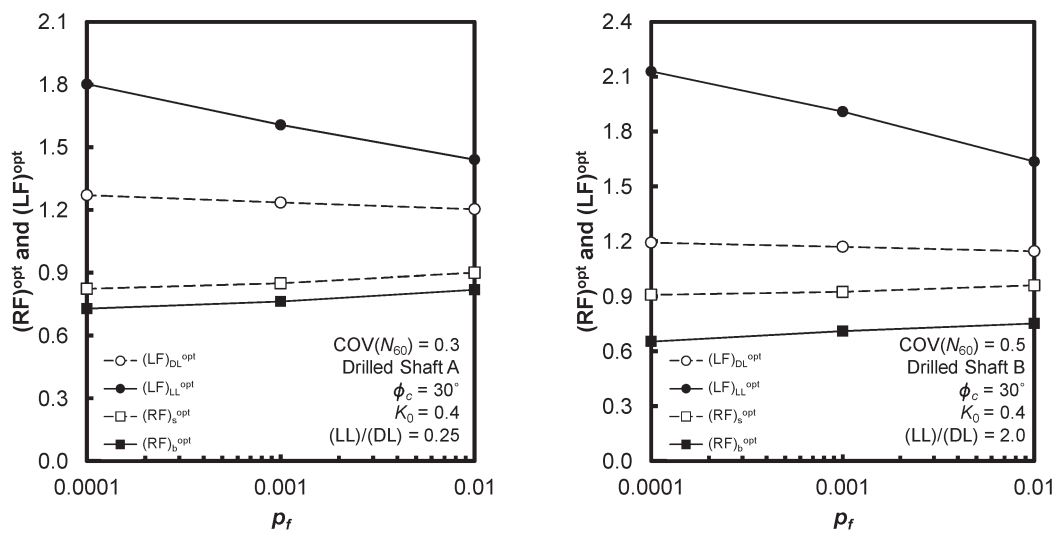

(a) (b)

Figure 4.15 Optimal resistance and load factors versus target probability of failure for (a) drilled shaft A and (b) drilled shaft B = 0.5 when $N_{60,mean}(z)$ is given as input

TABLE 4.3
Resistance factors for different drilled shafts and adjusted with $(LF)_{DL}^{code} = 1.25$ and $(LF)_{LL}^{code} = 1.75$ when $N_{60,mean}(z)$ is given as input

Probability of failure	Statistics	COV(N_{60}) = 0.3				COV(N_{60}) = 0.5			
		B_p / L_p = 0.3		B_p / L_p = 1.5		B_p / L_p = 0.3		B_p / L_p = 1.5	
		$(RF)_b^{code}$		$(RF)_b^{code}$		$(RF)_b^{code}$		$(RF)_b^{code}$	
10^{-3}	Mean	0.721	0.808	0.651	0.888	0.641	0.791	0.576	0.873
	SD	0.120	0.083	0.073	0.123	0.114	0.081	0.076	0.117
	Maximum	1.187	1.081	0.936	1.360	1.148	1.010	0.855	1.256
	Minimum	0.433	0.530	0.429	0.528	0.356	0.503	0.316	0.543
10^{-4}	Mean	0.645	0.725	0.588	0.806	0.559	0.697	0.508	0.794
	SD	0.109	0.079	0.062	0.117	0.103	0.081	0.063	0.113
	Maximum	1.000	0.911	0.774	1.208	0.914	0.895	0.704	1.137
	Minimum	0.393	0.500	0.402	0.501	0.324	0.510	0.334	0.497

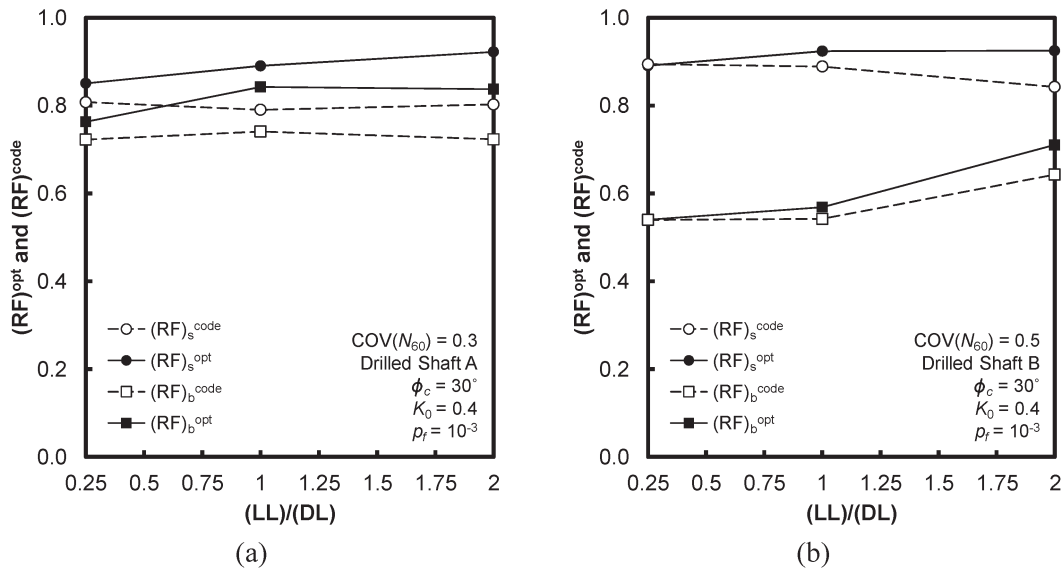

Figure 4.16 Optimal and code-adjusted resistance factors versus live load to dead load ratio for (a) drilled shaft A and (b) drilled shaft B when $N_{60,\text{mean}}(z)$ is given as input

reasonably, to increase with decreasing target probability of failure. The change in the mean factor of safety with the target probability of failure was a function of the live load to dead load ratio.

Based on our results, we recommended base and shaft resistance factors that can be used in design with the dead load and live load factors of 1.25 and 1.75 recommended by AASHTO (2007). When the CPT is used in the site investigation, the recommended base and shaft resistance values are 0.79 and 0.73 for a probability of failure of 10^{-3} and 0.63 and 0.57 for a probability of failure of 10^{-4}. These could be rounded to 0.80 and 0.75 and 0.65 and 0.60. When the SPT is used in site investigation, the recommended base and shaft resistance values are 0.45 and 0.59 for a probability of failure of 10^{-3} and 0.37 and 0.52 for a probability of failure of 10^{-4} considering COV of N_{60} as 0.3. These could be rounded to 0.45 and 0.60 and 0.35 and 0.50. In case of COV(N_{60}) = 0.5, the recommended base and shaft resistance values are 0.38 and 0.58 for a probability of failure of 10^{-3} and 0.33 and 0.49 for a probability of failure of 10^{-4}. These could be rounded to 0.40 and 0.60 and 0.35 and 0.50.

CHAPTER 5. RESISTANCE FACTORS FOR DRILLED SHAFT IN CLAY

5.1. Introduction

In this chapter, we develop the resistance factors for drilled shafts in clay for a soil variable-based design method. We first discuss the calculation of the limit unit base and shaft resistance in clay. Systematic probabilistic analyses are then performed with the uncertainties (probability density functions) associated with each of the soil variables appearing in the design equations carefully quantified. The analyses rely on Monte-Carlo (M-C) simulations and a target acceptable risk (i.e., target probability of failure) to identify the corresponding most probable limit state (at which the resistance equals imposed loads with probability equal to the probability of failure). The load and resistance factors are obtained by dividing the limit state values of loads and resistances by the corresponding nominal values.

5.2. Unit Base and Shaft Resistance: Purdue Clay Method for Nondisplacement Piles

To calculate the unit shaft resistance q_{sL} in clay, we used the α method, according to which:

$$q_{sL} = \alpha s_u \tag{5.1}$$

where s_u is the undrained shear strength. To determine α, Chakraborty et al. (2011) performed finite element analyses coupled with an advanced constitutive model to investigate the mechanics of load transfer at the interface of drilled shaft in clays. Based on their analysis, Chakraborty et al. (2011) proposed the following equation for α:

$$\alpha = \left(\frac{s_u}{\sigma_v'}\right)^{-0.05} \left[A_1 + (1 - A_1)\exp\left\{-\left(\frac{\sigma_v'}{p_A}\right)\left(\phi_c - \phi_{r,\min}\right)^{A_2}\right\}\right] \tag{5.2}$$

where σ_v' is the *in situ* vertical effective stress at the depth at which q_{sL} is calculated; ϕ_c is the critical-state friction angle; $\phi_{r,\min}$ is the minimum residual friction angle of the clay; p_A is the reference stress value (100*k*Pa); A_1 is a coefficient equal to 0.4 for $\phi_c - \phi_{r,\min} \geq 12$ degrees, 0.75 for $\phi_c - \phi_{r,\min} \leq 5$ degrees and a linearly interpolated value between 0.4 and 0.75 for 5

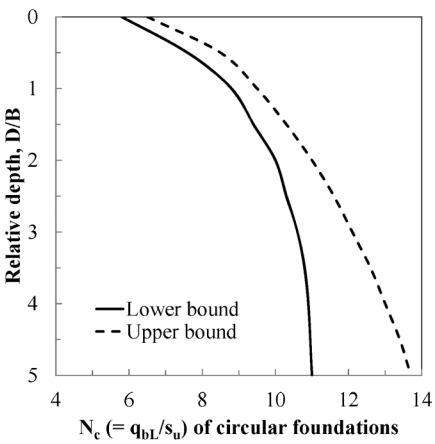

Figure 5.1 Limit unit base resistance of circular foundation versus depth (Salgado et al. 2004)

degrees $\leq \phi_c - \phi_{r,\min} \leq 12$ degrees; and A_2 is a coefficient determined by equation $A_2 = 0.4 + 0.3 \ln (s_u / \sigma_v')$. The above equation captures the dependence of shaft resistance on the undrained shear strength, effective normal stress and the difference between critical-state friction angle and minimum residual-state friction angle.

Salgado et al. (2004) used finite element limit analysis to investigate the upper and lower bound of the ratio of net bearing capacity q_{bL}^{net}, defined as

$$q_{bL}^{\text{net}} = q_{bL} - q_0 \tag{5.3}$$

where q_0 is the surcharge at the pile base level, to undrained shear strength s_u for piles. Based on their analysis, Salgado et al. (2004) found that the lower and upper bound values of N_c $\left(= q_{bL}^{\text{net}} / s_u\right)$ increase with increasing relative depth D/B (the ratio of the length of the pile to the width of the pile), as Figure 5.1 shows. For $D/B = 5$, the lower and upper bound values of N_c are 11.0 and 13.7, respectively.

By substituting N_c into equation (5.3), the equation of the limit unit base resistance is:

$$q_{bL} = N_c s_u + q_0 \tag{5.4}$$

Equations (5.1)–(5.4) constitute the basis for the Purdue Clay Method for Nondisplacement Piles (PCM-NP).

5.3. Uncertainty Assessment of Design Variables and Model Uncertainty

5.3.1. Uncertainties in Soil Variables

The soil variables required for pile capacity calculations in this analysis are ϕ_c, $\phi_{r,\min}$, s_u and soil unit weight γ (required to calculate the in situ stresses). Based on experimental observations, Bolton (1986) reported a $\pm 1^\circ$ band encompassing all measurements of the critical-state friction angle ϕ_c for sand. It is reasonable to assume that this forms an upper bound to the variability for clay. Thus, the expectation of the maximum error in the estimation of ϕ_c at a particular site is $\pm 1^\circ$. Assuming that ϕ_c follows a normal distribution, the spread of 2° results in a standard deviation of 0.33° for ϕ_c based on the 6σ method (Foye 2005). Because ϕ_c of different clays typically lie within the 15°–30° range (Salgado 2008), the maximum and minimum values of COV of ϕ_c are 0.33°/15° = 0.022 and 0.33°/30° = 0.011 at a particular site. In this study, we conservatively assume the COV of ϕ_c to be equal to 0.03, which is greater than the maximum value of 0.022 estimated in this manner.

We also assume that the maximum error in the estimation of $\phi_{r,\min}$ is $\pm 1^\circ$. For a clay such as Boston Blue Clay, there is no softening towards lower, residual values of friction angle, so $\phi_{r,\min}$ is equal to ϕ_c and is therefore within the 15°–30° range, which is a typical range of ϕ_c in clay. For a clay such as London Clay, however, $\phi_{r,\min}$ is within the 7.5°–9.4° range of much lower friction angles (Bishop et al. 1971). From these previous studies, we assume for the purpose of estimating the COV of $\phi_{r,\min}$ that the minimum value of $\phi_{r,\min}$ is 7.5°. Assuming that $\phi_{r,\min}$ follows a normal distribution with a standard deviation of 0.33°, the maximum COV of $\phi_{r,\min}$ is 0.33°/7.5° = 0.044. In this study, we conservatively assume the COV of $\phi_{r,\min}$ to be equal to 0.05, which is greater than the maximum value of 0.044 that we calculated.

Many researchers have studied the variability of soil unit weight. Baecher and Christian (2003) reported, based on studies by Lee et al. (1983), Lacasse and Nadim (1996) and Lumb (1974), that the COV of unit weight does not exceed 0.1. Kim (2008) corroborates the finding based on studies by Phoon and Kulhawy (1999), White et al. (2005) and Hammit (1966). In our research, we assumed that γ follows a normal distribution with a COV = 0.1.

Equations (5.1), (5.2) and (5.4) show that the limit unit base and shaft resistances are functions of undrained shear strength s_u. The equation for s_u in terms of cone resistance is:

$$s_u = \frac{q_c - \sigma_v}{N_k} \tag{5.5}$$

where q_c is cone resistance, σ_v is vertical stress and N_k is the cone factor. The minimum value of N_k is 11.0 and the maximum value of N_k is 13.7 (Salgado et al. 2004). In this research, we assume cone resistance q_c for a soil profile as the starting point in design and calculate the PDF of undrained shear strength s_u from the PDF of q_c and from the PDF of the relationship between q_c and s_u given by equation (5.5). According to Foye (2006), the COV of q_c in clay is 0.06 and q_c follows a normal distribution. In this study, we worked with COV = 0.06.

An alternative way to estimate the undrained shear strength s_u of clay, commonly used by some DOTs, is the unconfined compression (UC) test. Based on experimental observations, Fredlund and Dahlman (1971) reported that the COV of s_u from UC tests lie within the 0.40 to 0.50 range. This range is 0.27 to 0.41

according to Ladd, et al. (1971)(based on data for soft Bangkok clay), 0.11 to 0.45 according to Wolff (1985). and 0.30 to 0.40 according to Shannon and Wilson Inc. and Wolff (1994). Based on these studies, the COV of s_u from UC tests lies in the 0.11 to 0.50 range. In this study, we conservatively assumed the COV of s_u from UC tests to be 0.45. According to the studies by Spry et al. (1988) and Phoon and Kulhawy (1999), a lognormal distribution can be assumed for most soil properties. Using a lognormal distribution for s_u from UC test prevents random realizations of s_u from being negative, which would happen if a normal distribution with a high COV were assumed for possibly low to moderate values of nominal s_u. For these reasons, we assume the undrained shear strength s_u from UC test following lognormal distribution.

5.3.2. Model Uncertainties

If the input data are values of cone resistance q_c, the uncertainties in the $q_c \rightarrow s_u$ relationship must be considered. Equation (5.5) already implies the level of uncertainty in the $q_c \rightarrow s_u$ relationship since the cone factor N_k is expressed as a range. The upper and lower bound values of N_k are 13.7 and 11.0, respectively, with a range for N_k of 2.7. We can estimate the standard deviation for a variable that has upper and lower bound values and follows a normal distribution using the 6σ method (Withiam et al. 1997, Foye et al. 2006):

$$\sigma = \frac{\text{Range}}{6} \tag{5.6}$$

where σ is the standard deviation. In this study, we assumed that the mean value of N_k is 12.35, and, assuming that N_k follows normal distribution, the standard deviation of N_k is 0.45, which is equal to the range divided by 6.0.

The relationship $s_u \rightarrow q_{bL}$ for a pile is similar physically to the $s_u \rightarrow q_c$ relationship. If the dimensions of the pile are given, we can obtain the lower and upper bound values of N_c from Figure 5.1. We assumed that the mean value of N_c is equal to the mean value of the lower and upper bound values. The range of N_c is the difference between the lower and upper bound value and we calculated the standard deviation of N_c based on the 6σ method from this range by assuming that N_c follows normal distribution. Typically, the relative depth of a pile is much greater than 5.0, so the maximum and minimum values of N_c are taken as 13.7 and 11.0. From this range, it is reasonable to set the mean and the standard deviation of N_c as 12.35 and 0.45, respectively. The tacit assumption here is that the ultimate load for a pile will be taken as equal to q_{bL}, which is a reasonable assumption for piles in normally to lightly overconsolidated soils, but overestimates $q_{b,ult}$ for piles in stiff clay.

The model uncertainty associated with q_{sL} arises in the estimation of α through the use of equation (5.2). Equation (5.2) follows from rigorous finite element analyses, which themselves introduce essentially no error in the results. To the extent that (5.2) is a fit to the results of those analyses, there is an error. To estimate the uncertainty in equation (5.2), we used the elemental simulations based on the two surface plasticity model for clay proposed by Basu et al. (2009) of rate-independent, K_0-consolidated, undrained triaxial compression tests and direct simple shear tests.

In equation (5.1), α is the ratio of the limit shaft resistance q_{sL} to the undrained shear strength s_u. To estimate the variability of the undrained shear strength s_u, we simulated CK0UTXC tests for random values of the critical-state friction angle and the minimum residual-state friction angle as determined from their probability density functions. From these CK0UTXC test simulations, we obtained the distribution of undrained shear strength of the model, $s_{u,model}$.

Since the limit shaft resistance of drilled shafts is arrived at through a simple shear loading path and is controlled purely by the shear strength of the soil (Basu et. al 2009), the limit shaft resistance q_{sL} would be equal to the simple shear strength τ_{ss} of the soil for a rough soil-pile interface as long as the correct loading history is reproduced. Thus, we assumed the limit unit shaft resistance q_{sL} to be equal to the simple shear strength τ_{ss}. For the purposes of assessing the uncertainty in the equation for q_{sL}, that history (associated with drilling operations and concrete placement) should have at most a small impact, and we therefore neglect it in the evaluation of the uncertainty of q_{sL}.

Clay particles, unlike sand particles, align along shear bands with increasing shear deformation. The resulting state, the residual state, is in effect as long as the direction of shearing stays the same during loading (as is the case along the shaft of an axially loaded pile). In order to capture the variability in q_{sL} resulting from basic soil property variability, we estimated q_{sL} using the residual shear strength at very large strains resulting from simple shear loading (same as in simulated CK0UDSS tests) from random values of the critical-state angle and the minimum residual-state friction angle.

To estimate the uncertainty of $\alpha_{equation}$ (given by equation (5.2)) we first generated the random values of the critical-state friction angle ϕ_c and the minimum residual-state friction angle $\phi_{r,min}$ from their probability density functions. Then we estimated the undrained, critical-state shear strength, which we denote by $s_{u,model}$, obtained from elemental simulation of undrained triaxial compression tests (CK0UTXC) with random values of ϕ_c and $\phi_{r,min}$. Subsequently, we estimated q_{sL} (assumed equal to the simple shear strength τ_{ss} obtained for the same initial soil state as the point on the pile shaft where q_{sL} is desired) obtained from elemental simulation of undrained simple shear tests (CK0UDSS) with random values of ϕ_c and $\phi_{r,min}$. From $s_{u,model}$ and q_{sL}, we can estimate α_{model} ($= q_{sL} / s_{u,model}$). We repeated this procedure two hundred times to get reliable distributions of α_{model} and $\alpha_{equation}$ for several stress states (σ_v = 100 kPa, σ_v = 150 kPa, σ_v = 200 kPa, σ_v = 300 kPa and σ_v = 400 kPa).

The error in α estimates can be calculated as $|(\alpha_{equation}/\alpha_{model}) - 1.0|$. The distribution of the ratio $(\alpha_{equation}/\alpha_{model})$ suggests that there is no bias. (i.e., $\alpha_{equation}/\alpha_{model} \approx 1$) in our estimates. The estimated absolute maximum value of $|(\alpha_{equation}/\alpha_{model}) - 1.0|$ is about 0.20 so that $\alpha_{equation}$ is within the range of approximately 80% to 120% of α_{model}. From this, with the assumption that the ratio $(\alpha_{equation}/\alpha_{model})$ follows a normal distribution, the 6σ method leads to an estimate of the standard deviation of this ratio as 0.067 (= 0.4 / 6.0). So, to incorporate the model uncertainty of shaft resistance in our analysis, we introduced a new variable M_α that follows a normal distribution with expectation $E(M_\alpha) = 1.0$ and standard deviation $S_{M\alpha} = 0.1$, which is conservatively used in place of 0.067. The equation used to calculate the unit limit shaft resistance in the Monte-Carlo simulation is:

$$q_{sL} = M_\alpha \left(\frac{s_u}{\sigma_v'}\right)^{-0.05} \left[A_1 + (1 - A_1)\exp\left\{-\left(\frac{\sigma_v'}{p_A}\right)(\phi_c - \phi_{r,\min})^{A_2}\right\}\right] s_u \tag{5.7}$$

5.3.3. Uncertainties in Applied Loads

According to Ellingwood and Tekie (1999), dead load follows a normal distribution with a bias factor of 1.05 and COV equal to 0.1. According to Nowak (1994) and FHWA (2001), the bias factor and COV for dead load are in the range 1.03−1.05 and 0.08−0.1, respectively, depending on the type of structural components. In this analysis, we assumed, that dead load follows a normal distribution with a bias factor = 1.05 and COV = 0.1.

Live load is generally assumed to follow a lognormal distribution (Foye et al. 2006a). According to FHWA (2001), live load has a bias factor of 1.1–1.2 and a COV of 0.18. According to Ellingwood and Tekie (1999), however, live load is represented by a Type 1 distribution of largest values with a bias factor = 1.0 and COV = 0.25. We plotted the PDFs of the Type 1 extreme value distribution and the lognormal distribution for identical values of bias factor and COV, and found that the PDFs of both distributions are nearly identical for the range of live load values encountered in practice for piles. This finding is indirectly corroborated by Ghosn and Moses (1998), who separately calculated reliability indices for highway bridge structures with live loads following a lognormal distribution and a Type 1 extreme value distribution, and found that the results of both calculations were sufficiently close. Consequently, we decided to use the widely-used lognormal distribution to describe live loads. For most of the problems analyzed in this research, we conservatively chose a COV = 0.25 and the corresponding bias factor = 1.0, as recommended by Ellingwood and Tekie (1999).

5.3.4. Uncertainties in Pile Dimensions

Drilled shafts are constructed by removing soil from the ground by drilling and filling the resulting cylindrical void with concrete and reinforcement. The construction process is controlled; so the as-built diameter of the drilled shaft varies little. As far as we know, there is no systematic study available regarding the variability of the drilled shaft diameter. Based on experience and typical construction tolerances, we assume that the drilled shaft diameter B_p (= B_s = B_b) follows a normal distribution with a COV = 0.02.

Typically, drilling is done to refusal or to a minimal embedment into the bearing layer noticeable by a substantial change in drilling resistance. Thus, the lengths of drilled shafts do not vary greatly, and any variation that may occur, if still greater than the minimum length specified by the designer, results in lengths slightly greater than the design lengths. Therefore, in our analysis, we assume that the pile length L_p is deterministic (equal to the design length) because any additional length (due to variability in the depth to the bearing layer, for example) will work towards a conservative design.

5.4. Analysis

Monte-Carlo (M-C) simulations were performed to obtain the probability distributions of the capacity ($Q_{b,\text{ult}}$ + $Q_{s\text{L}}$), the demand (DL + LL) and their difference. We assumed in our analysis that the capacity and the demand are statistically independent. We also assumed that all the random variables — soil properties, loads and the variables representing model uncertainties — are uncorrelated.

We start with a soil profile with known (or assumed) mean values of ϕ_c, $\phi_{r,\min}$ and γ. If undrained shear strength s_u is estimated from q_c, we start with an assumed mean trend of CPT profile $q_c(z)$, where z is the depth. If unconfined compression (UC) tests are used to estimate s_u, we start with an assumed mean value of s_u within the soil layers. We also assume a mean value of applied dead load $(DL)^{(mean)}$ and an (LL)/(DL) ratio (which gives the mean live load $(LL)^{(mean)}$). Then, we consider a drilled shaft with an assumed length and an assumed mean diameter embedded in the soil profile. With the mean soil profile, applied loads and pile dimensions established, we start the first run of the M-C simulations (Figure 5.2).

We start with shaft resistance calculations at depth z = 0 m and move down along the pile shaft. If mean cone resistance trend is given as input, random values of q_c, γ and N_k are generated for a particular depth to calculate a random value of s_u using equation (5.5). If mean undrained shear strength data from UC tests within the soil layers are given as input, random values of s_u and γ are generated for a particular depth. Subsequently, a random value of M_α is generated to calculate a random value of shaft resistance for that depth using equation (5.7). This shaft capacity

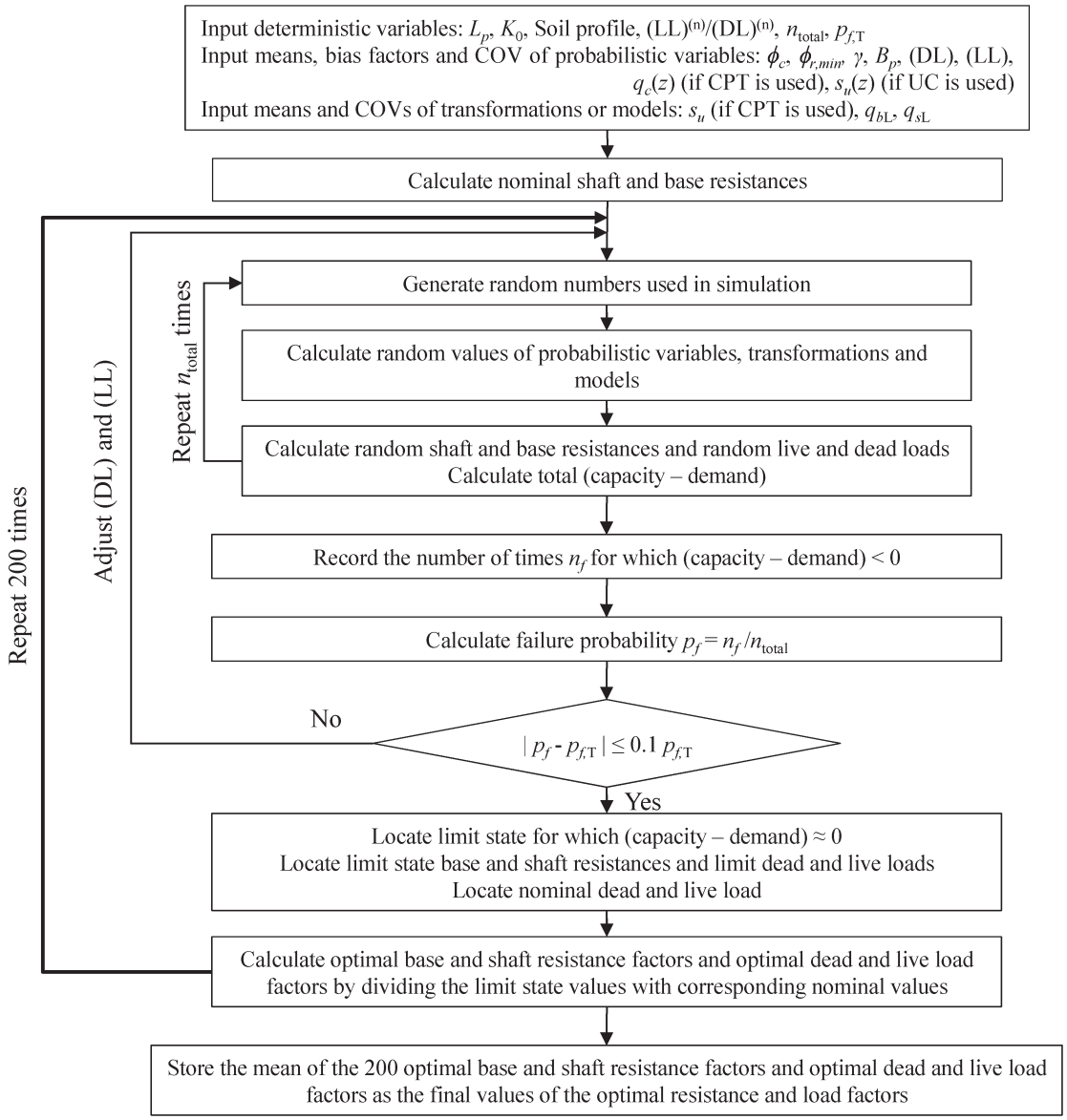

Figure 5.2 Flow chart of Monte-Carlo simulations

calculation is repeated for different depths along the pile shaft with new random values of q_c (typically, soil sub-layers of 1 m thickness with different mean q_c were assumed), s_u and the other variables. By summation of the calculated shaft capacities at the different depths over the entire pile length, we can obtain the random value of the total shaft resistance Q_{sL}. Then, as we reach the pile base, a random value of the base resistance $Q_{b,ult}$ is calculated using the random values of soil variables, a random value of s_u, a random value of B_p and a random value of N_c. Equations (5.4) and (5.7) were used to obtain these random values of $Q_{b,ult}$ and Q_{sL}. After calculating the random $Q_{b,ult}$ and Q_{sL}, random values of (DL) and (LL) are generated and the difference $(Q_{b,ult} + Q_{sL}) - (DL + LL)$ between the random values of capacity $C = Q_{b,ult} + Q_{sL}$ and demand D = (DL + LL) is calculated. The above set of calculations completes one run of the M-C simulations.

The above set of calculations (corresponding to one M-C run) was repeated n_{total} times; the value of n_{total} depends on the target probability of failure. We will call this repeated n_{total} number of calculations one set of M-C simulations. Each set of M-C simulations generated the probability distributions (or histograms) of the capacity and demand. The number of runs n_f for which $(Q_{b,ult} + Q_{sL}) - (DL + LL)$ was less than zero (i.e., the number of times for which demand exceeded capacity) was noted. The ratio n_f / n_{total} approximates the probability of failure p_f. Theoretically, for a continuous probability distribution of (capacity – demand), the area under the PDF curve on the negative side of the (capacity – demand) axis gives p_f.

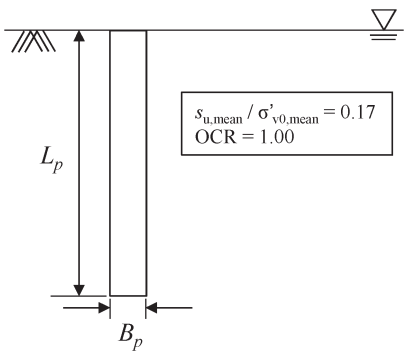

Figure 5.3 Details of soil profile

5.5. Results

The primary goal we have with this chapter is to provide resistance factors that can be useful in design of drilled shafts in clay deposits. However, before doing that, we will investigate how the optimal resistance and load factors change with different field conditions and variables. We will consider a range of soil properties and pile dimensions that may occur in field conditions.

Figure 5.3 shows the details of a homogeneous, completely saturated deposit of normally consolidated clay with $s_{u,mean}$ / $\sigma'_{v0,mean}$ = 0.17 with the water table located at the ground surface. For this deposit, we considered three different clay types. All clay deposits have identical mean critical-state friction angle $\phi_{c,mean}$ = 21°. However, we considered three different values of mean minimum residual-state friction angle $\phi_{r,min,mean}$: 21°, 16°, and 9°. We estimated the mean unit weight, the mean void ratio and the mean vertical stress at the desired depth along the pile using the relation between unit weight and void ratio in clay, $\gamma = (G_s + Se)/(1 + e)$ (G_s = specific gravity of clay solid particles = 2.67, S = degree of saturation = 1.0), and the relation between mean effective stress and void ratio, $e = N - \lambda \ln (p'/p'_A)$ (p'_A = reference mean effective stress, N = void ratio at the reference mean effective stress, λ = the slope of normal consolidation line on e-ln(p') plane). If the mean cone resistance profiles $q_{c,mean}(z)$ are given as input, the mean undrained shear strength s_u follows from equation (5.5). The $q_{c,mean}(z)$ curves were initially back-calculated from void ratio, stress state and a pre-assumed ratio of undrained shear strength to effective vertical stress (s_u / σ'_{v0}). For the case of design based on given undrained shear strength values, we back-calculated the mean undrained shear strength $s_{u,mean}$ from void ratio, stress state and a pre-assumed ratio of undrained shear strength to effective vertical stress (s_u / σ'_{v0}).

The relative depth or slenderness ratio (D / B = L_p / B_p) and diameter and length of drilled shafts that we considered in this research ranged from values that would be considered very low to values considered high for real field conditions. We studied the responses of three drilled shafts with (A) mean diameter $B_{p,mean}$ = 0.3 m and length L_p = 10 m, (B) mean diameter $B_{p,mean}$ = 0.9 m and length L_p = 10 m and (C) mean diameter $B_{p,mean}$ = 1.5 m and length L_p = 10 m.

The proportion of live and dead loads acting on a bridge structure depends on the span length (Hansell and Viest 1971). Titi et al. (2004) tabulated the (LL)/(DL) ratios recommended by AASHTO and FHWA for design of bridge structures; the recommended values vary over a wide range of 0.28–1.92. Accordingly, we considered (LL)/(DL) = 0.25, 1.0 and 2.0.

5.5.1. Results for CPT-Based Design

In this section, we describe how the optimal resistance and load factors change with different field conditions for CPT-based design. We also propose

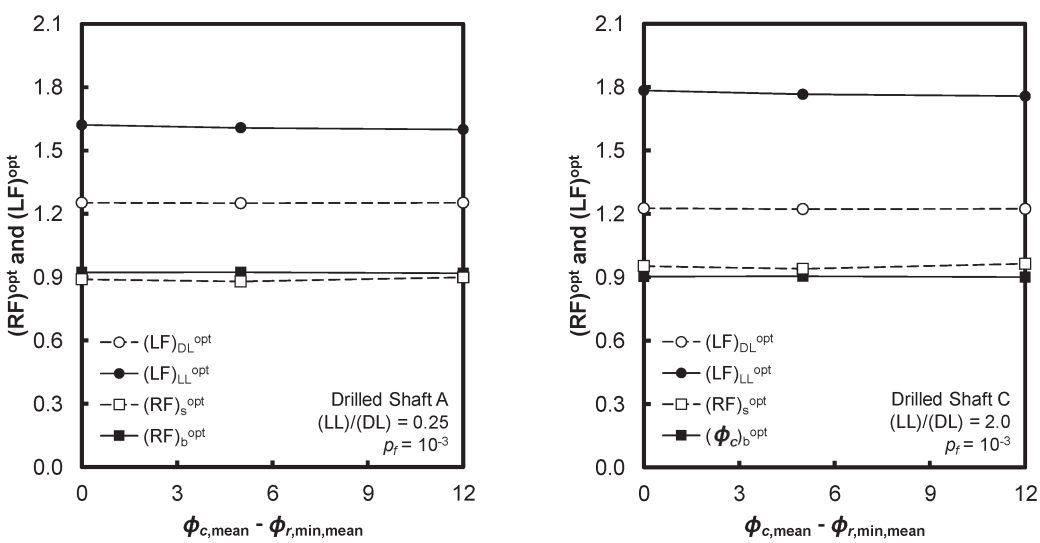

Figure 5.4 Optimal load and resistance factors versus $\phi_{c,mean}$ - $\phi_{r,min,mean}$ for (a) drilled shaft A and (b) drilled shaft C when $q_{c,mean}(z)$ is given as input

design values of code-adjusted resistance factors for use with CPT data as input.

Figure 5.4(a) shows the plots of the load and resistance factors with respect to ($\phi_{c,\text{mean}}$ - $\phi_{r,\text{min,mean}}$) for drilled shafts A with (LL)/(DL) = 0.25 with target failure probability $p_f = 10^{-3}$ when mean cone resistance trend is given as input. Figure 5.4 (b) shows the plots of the load and resistance factors with respect to ($\phi_{c,\text{mean}}$ - $\phi_{r,\text{min,mean}}$) for drilled shafts C with (LL)/(DL) = 2.0 with target failure probability $p_f = 10^{-3}$. In Figure 5.4(a) and Figure 5.4(b), it is evident that the optimal load and resistance factors are independent of $\phi_{c,\text{mean}}$ - $\phi_{r,\text{min,mean}}$. The minor variations in the resistance and load factors observed in Figure 5.4 are typical of all drilled shafts; the fluctuations in the load and resistance factors were rather random without any particular trend.

Figure 5.5(a) shows the plots of the load and resistance factors with respect to diameter to length ratio (B_p/L_p) for the drilled shafts considered in our study with (LL)/(DL) = 0.25, $\phi_{c,\text{mean}} - \phi_{r,\text{min,mean}} = 12^\circ$ and target failure probability $p_f = 10^{-3}$ when mean cone resistance trend is given as input. Figure 5.5(b) shows the plots of the load and resistance factors with respect to diameter to length ratio for considered drilled shafts with (LL)/(DL) = 2.0, $\phi_{c,\text{mean}} - \phi_{r,\text{min,mean}} = 12^\circ$ and target failure probability $p_f = 10^{-3}$. In both Figure 5.5 (a) and (b), as diameter to length ratio B_p/L_p increases, the shaft resistance factor increases slightly and the base resistance factor decreases slightly. That said, Figure 5.5 also shows that the load factors are nearly independent on the diameter to length ratio B_p/L_p. The trends observed in Figure 5.5, are typical of all the other cases. Although there are slight variations in resistance factor with respect to diameter to length ratio, these variations can be considered negligible for practical purposes.

Soil properties and pile dimensions have practically no effect on the resistance and load factors. The (LL)/(DL) ratio, however, has a non-negligible effect on the live load factor. Figure 5.6 (a) and Figure 5.6(b) show the plots of the load and resistance factors with respect to the (LL)/(DL) ratio for drilled shafts A and B, respectively, when $\phi_{c,\text{mean}} - \phi_{r,\text{min,mean}} = 12^\circ$, target failure probability $p_f = 10^{-3}$, and mean cone resistance trend is given as input. In both Figure 5.6(a) and Figure 5.6(b), the optimal resistance factors increase slightly and the optimal dead load factor decreases slightly with increase in (LL)/(DL) ratio; however, the optimal live load factor increases significantly with increase in (LL)/(DL) ratio.

Figure 5.6 implies that (LL)/(DL) ratio affects the mean factor of safety $(\text{FS})_{\text{mean}}$ because of a significant change of live load factor. Figure 5.7(a) and Figure 5.7(b) show $(\text{FS})_{\text{mean}}$ versus p_f for drilled shafts A and C, respectively, when mean cone resistance trend is given as input. To study the effect of p_f, we performed additional M-C simulations with target $p_f = 10^{-2}$. Both Figure 5.7(a) and Figure 5.7(b) show that $(\text{FS})_{\text{mean}}$ increases with decrease of p_f. Also, the larger the (LL)/(DL) ratio, the higher the $(\text{FS})_{\text{mean}}$ is. This shows that $(\text{FS})_{\text{mean}}$ is not a true indicator of the reliability of a design; for the same mean factor of safety, the probabilities of failure are different for different proportions of applied live to dead load. From another viewpoint, for the same probability, a higher factor of safety is required to account for the higher uncertainty levels of live loads if (LL)/(DL) ratio increases.

Figure 5.8(a) and Figure 5.8(b) plot the optimal resistance and load factors versus the probability of failure p_f for drilled shaft A with $\phi_{c,\text{mean}} - \phi_{r,\text{min,mean}} = 12^\circ$ when (LL)/(DL) = 0.25 and (LL)/(DL) = 2.0, respectively. Both figures show the effect of p_f on the

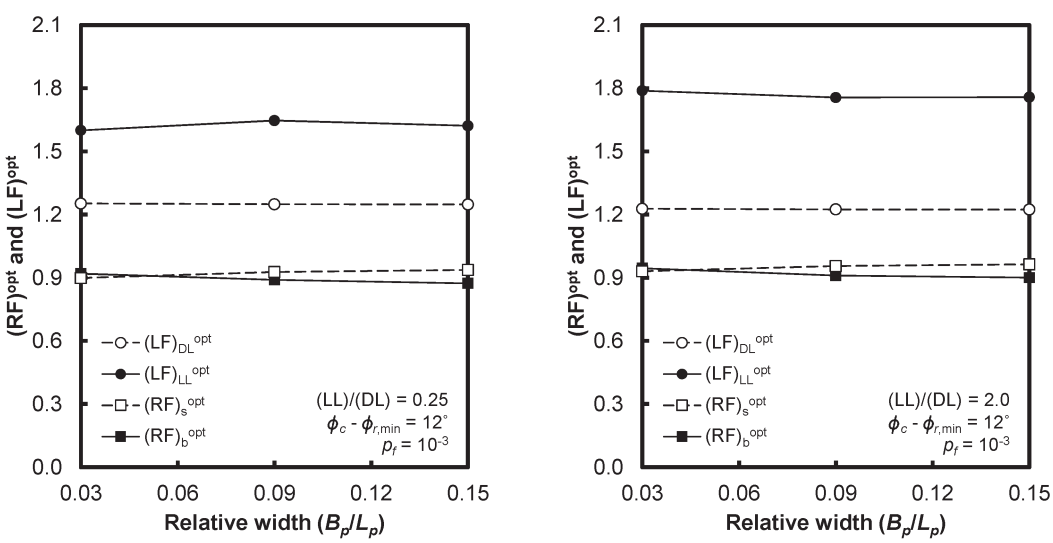

Figure 5.5 Optimal load and resistance factors versus diameter to length ratio for (a) LL/DL = 0.25 and (b) LL/DL = 2.0 when $q_{c,\text{mean}}(z)$ is given as input

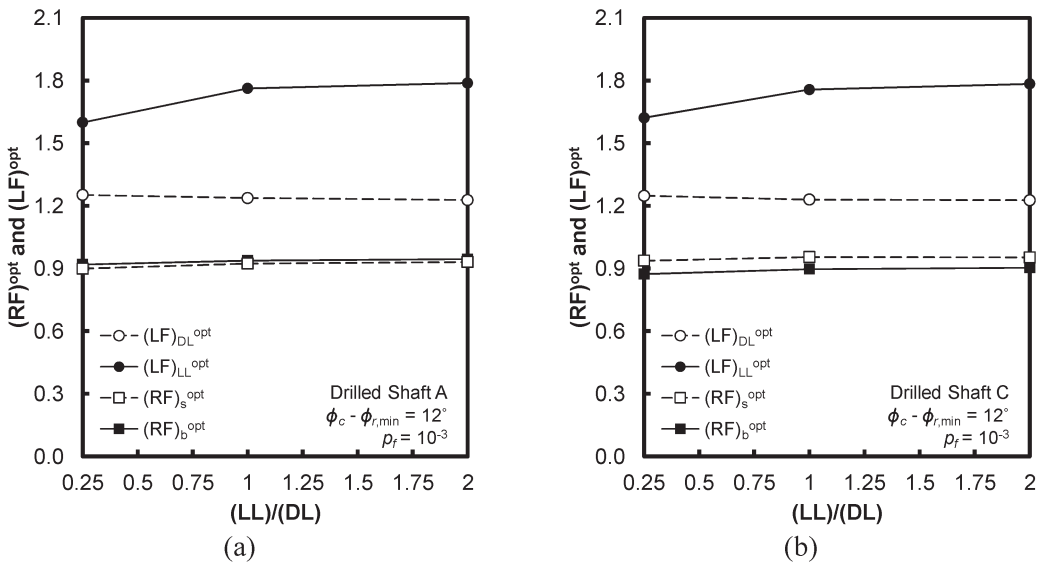

Figure 5.6 Optimal load and resistance factors versus live load to dead load ratio for (a) drilled shaft A and (b) drilled shaft C when $q_{c,\text{mean}}(z)$ is given as input

optimal resistance and load factors. As p_f increases, the resistance factors increase slightly and the dead load factor decreases slightly. The live load factor, however, significantly decreases with increase of p_f. So, it is evident that the change in $(\text{FS})_{\text{mean}}$ due to change in p_f is mainly influenced by the live load.

Figure 5.9(a) and Figure 5.9(b) show the optimal and code-adjusted resistance factors for drilled shaft A and drilled shaft C, respectively, when $p_f = 10^{-3}$ and mean cone resistance trend is given as input. The code-adjusted resistance factors were obtained from the optimal resistance factors by using equation (3.10). For both drilled shafts, the code-adjusted resistance factors are slightly more conservative than the optimal resistance factors. Moreover, the code-adjusted resistance factors do not vary as much as the optimal resistance factors with (LL)/(DL) ratio.

Since the code-adjusted resistance factors do not vary significantly for the different drilled shafts and soil properties, we consolidate the results of the code-adjusted resistance factors obtained for drilled shafts A, B and C and the range of soil properties considered. We calculated the mean, standard deviation (SD), maximum and minimum of the resistance factor obtained for the three drilled shafts. We report these statistics in Table 5.1. We present the data separately for $p_f = 10^{-3}$ and 10^{-4}. Based on the values of the mean and standard deviation of the resistance factors, we calculated the code-adjusted resistance factor with 99% confidence as: $(\text{RF})_b^{\text{code}} = 0.70$ and $(\text{RF})_s^{\text{code}} = 0.73$

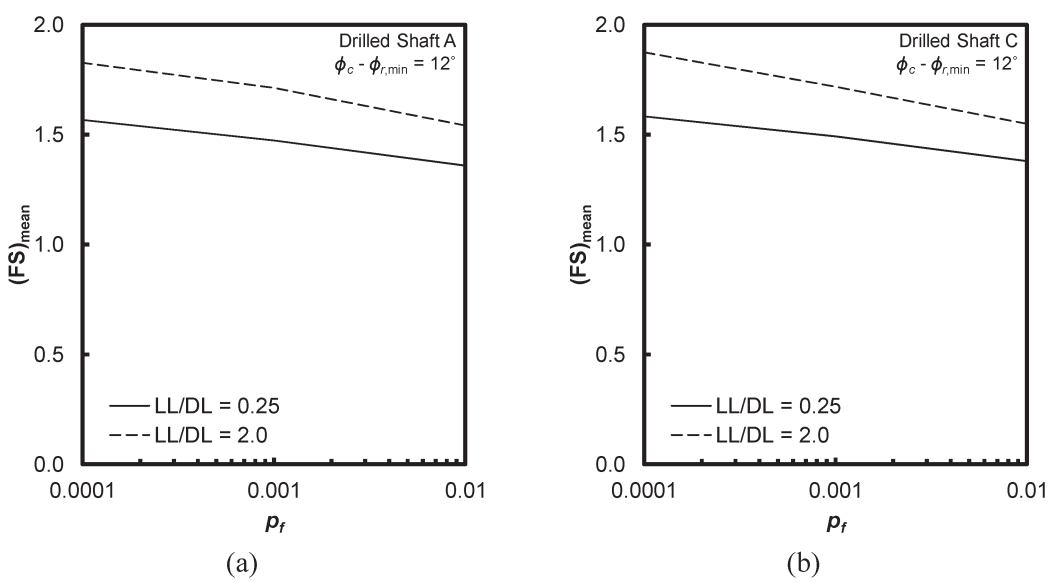

Figure 5.7 Mean factor of safety versus target probability of failure for (a) drilled shaft A and (b) drilled shaft C when $q_{c,\text{mean}}(z)$ is given as input

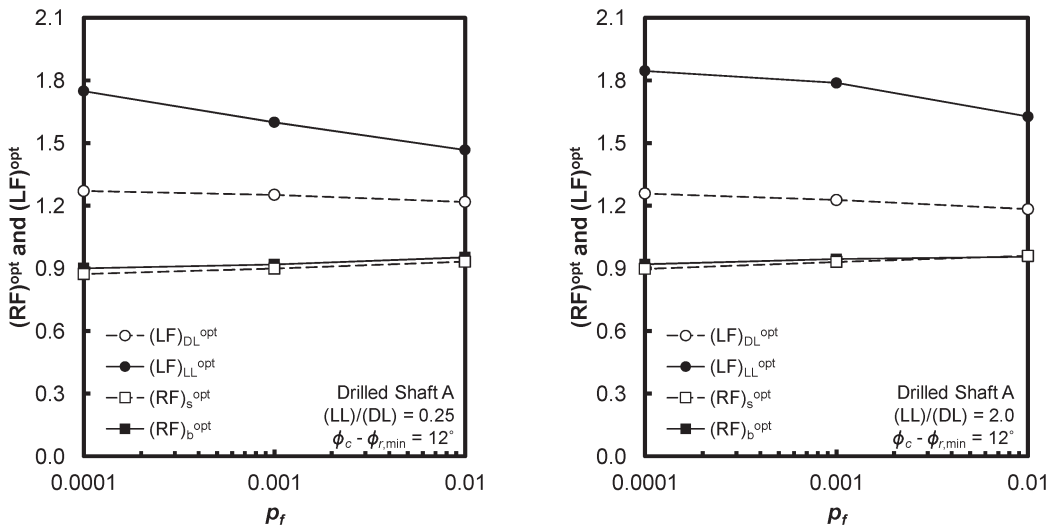

(a) (b)

Figure 5.8 Optimal resistance and load factors versus target probability of failure for drilled shaft A and (a) LL/DL = 0.25 and (b) LL/DL = 2.0 when $q_{c,\text{mean}}(z)$ is given as input

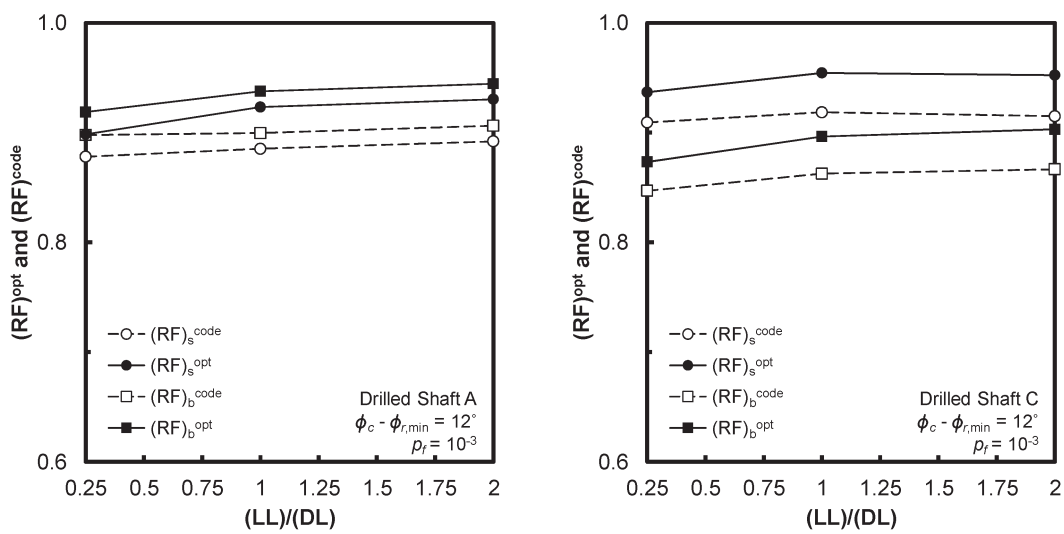

(a) (b)

Figure 5.9 Optimal and code-adjusted resistance factors versus live load to dead load ratio for (a) drilled shaft A and (b) drilled shaft C when $q_{c,\text{mean}}(z)$ is given as input

TABLE 5.1
Resistance factors for different drilled shafts and adjusted with $(\text{LF})_{\text{DL}}^{\text{code}} = 1.25$ and $(\text{LF})_{\text{LL}}^{\text{code}} = 1.75$ when $q_{c,\text{mean}}(z)$ is given as input

		Diameter to length ratio			
		B_p / L_p = 0.3		B_p / L_p = 1.5	
Probability of failure	Statistics	$(\text{RF})_b^{\text{code}}$	$(\text{RF})_s^{\text{code}}$	$(\text{RF})_b^{\text{code}}$	$(\text{RF})_s^{\text{code}}$
10^{-3}	Mean	0.902	0.885	0.861	0.923
	SD	0.083	0.063	0.063	0.079
	Maximum	1.161	1.041	1.018	1.150
	Minimum	0.581	0.676	0.679	0.684
10^{-4}	Mean	0.852	0.829	0.801	0.874
	SD	0.076	0.057	0.058	0.074
	Maximum	1.065	0.955	0.939	1.070
	Minimum	0.627	0.628	0.615	0.674

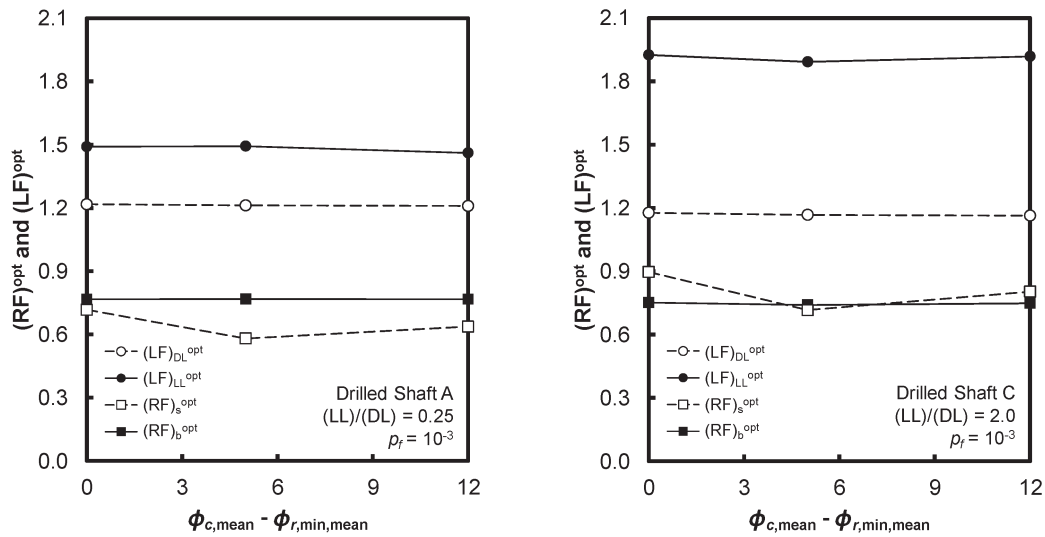

(a) (b)

Figure 5.10 Optimal load and resistance factors versus $\phi_{c,\text{mean}} - \phi_{r,\text{min,mean}}$ for (a) drilled shaft A and (b) drilled shaft C when $s_{u,\text{mean}}$ from UC testing is given as input

for $p_f = 10^{-3}$ and $(\text{RF})_b^{\text{code}} = 0.66$ and $(\text{RF})_s^{\text{code}} = 0.69$ for $p_f = 10^{-4}$.

5.5.2. Results for Designs Based on Unconfined Compressive Strength

In this section, we describe how the optimal resistance and load factors change with different field conditions when unconfined compression tests are used to obtain undrained shear strength. We also propose design values of code-adjusted resistance factors for use with UC test data as input.

Figure 5.10(a) shows the plots of the load and resistance factors with respect to $\phi_{c,\text{mean}} - \phi_{r,\text{min,mean}}$ for drilled shaft A with (LL)/(DL) = 0.25 with target failure probability $p_f = 10^{-3}$ when mean undrained shear strength data from unconfined compression (UC) test are given as input. Figure 5.10(b) shows the plots of the load and resistance factors with respect to $\phi_{c,\text{mean}} - \phi_{r,\text{min,mean}}$ for drilled shaft C with (LL)/(DL) = 2.0 with target failure probability $p_f = 10^{-3}$. In Figure 5.10(a) and Figure 5.10(b), it is evident that the optimal load and resistance factors are independent on $\phi_{c,\text{mean}} - \phi_{r,\text{min,mean}}$. The minor variations in the resistance and load factors observed in Figure 5.10 are typical of all drilled shafts; the fluctuations in the load and resistance factors were rather random without any particular trend.

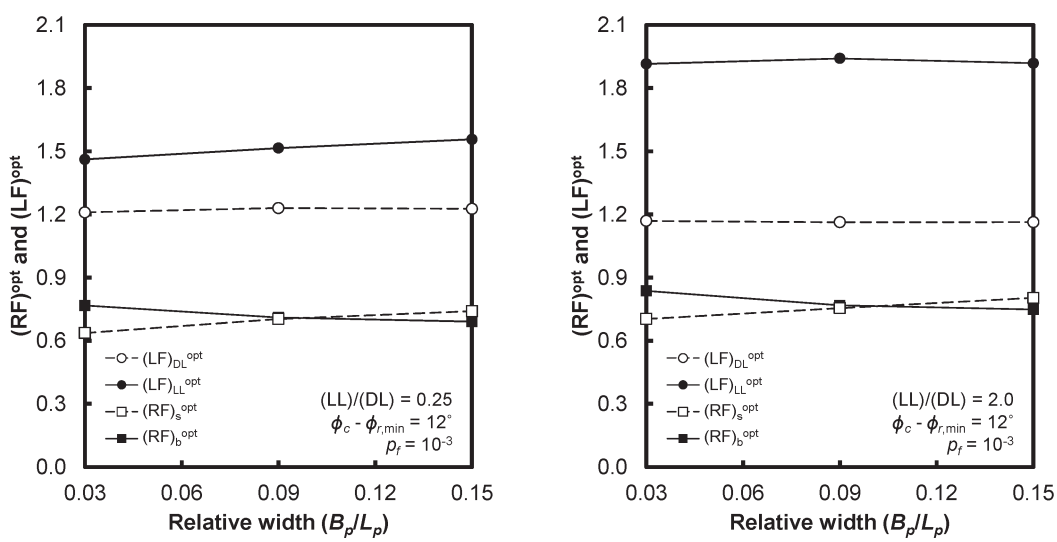

(a) (b)

Figure 5.11 Optimal load and resistance factors versus diameter to length ratio for (a) LL/DL = 0.25 and (b) LL/DL = 2.0 when $s_{u,\text{mean}}$ from UC testing is given as input

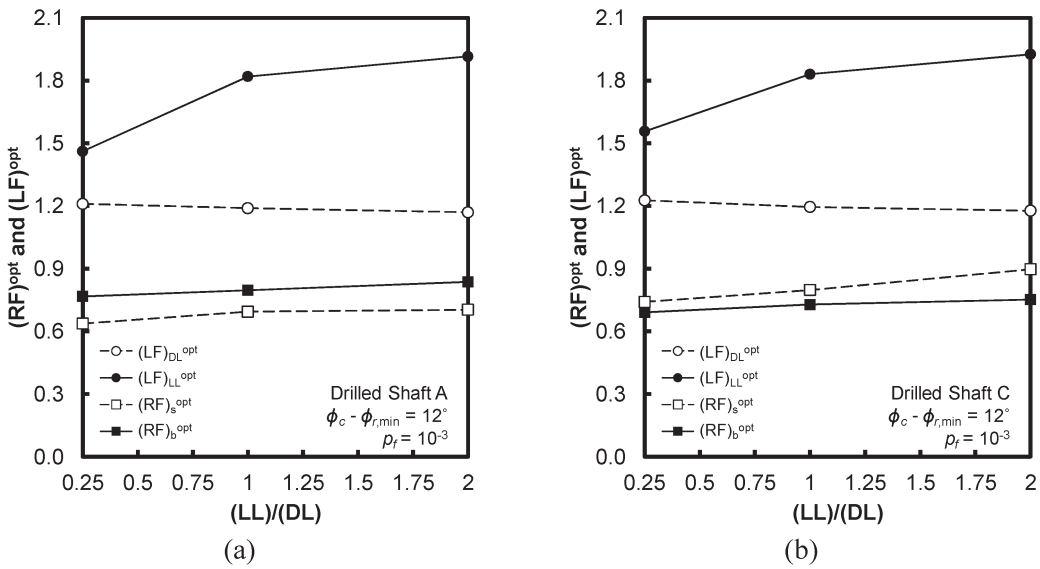

Figure 5.12 Optimal load and resistance factors versus live load to dead load ratio for (a) drilled shaft A and (b) drilled shaft C when $s_{u,\text{mean}}$ from UC testing is given as input

Figure 5.11(a) shows the plots of the load and resistance factors with respect to diameter to length ratio (B_p/L_p) for the drilled shafts considered in this study with (LL)/(DL) = 0.25, $\phi_{c,\text{mean}} - \phi_{r,\text{min,mean}} = 12°$ and target failure probability $p_f = 10^{-3}$ when mean undrained shear strength data are given as input. Figure 5.11(b) shows the plots of the load and resistance factors with respect to diameter to length ratio for the drilled shafts with (LL)/(DL) = 2.0, $\phi_{c,\text{mean}} - \phi_{r,\text{min,mean}} = 12°$ and target failure probability $p_f = 10^{-3}$. In both Figure 5.11(a) and (b), as diameter to length ratio B_p/L_p increases, the shaft resistance factor increases slightly and the base resistance factor decreases slightly. That said, the changes are so slight that Figure 5.11 in essence shows that the load factors are nearly independent of the diameter to length ratio B_p/L_p. The trends observed in Figure 5.11, are typical of all the other cases. Although there are slight variations in resistance factor with respect to diameter to length ratio, these variations can be considered negligible for practical purposes.

Soil properties and pile dimensions have practically no effect on the resistance and load factors. The (LL)/(DL) ratio, however, has a non-negligible effect on the live load factor. Figure 5.12(a) and Figure 5.12(b) show the plots of the load and resistance factors with respect to the (LL)/(DL) ratio for a drilled shaft A and C, respectively when $\phi_{c,\text{mean}} - \phi_{r,\text{min,mean}} = 12°$ and target failure probability $p_f = 10^{-3}$ when mean undrained shear strength data are given as input. In both of

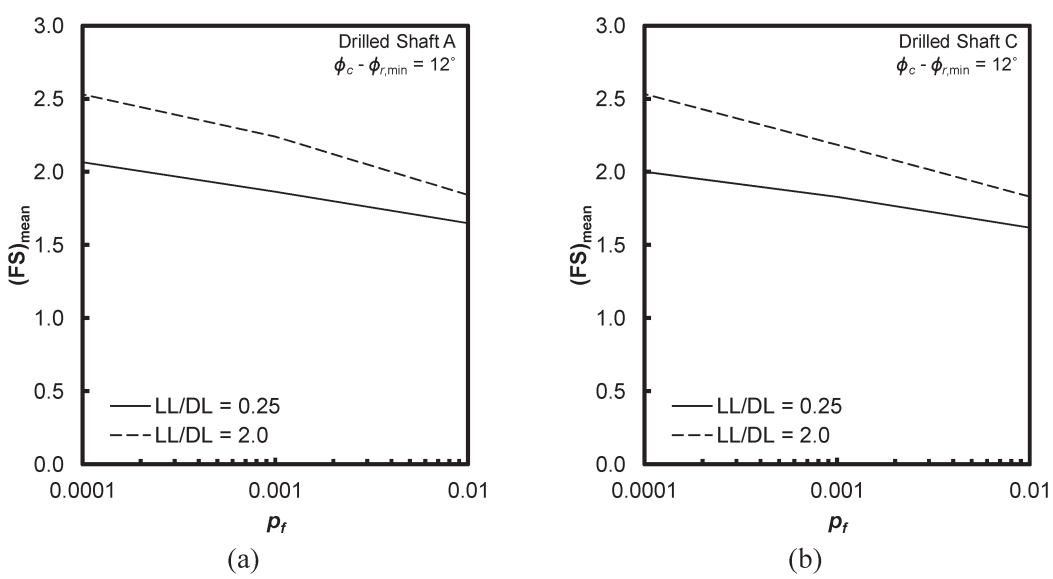

Figure 5.13 Mean factor of safety versus target probability of failure for (a) drilled shaft A and (b) drilled shaft C when $s_{u,\text{mean}}$ from UC testing is given as input

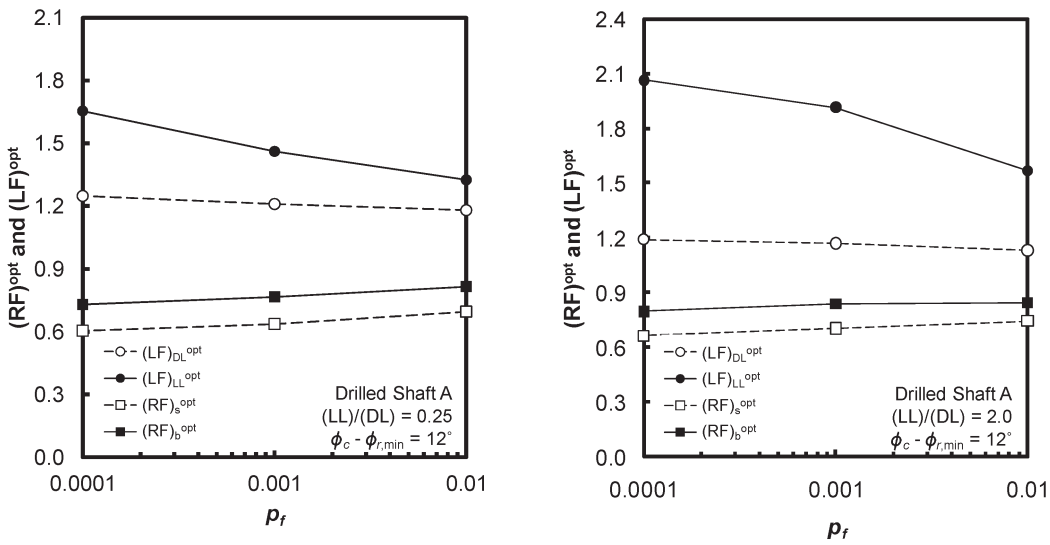

(a) (b)

Figure 5.14 Optimal resistance and load factors versus target probability of failure for drilled shaft A and (a) LL/DL = 0.25 and (b) LL/DL = 2.0 when $s_{u,\text{mean}}$ from UC testing is given as input

Figure 5.12(a) and Figure 5.12(b), the optimal resistance factors increase slightly and the optimal dead load factor decreases slightly with increase in (LL)/(DL) ratio; however, the optimal live load factor increases significantly with increase in (LL)/(DL) ratio.

Figure 5.12 implies that (LL)/(DL) ratio affects the mean factor of safety $(\text{FS})_{\text{mean}}$ because of a significant change of live load factor. Figure 5.13(a) and Figure 5.13(b) show $(\text{FS})_{\text{mean}}$ versus p_f for drilled shafts A and C, respectively, when mean undrained shear strength data are given as input. To study the effect of p_f, we performed additional M-C simulations with target $p_f = 10^{-2}$. Both Figure 5.13(a) and Figure 5.13(b) show that $(\text{FS})_{\text{mean}}$ increases with decreasing p_f. Also, the larger the (LL)/(DL) ratio, the higher the $(\text{FS})_{\text{mean}}$ is. This shows that $(\text{FS})_{\text{mean}}$ is not a true indicator of the reliability of a design; for the same mean factor of safety, the probabilities of failure are different for different proportions of applied live load. From another viewpoint, for the same probability, a higher factor of safety is required to account for the higher uncertainty levels of live loads if the (LL)/(DL) ratio increases.

Figure 5.14(a) and Figure 5.14(b) plot the optimal resistance and load factors versus the probability of failure p_f for drilled shaft A with $\phi_{c,\text{mean}} - \phi_{r,\text{min,mean}} = 12^\circ$ when (LL)/(DL) = 0.25 and (LL)/(DL) = 2.0, respectively. Both figures show the effect of p_f on the optimal resistance and load factors. As p_f increases, the resistance factors increase slightly and the dead load factor decreases slightly. The live load factor, however, significantly decreases with increasing p_f. So, it is evident that the change in $(\text{FS})_{\text{mean}}$ due to change in p_f is mainly influenced by the live load.

Figure 5.15(a) and Figure 5.15(b) show the optimal and code-adjusted resistance factors for drilled shaft A and drilled shaft C, respectively, when target $p_f = 10^{-3}$ and mean undrained shear strength data are given as input. The code-adjusted resistance factors were obtained from the optimal resistance factors by using equation (3.10). The code-adjusted resistance factors do not vary as much as the optimal resistance factors with (LL)/(DL) ratio.

Since the code-adjusted resistance factors do not vary significantly for the different drilled shafts and soil properties, we consolidate the results of the adjusted resistance factors obtained from drilled shafts A, B and C and the range of soil properties considered. We calculated the mean, standard deviation (SD), maximum and minimum of the resistance factor obtained for the three drilled shafts. We report these statistics in Table 5.2. We present the data separately for $p_f = 10^{-3}$ and 10^{-4}. Based on the values of mean and standard deviation of the resistance factors, we calculated the code-adjusted resistance factors with 99% confidence: $(\text{RF})_b^{\text{code}} = 0.48$ and $(\text{RF})_s^{\text{code}} = 0.43$ for $p_f = 10^{-3}$ and $(\text{RF})_b^{\text{code}} = 0.42$ and $(\text{RF})_s^{\text{code}} = 0.40$ for $p_f = 10^{-4}$.

5.6. Conclusions

We performed a systematic probabilistic analysis to develop the resistance factors for drilled shafts in normally consolidated clay for a soil variable-based design method. The analysis involved identification of a robust design method, the Purdue Clay method for Nondisplacement Piles, quantification of the uncertainties (probability distributions) associated with the design variables and the design equations, and subsequent performance of Monte-Carlo simulations to generate the probability distributions of the pile capacities and applied loads. The limit state loads and shaft and base capacities were then identified from these distributions based on a target probability of failure. From the calculated limit state and nominal

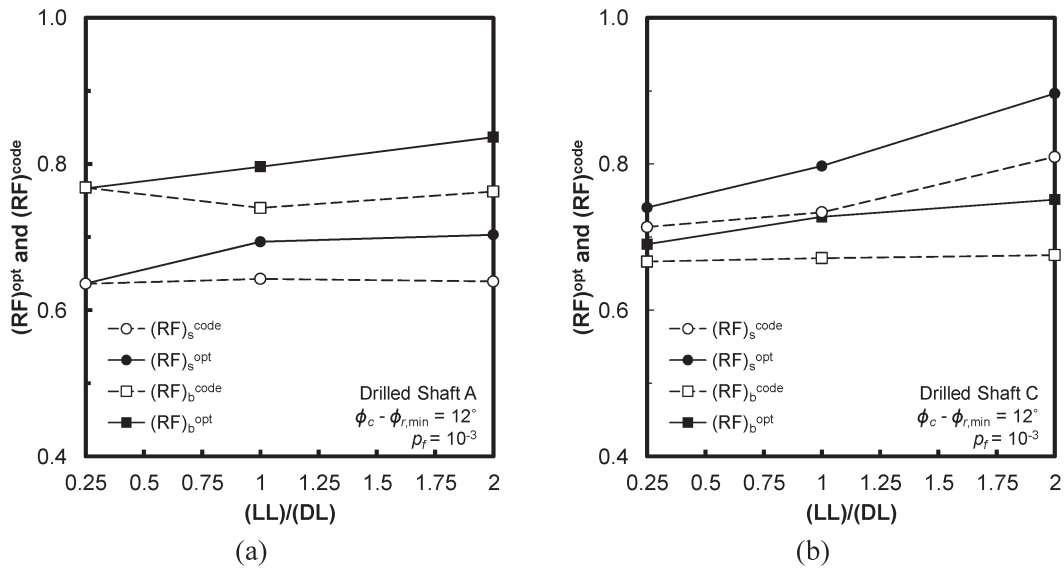

Figure 5.15 Optimal and code-adjusted resistance factors versus live load to dead load ratio for (a) drilled shaft A and (b) drilled shaft C when $s_{u,\text{mean}}$ from UC tests is given as input

values of shaft and base capacities and dead and live loads, the optimal resistance and load factors were obtained. The optimal resistance factors were then adjusted to make them compatible with the dead and live load factors recommended by AASHTO (2007).

In the course of the study, performed with different soil properties and for three different dimensions of drilled shafts, we found that the resistance and load factors did not vary to any significant extent between the different soil properties and drilled shafts considered. The ratio of live to dead load was identified as the only variable that affected the results; however, it affected mostly the live load factor, with minimal effect on the resistance and dead load factors (of course, after adjustment of the factors to code-proposed load factors, there would be an effect on all resistance and load factors). The mean factor of safety was found, reasonably, to increase with decreasing target probability of failure. The change in the mean factor of safety with the target probability of failure was found to be a function of the live load to dead load ratio.

Based on the study, we recommend base and shaft resistance factors that can be used in design together with the dead load and live load factors of 1.25 and 1.75, respectively, recommended by AASHTO (2007). In CPT-based design, the recommended base and shaft resistance values are 0.70 and 0.73 for a probability of failure of 10^{-3} and 0.66 and 0.69 for a probability of failure of 10^{-4}. These could be rounded to 0.70 and 0.75 and 0.65 and 0.70. When unconfined compression tests are used in the estimation of undrained shear strength, the recommended base and shaft resistance values are 0.48 and 0.43 for a probability of failure of 10^{-3} and 0.42 and 0.40 for probability of failure of 10^{-4}. These could be rounded to 0.50 and 0.45 and 0.40 and 0.40.

TABLE 5.2
Resistance factors for different drilled shafts and adjusted with $(\text{LF})_{\text{DL}}^{\text{code}} = 1.25$ and $(\text{LF})_{\text{LL}}^{\text{code}} = 1.75$ when $s_{u,\text{mean}}$ from UC tests is given as input

Probability of failure	Statistics	Diameter to length ratio $B_p / L_p = 0.3$ $(\text{RF})_b^{\text{code}}$	$(\text{RF})_s^{\text{code}}$	$B_p / L_p = 1.5$ $(\text{RF})_b^{\text{code}}$	$(\text{RF})_s^{\text{code}}$
10^{-3}	Mean	0.756	0.638	0.674	0.729
	SD	0.109	0.076	0.072	0.127
	Maximum	1.123	0.935	0.960	1.275
	Minimum	0.440	0.414	0.419	0.317
10^{-4}	Mean	0.684	0.565	0.598	0.643
	SD	0.102	0.056	0.064	0.093
	Maximum	0.995	0.727	0.809	0.897
	Minimum	0.396	0.385	0.407	0.424

CHAPTER 6. RESISTANCE FACTORS OF DRIVEN PILES IN SAND

6.1. Introduction

For the development of resistance factors of axially loaded driven piles in sands, equations for the ultimate unit base resistance and limit unit shaft resistance are proposed based on field and model test data. The uncertainties of dead and live loads and the component variables, transformations, and models associated with the resistance equations are assessed. Based on these uncertainties, rigorous reliability analyses were performed using Monte-Carlo simulations.

Calculations of resistance factors for piles have attracted considerable attention. Kim et al. (2005) obtained resistance factors for the ultimate resistance $Q_{b,ult}$ of driven piles based on the results of the driving analyzer (PDA) and static load tests. Others [McVay et al. (2000), Paikowsky et al. (2004), Titi et al. (2004), Kwak et al. (2010), Yoon and O'Neil (1996), and Allen (2005)] proposed resistance factors for the ultimate resistance Q_{ult} of axially loaded driven piles. Yoon et al. (2008) proposed resistance factors for axially loaded driven piles in soft Louisiana soils. The work we present in this chapter differs from past work in that we are developing resistance factors for a specific method, which we have validated against model tests and field work, and in that we have separate resistance factors for base and shaft resistance.

6.2. Unit Base and Shaft Resistance: Purdue Sand Method for Driven Piles

In this study, resistance factors for driven piles in sand are calculated for a property-based design method. To perform reliability analysis, the equations for ultimate unit base resistance $q_{b,ult}$ and limit unit shaft resistance q_{sL} should be selected or developed together with an assessment of the uncertainties of their component variables and of the transformations themselves.

For a pile problem, the limit unit base resistance q_{bL} of a pile at a certain depth within a given soil layer is approximately equivalent to the cone penetration resistance q_c at the same depth within the same soil layer (Salgado, 2008 and Ghionna et al. 1994). According to the results from Salgado and Prezzi (2007), the limit unit base capacity q_{bL} can be expressed as:

$$\frac{q_{bL}}{p_A} = 1.64e^{0.1041\phi_c + (0.0264 - 0.0002\phi_c)D_R}\left(\frac{\sigma'_h}{p_A}\right)^{0.841 - 0.0047D_R} \quad (6.1)$$

where p_A is the reference stress (=100 kPa), ϕ_c is the critical-state friction angle, D_R (%) is the relative density of cohesionless soil, σ_h' is the effective horizontal stress obtained by $K_0\sigma_v'$, and K_0 is the coefficient of lateral earth pressure at rest.

Based on previous studies (Randolph, 2003, Salgado et al., 2004, and Foye et al. 2009), the limit unit shaft resistance $q_{b,ult}$ (or $q_{b,10\%}$) of a driven pile is a function of D_R in the bearing layer. By performing regression analysis using the pile load test results [measured values of $q_{b,ult}/q_{bL}$ (or $q_{b,ult}/q_c$) for different D_R; data shown in Figure 6.1 of axially loaded instrumented driven piles reported by Altaee et al. (1992 and 1993), Beringen et al. (1979), BCP Committee (1971), Briaud et al. (1989), Gregersen et al. (1973), Jardine et al. (2005) , Paik et al. (2003), and Vesic (1970), the ultimate unit base resistance $q_{b,ult}$ equation for a driven pile in sand is proposed as the follows:

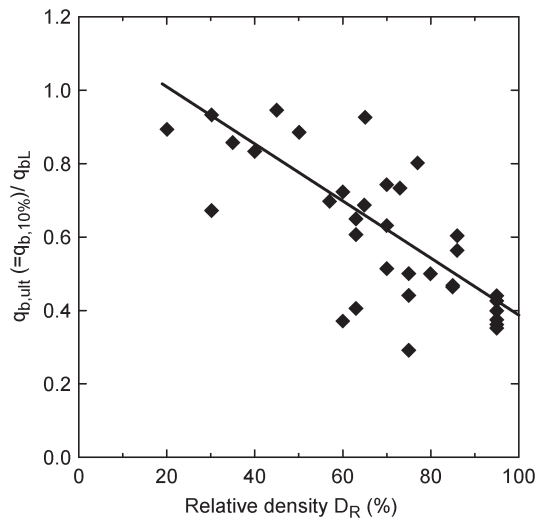

Figure 6.1. Relationship between $q_{b,ult}$ / q_{bL} and D_R

$$q_b,ult = q_b,10\% = (1.09 - 0.007D_R)q_{bL} \quad (6.2)$$

The limit unit shaft resistances q_{sL} can be simply expressed as the normal stress σ'_n on the pile shaft times the tangent of the interface friction angle δ:

$$q_{sL} = \sigma'_h \tan\delta = K\sigma'_v \tan\delta \quad (6.3)$$

where K is the coefficient of lateral earth pressure and σ'_v is the vertical effective stress. Foye et al. (2009) established the following relationship between interface friction angle δ and the critical-state friction angle ϕ_c for an interface between rough-surface steel (average roughness $R_a > 4\mu$m) and sand using the test data reported by Rao et al. (1998), Lehane et al. (1993), and Jardine and Chow (1998):

$$\delta = 0.9\phi_c \quad (6.4)$$

The coefficient K of lateral earth pressure is truly a function of soil state (relative density D_R and K_0); however, a rigorous analysis to calculate K surrounding a driven pile has not yet been possible due to the difficulties explained by Salgado (2008). This makes the use of equation (6.3) less convenient. In order to arrive at a practical way of estimating q_{sL}, we assumed that the q_{sL} is a function of D_R, the tangent of interface friction angle, and q_{bL}. The assumed mathematical form for this relationship is:

$$q_{sL} = f(D_R,\ \tan\delta,\ q_{bL}) = f'(D_R)\tan\delta\ q_{bL} \quad (6.5)$$

Based on the results of high-quality model pile tests in sands by Yazdanbod et al. (1984) and Lee et al. (2003), the ratios of q_{sL}/q_{bL} for closed-ended model piles are collected. Yazdanbod et al. (1984) provided values of ϕ_c, D_R, and σ'_h for the depths where q_{sL} was being calculated in their paper; therefore, the calculations of q_{bL} values were possible using equation (6.1). Lee et al. (2003) reported ϕ_c and D_R of sands in a calibration chamber and q_c values at the depths of q_{sL} measurements. As mentioned earlier, q_c is approximately assumed to be equal to q_{bL}.

For the model pile tests, D_R values along the pile shaft are well controlled, ranging from 24% to 91%. For the estimates of δ values of the model load tests, equation (6.4) ($\delta = 0.9\phi_c$) is used to estimate the ϕ_c values of Yazdanbod et al. (1984) and Lee et al. (2003). A regression analysis is performed, leading to the following equation for the limit unit shaft resistance q_{sL}:

$$q_{sL} = \left(0.0574 D_R^{0.013} - 0.051\right)\tan(0.9\phi_c)\ q_{bL} \quad (6.6)$$

The measured values of q_{sL}/q_{bL} (or q_{sL}/q_c) ratios from Yazdanbod et al. (1984) and Lee et al. (2003) and lines represented by equation (6.6) assuming $\phi_c = 30°$ and $\phi_c = 33.7°$ are plotted versus D_R, as shown in Figure 6.2.

6.3. Uncertainty Assessment of Design Variables and Model Uncertainty

The component variables in the $q_{b,ult}$ equation are B_p, D_R, K_0, γ, ϕ_c, and those in the q_{sL} equation are B_p, ΔL_p, D_R, K_0, γ, ϕ_c (or δ). We assumed that the pile geometry (defined by B_p and L_p) is deterministic. This is because driven piles are typically prefabricated and minimum design length is preset. For normally consolidated cohesionless soils, K_0 tends to increase with increasing

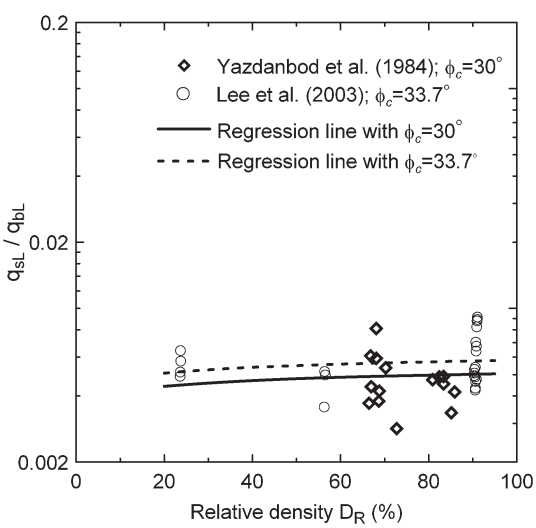

Figure 6.2. Relationship between q_{sL} / q_{bL} and D_R

void ratio. Based on research on K_0 for several sands (Ottawa sand, Minnesota sand, Toyoura sand), the range of K_0 for sands is 0.35 – 0.5 (Fang et al., 1997, Hendron, 1963, and Okichi and Tatsuoka, 1984). A K_0 of 0.35 exists only for extremely dense sand, which would typically not be crossed by a driven pile; therefore, in this study, we assumed K_0 to be deterministic and range from 0.4 to 0.5. Three different K_0 values (0.4, 0.45, and 0.5) were assumed.

6.3.1. Uncertainties in Soil Variables

Critical-State Friction Angle ϕ_c

Negussey et al. (1987) reported that ϕ_c of medium and fine Ottawa sands measured using ring shear tests varies within the 29.8° – 30.2° range, depending on whether dry/saturated conditions existed during the tests. Kim (2008) calculated COV of ϕ_c using these data and found that COV of ϕ_c varied from 0.0081 to 0.0172. Based on the standard deviation of ϕ_c estimated from Bolton (1986), Foye (2005) and Kim (2008) concluded that the standard deviation of ϕ_c is 0.333°. Kim (2008) calculated that the maximum COV of ϕ_c within the ϕ_c range assumed to contain the vast majority of ϕ_c values found in real soils (28°–36°) is 0.012 (0.333° / 28°). Considering these results, we conservatively assumed the COV of ϕ_c in our analysis to be 0.02. The distribution of ϕ_c is assumed to be a normal distribution.

Soil Unit Weight γ

Soil unit weight γ is used for the calculation of the horizontal effective stress σ'_h in equation (6.1) and in the calculation of D_R, which will be explained later. Hammit (1966) concluded that the COV of γ is 0.03, while Phoon and Kulhawy (1999) suggested a COV of γ ranging from 0.01 to 0.12 for dry γ and from 0.03 to 0.2 for saturated or partially-saturated γ. White et al. (2005) found that a COV of γ for compacted fill is about 0.08. Kim (2008) assumed γ to follow a normal distribution with a COV of 0.1 based on prior studies. Malkawi et al. (2000) assumed the COV of γ to range from 0.01 to 0.03 in their reliability analysis for slopes. In this study, the distribution of γ is assumed to follow a normal distribution with a COV of 0.1.

In addition to these design variables' uncertainties, only the assessment of uncertainties of the transformations of the relative density D_R and the interface friction angle δ [equation (6.4)] and the models [equations (6.2) and (6.6)] for $q_{b,ult}$ and q_{sL} are needed for the reliability analysis of driven piles in sand.

6.3.2. Transformation and Model Uncertainties

Relative Density D_R

Estimation of D_R values directly from its definition [$(e_{max} - e)$ / $(e_{max} - e_{min})$] along the pile shaft and near the pile base in the field is impossible; therefore, we calculate D_R using cone resistance q_c and horizontal effective stress σ'_h from equation (6.1) proposed by

Salgado and Prezzi (2007), rewritten as:

$$D_R(\%) = \frac{\ln\left(\frac{q_c}{p_A}\right) - 0.4947 - 0.1041\phi_c - 0.841n\left(\frac{\sigma'_h}{p_A}\right)}{0.0264 - 0.0002\phi_c - 0.0047\ln\left(\frac{\sigma'_h}{p_A}\right)} \quad (6.7)$$

$$= f(q_c, \phi_c, \sigma')$$

For the assessment of the uncertainty in D_R calculated using equation (6.7), we must assess the uncertainties of the component variables of the equation and the uncertainty of transformation equation itself. The uncertainties of the component variables other than q_c were discussed earlier. Foye et al. (2006, 2009) decided to use a normal distribution with a COV of 0.08 for q_c. Foye (2005) performed regression analysis based on the good-quality chamber tests results reported by Salgado (1993). The resulting bias factor and COV of transformation equation (6.7) of D_R were 0.97 and 0.1, respectively.

Interface Friction Angle δ

Using the date sets of δ and ϕ_c reported by Rao et al. (1998), Lehane et al. (1993), and Jardine and Chow (1998), Foye et al. (2009) assessed the uncertainty of transformation equation (6.4) and concluded that the bias factor and COV value of transformation equation (6.4) are 1.0 and 0.10, respectively.

Ultimate Unit Base Resistance

In order to assess the uncertainty of $q_{b,ult}$, the data from the axial load tests on instrumented piles of Figure 6.1, fit with Equation (6.2), was used. The histogram of the ratios of the measured $q_{b,ult}$ ($q_{b,ult,meas.}$) to the predicted $q_{b,ult}$ ($q_{b,ult,pred.}$) and the equivalent distribution of these ratios are plotted in Figure 6.3. The bias factor and COV of measured-to-predicted $q_{b,ult}$ [equation (6.2)] are 1.00 and 0.217, respectively, and its distribution follows closely a normal distribution.

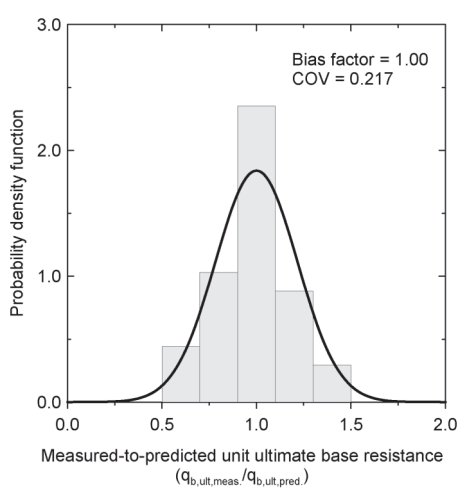

Figure 6.3. Bias factor, COV, and distribution of $q_{b,ult,meas.}/q_{b,ult.pred.}$

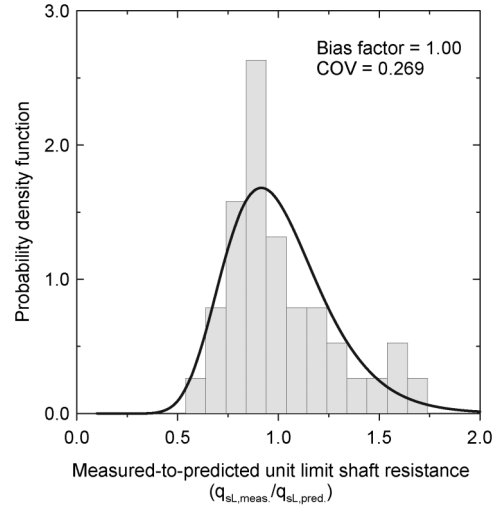

Figure 6.4. Bias factor, COV, and distribution of $q_{sL,meas.}/q_{sL.pred.}$

Limit Unit Shaft Resistance

The histogram and its equivalent distribution of the measured-to-predicted q_{sL}/q_{bL} data are shown in Figure 6.4. The distribution of the measured-to-predicted q_{sL}/q_{bL} values approximately follows a lognormal distribution. The bias factor and COV values of q_{sL}/q_{bL} [equation (6.6)] are 1.00 and 0.269, respectively.

6.3.3. Uncertainties of Applied Loads

Dead Load DL

According to Nowak (1999) and FHWA (2001), the bias factor and COV for DL vary from 1.03 to 1.05 and from 0.08 to 0.1, respectively, depending on materials used in the structure. In this study, a normal distribution with a bias factor = 1.05 and COV = 0.1 is assumed as the distribution of DL.

Live Load LL

Live load is generally described using a lognormal distribution (Nowak, 1999, Foye et al. 2006, Kim, 2008) because Nowak (1999) found that the distribution of LL associated with vehicular load is approximately lognormal; thus, Foye et al. (2006, 2009) and Kim (2008) assumed the distribution of LL follows a lognormal distribution. According to Nowak (1999), the ranges of bias factor and COV of LL are 0.6 – 1.2 and a COV of 0.17 – 0.205, respectively. We have used a bias factor of 1.15 and a COV of 0.18 for LL, values recommended in FHWA (2001).

6.4. Analysis

6.4.1. Procedure for Calculation of Optimal Factors

The procedure for determining optimal factors is illustrated in the flow chart of Figure 6.5. For pile problems, it is acceptable to assume that pile capacity ($Q_{b,\mathrm{ult}} + Q_{s\mathrm{L}}$) is independent of demand (DL + LL) on

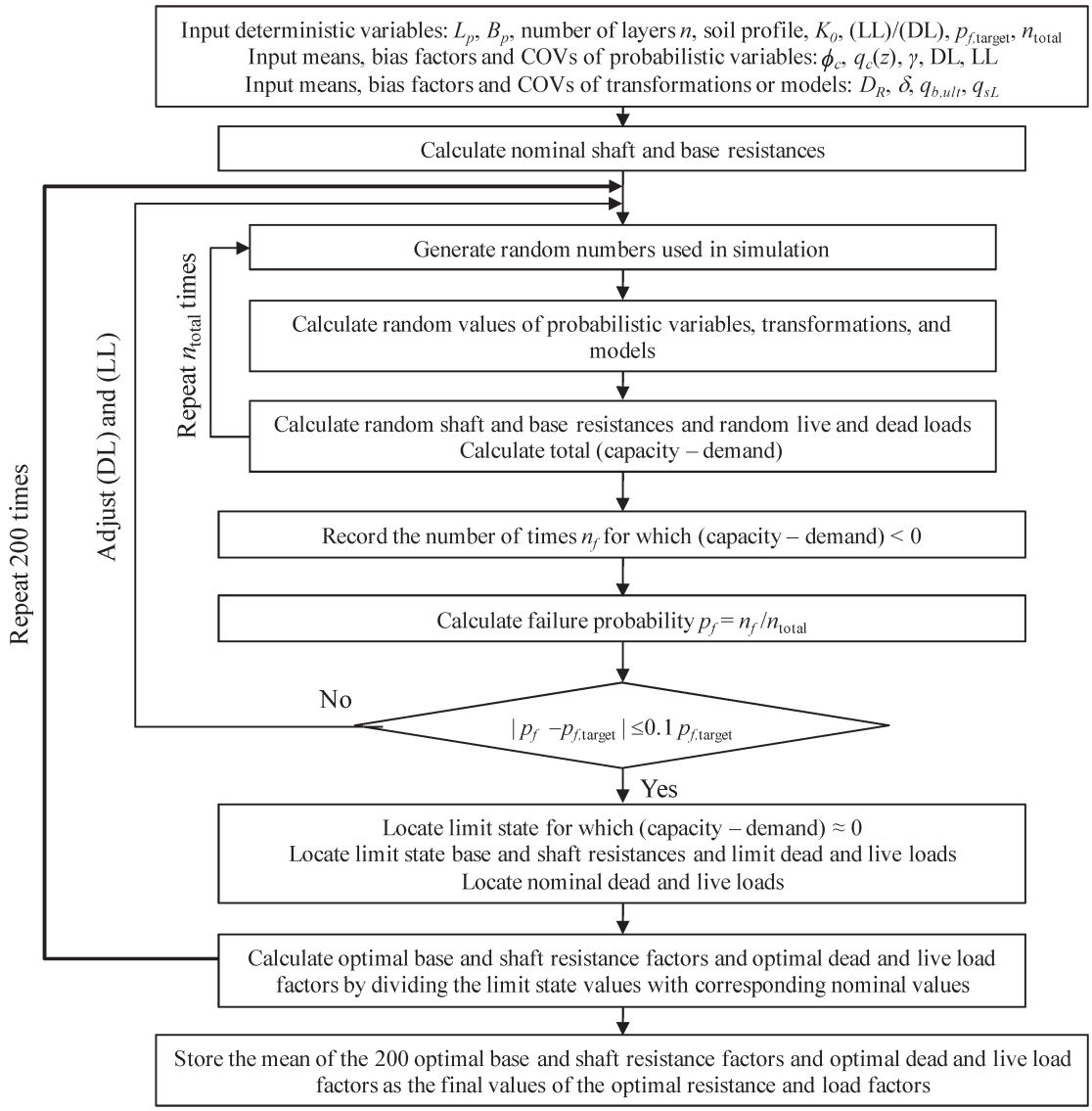

Figure 6.5. Procedure of calculations of optimal factors

the pile head. In the reliability analysis using Monte-Carlo simulations, we assumed that all the random variables generated for the representation of the uncertainties of design variables, transformations, and models are statistically independent.

The process starts with setting the values of the deterministic variables [L_p, B_p, number of layers n, soil profile, K_0, (LL)/(DL), $p_{f,\text{target}}$, n_{total}]. That is followed by setting the values of the means, bias factors, and COVs of the probabilistic variables [ϕ_c, $q_c(z)$, γ, DL, LL], the transformations [equation (6.4) for δ and equation (6.7) for D_R], and the models [equation (6.2) for $q_{b,ult}$ and equation (6.6) for q_{sL}]. For all the examples in this report, we divided soil layers into 1m-thick sub-layers. Near the pile base, layers may be thinner because of the presence of the bearing layer. Salgado (2008) proposed that a pile should be driven into a bearing layer by at least twice its diameter for the full mobilization of the base resistance associated with that layer. Accordingly, we assumed that piles were embedded into the bearing layer by $2B_p$. The representative nominal values of soil parameters and horizontal effective stress for the calculation of base resistance were assumed as those values at $0.5B_p$ below the pile base.

Nominal values of ultimate base resistance $Q_{b,ult}$ and limit shaft resistance Q_{sL} were calculated and were stored separately. Next, we generated separate random numbers for the probabilistic variables, the transformations, and the models reflecting their bias factors, COVs, and distribution types to have random values of $Q_{b,\text{ult}}$, $Q_{s\text{L}}$, DL and LL. The generations of sets of $Q_{b,\text{ult}}$, $Q_{s\text{L}}$, DL and LL were repeated until the total number of sets was equal to n_{total} (n_{total} depends on $p_{f,\text{target}}$, as discussed in Chapter 2). For each of the n_{total} sets of $Q_{b,\text{ult}}$, $Q_{s\text{L}}$, DL and LL, the difference between capacity ($Q_{b,\text{ult}} + Q_{s\text{L}}$) and demand (DL + LL) was also calculated. The number n_f of cases for which the

demand was equal to or less than the capacity was counted. The probability of failure p_f is n_f / n_{total}. If the difference between p_f and $p_{f,target}$ was not less than 10% of $p_{f,target}$, total load (DL + LL) was adjusted until $| p_f - p_{f,target} | < 0.1\ p_{f,target}$. Having met $| p_f - p_{f,target} | < 0.1\ p_{f,target}$, the ultimate limit state is then defined by the values of $Q_{b,ult}$, Q_{sL}, DL, and LL corresponding to $| Q_{b,ult} + Q_{sL} - DL - LL | = 0$. Since it is not possible to get this result from calculations that are done numerically, we find the combination of these four variables that give us the lowest value of $| Q_{b,ult} + Q_{sL} - DL - LL |$. The optimal base and shaft resistance factors and dead and live load factors were then calculated using Equations (3.5) through (3.8).

As explained in Chapter 3, because of the non-uniqueness of the ultimate limit state, the calculations of optimal factors were repeated 200 times and their average values (means of the 200 base and shaft resistance factors and dead and live load factors) were used as (very good) estimates of the optimal resistance and load factors. To find approximations to the most probable ultimate limit state values of $Q_{b,ult}$, Q_{sL}, DL, and LL, we generated 200 sets of ultimate limit state values of $Q_{b,ult}$, Q_{sL}, DL, and LL and took the means of the 200 optimal base and shaft resistance factors and dead and live load factors as the optimal values of $Q_{b,ult}$, Q_{sL}, DL, and LL.

6.4.2. Monte-Carlo Simulations

Following the procedure shown in Figure 6.5, optimal factors were calculated for different pile geometries, different levels of water tables, and soil profiles. Six combinations [profiles (1) – (6)] of soil profiles with different water table conditions were assumed: details of soil properties, pile geometries, and water table existence/location are represented in Figure 6.6 for profile (1) and (2), in Figure 6.7 for profile (3) – (5) and in Figure 6.8 for profile (6).

For each profile, three different values (30°, 33° and 36°) within the range of possible ϕ_c values and three different possible values (0.4, 0.45, and 0.5) of K_0 were assumed. The unit weight γ of each layer was calculated from the following equation:

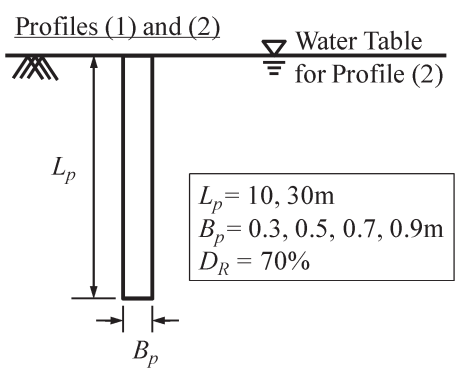

Figure 6.6. Description of pile and soil profiles: profiles (1) and (2)

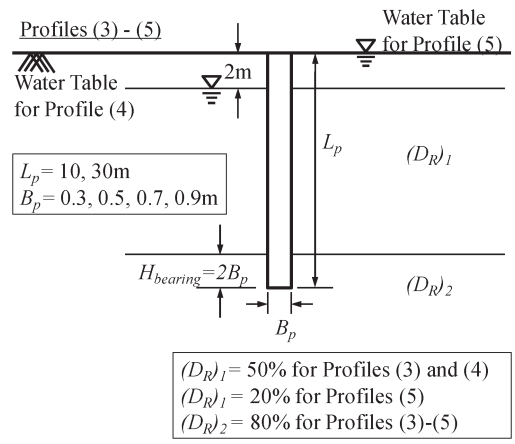

Figure 6.7. Description of pile and soil profiles: profiles (3) – (5)

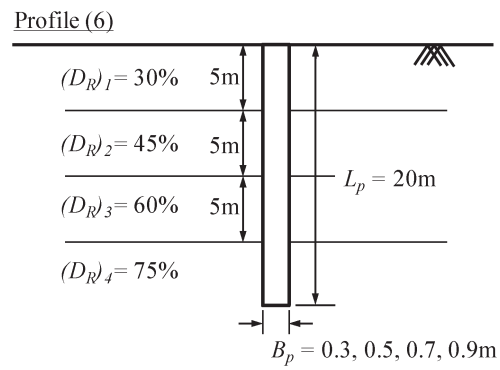

Figure 6.8. Description of pile and soil profile: profiles (6)

$$\gamma = \frac{G_s + Se}{1+e}\gamma_w \tag{6.8}$$

where G_s is the specific gravity; S is the degree of saturation; e is the void ratio; and γ_w is the unit weight of water. For given D_R and e_{max} and e_{min} (in this research, we assumed that e_{max} = 0.9 and e_{min} = 0.45), the void ratio e is determined from the relationship, D_R (%) = 100 ($e_{max} - e$) / ($e_{max} - e_{min}$).

The limit unit base capacity q_{bL} can be calculated using equation (6.1) using the assumed values of D_R, ϕ_c, K_0, and γ. Optimal resistance and load factors were calculated for L_p = 10 and 30m and B_p = 0.3, 0.5, .0.7 and 0.9m for profiles (1) – (5) and L_p = 20m and B_p = 0.3, 0.5, .0.7 and 0.9m for profiles (6). Based on the pre-assessed uncertainties of components variables of $q_{b,ult}$ and q_{sL}, transformations, and $q_{b,ult}$ and q_{sL} equations themselves, the Monte Carlo simulations detailed in Figure 6.5 were performed.

6.5. Results

For profile (1) [with L_p = 10m, B_p = 0.3m, K_0 = 0.45, (LL)/(DL) = 1.0], Figure 6.9 shows values of optimal resistance factors for $p_f = 10^{-3}$ plotted versus ϕ_c. The optimal factors were not highly dependent on ϕ_c.

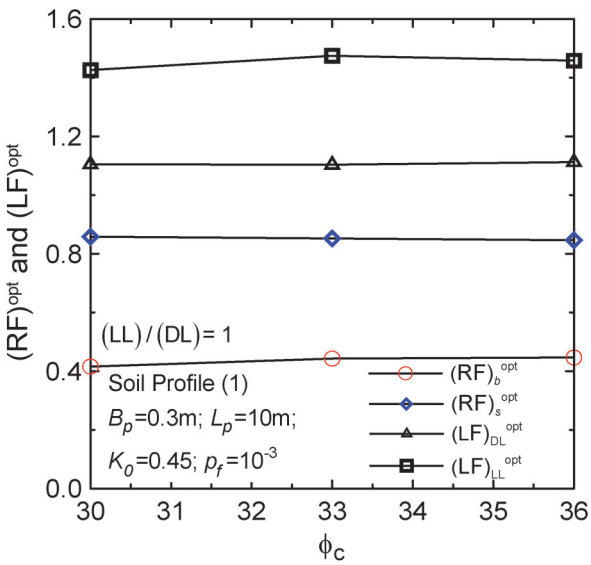

Figure 6.9. Optimal resistance and load factors versus ϕ_c

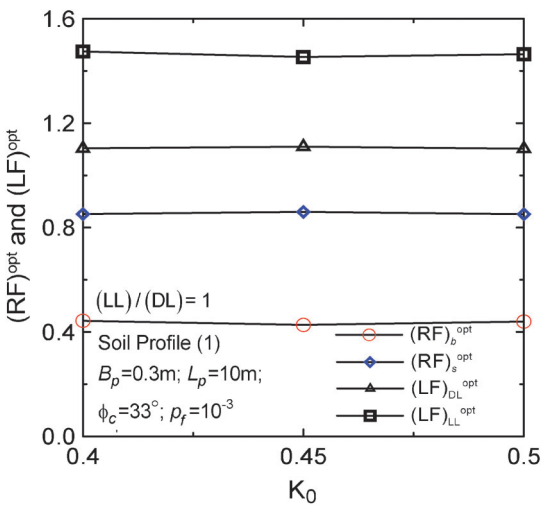

Figure 6.10. Optimal resistance and load factors versus K_0

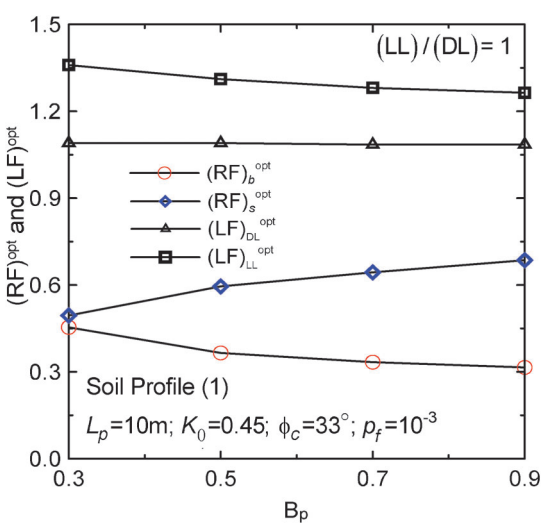

Figure 6.11. Optimal resistance and load factors versus B_p for L_p = 10m

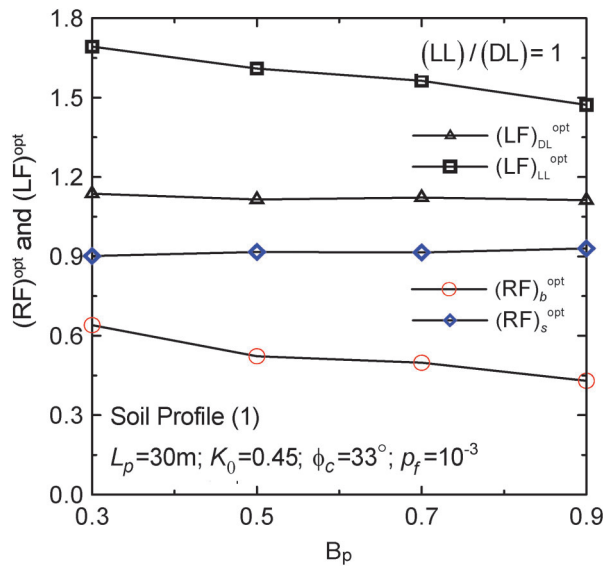

Figure 6.12. Optimal resistance and load factors versus B_p for L_p = 30m

Changes of optimal factors with respect to change of K_0 were examined for profile (1) with L_p = 10m, B_p = 0.3m, ϕ_c = 33°, (LL)/(DL) = 1.0, and $p_f = 10^{-3}$, as shown in Figure 6.10. The figure shows that the optimal factors are insensitive to K_0 changes.

Figure 6.11 shows a plot of the optimal factors versus the pile diameter B_p for L_p = 10m, and Figure 6.12 represents a plot of those with respect to B_P for L_p = 30m for profile (1) [K_0 = 0.45, ϕ_c = 33°, (LL)/(DL) = 1.0, and $p_f = 10^{-3}$]. In both cases, although the optimal factor for dead load was insensitive to B_p, the other optimal factors did vary significantly as B_p increased. This was mainly because $Q_{b,ult}/Q_{sL}$ increased as B_p increased and the degree of uncertainty of $\underline{Q}_{b,ult}$ was different from that of Q_{sL}.

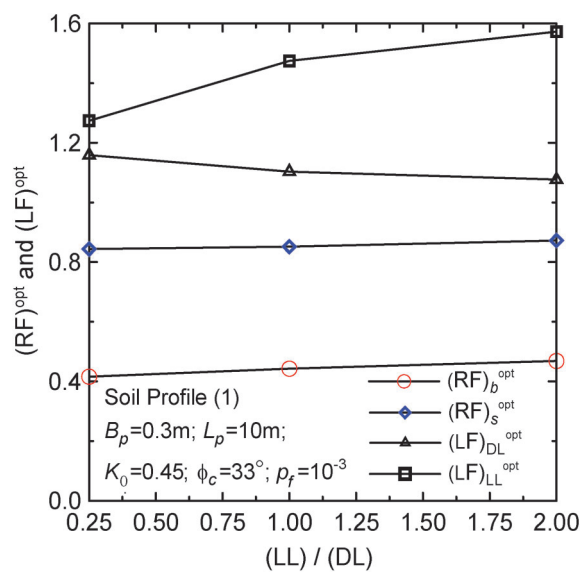

Figure 6.13. Optimal resistance and load factors versus (LL)/(DL)

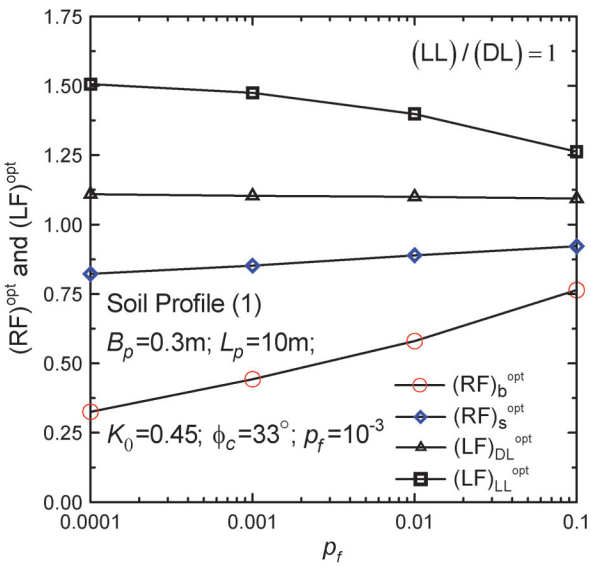

Figure 6.14. Optimal resistance and load factors versus p_f for soil profile (1).

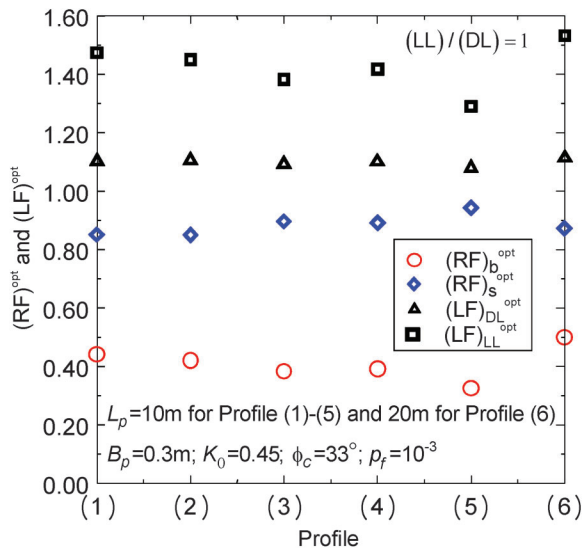

Figure 6.15. Optimal resistance and load factors for different profiles [profile (1) – (6)]

The optimal factors for $Q_{b,ult}$, Q_{sL}, and LL increase and that for DL decreases as (LL)/(DL) increases, as shown in Figure 6–13 for profile (1) with L_p = 10m, B_p = 0.3m, K_0=0.45, ϕ_c = 33°, and p_f = 10^{-3}.

Figure 6.14 illustrates, for soil profile (1), the gradual increase of resistance factors and decrease of load factors with increasing p_f.

Figure 6.15 shows the optimal resistance and load factors calculated for all the schematic profiles with L_p = 10m for profile (1) – (5) and L_p = 20m for profile (6), B_p = 0.3m, K_0 = 0.45, ϕ_c = 33°, (LL)/(DL) = 1.0, and p_f = 10^{-3}. It shows that the resistance factors are quite insensitive to details in the soil profile, and selection of conservative values based on a number of soil profiles will not lead to over-conservative design.

From extensive calculations of resistance factors, we found that the optimum factors were dependent on the profile and on the ratio $Q_{b,ult}^{(n)}$/ $Q_{sL}^{(n)}$. To quantify the effect of $Q_{b,ult}^{(n)}$/ $Q_{sL}^{(n)}$ on resistance factors, we calculated $(RF)_b$ and $(RF)_s$ using equation (3.10) varying L_p (10 – 30m), B_p (0.3– 0.9m) for each profile assuming that K_0 = 0.45 and ϕ_c = 33° (Figure 6–16 for p_f = 10^{-3} and Figure 6–17 for p_f = 10^{-4}). From Figure 6.16 and Figure 6.17, it is clear that $(RF)_b$ increases and $(RF)_s$ decreases as $Q_{b,ult}^{(n)}$/ $Q_{sL}^{(n)}$ increases.

It should be noted that we believe the equation used to calculate unit shaft resistance to be conservative, perhaps more than just slightly so, for lower relative densities. This means that research is still needed on this topic. An implication is that equivalent factors of safety will result somewhat on the high end of the range.

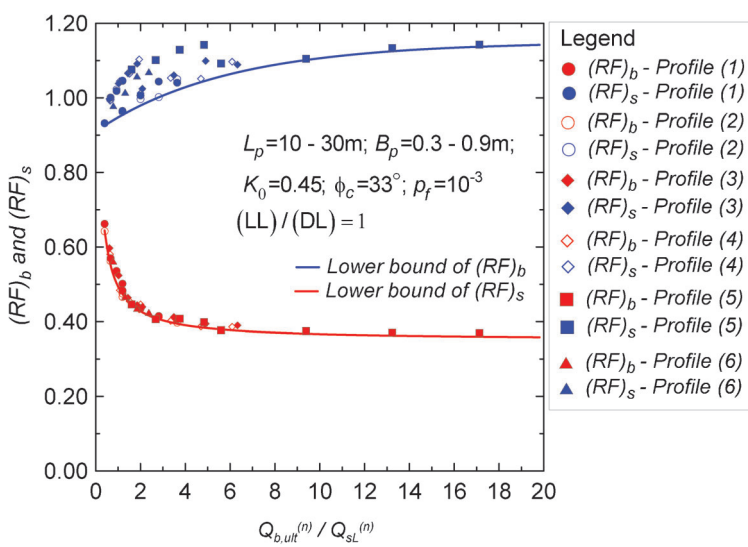

Figure 6.16. $(RF)_b$ and $(RF)_s$ versus $Q_{b,ult}^{(n)}$/ $Q_{sL}^{(n)}$ for all the profiles (1) – (6) for p_f = 10^{-3}

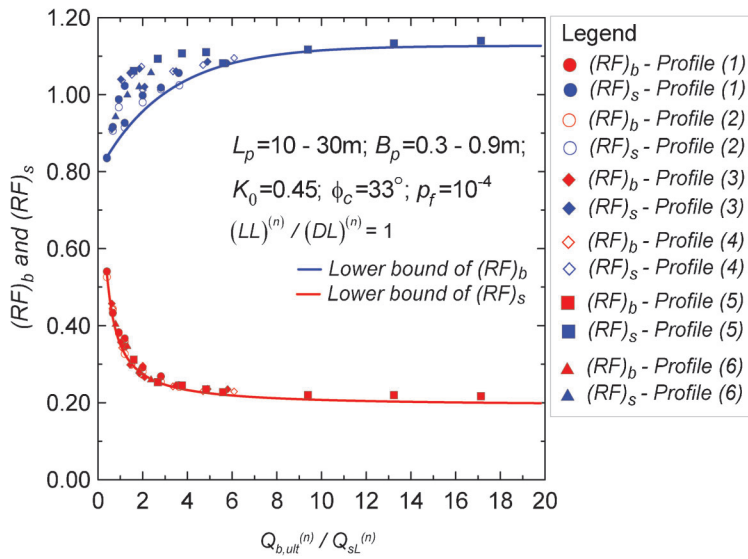

Figure 6.17. $(RF)_b$ and $(RF)_s$ versus $Q_{b,ult}^{(n)}/\ Q_{sL}^{(n)}$ for profiles (1) – (6) for $p_f = 10^{-4}$.

6.6. Suggested values of Resistance Factors

From Figure 6.16 and Figure 6.17, which were prepared for (LL)/(DL) = 1.0, the equations representing the lower bounds of $(RF)_b$ and $(RF)_s$ for $p_{f,\text{target}} = 10^{-3}$ and 10^{-4} are:

$$(RF)_{b,(\text{LL})/(\text{DL})=1} = 0.35\exp\left[\frac{0.48}{\left(Q_{b,ult}^{(n)}/Q_{sL}^{(n)}\right)+0.39}\right] \tag{6.9}$$

$$(RF)_{s,(\text{LL})/(\text{DL})=1} = 1.15-0.24\exp\left[-0.17\left(Q_{b,ult}^{(n)}/Q_{sL}^{(n)}\right)\right] \tag{6.10}$$

for $p_{f,\text{target}} = 10^{-3}$ and

$$(RF)_{b,(\text{LL})/(\text{DL})=1} = 0.20\exp\left[\frac{0.87}{\left(Q_{b,ult}^{(n)}/Q_{sL}^{(n)}\right)+0.47}\right] \tag{6.11}$$

$$(RF)_{s,(\text{LL})/(\text{DL})=1} = 1.14-0.33\exp\left[-0.33\left(Q_{b,ult}^{(n)}/Q_{sL}^{(n)}\right)\right] \tag{6.12}$$

for $p_{f,\text{target}} = 10^{-4}$.

The calculations of $(RF)_b$ and $(RF)_s$ using equations (6.9) – (6.12) were done for (LL)/(DL) = 1. To account for the effects of (LL)/(DL) on $(RF)_b$ and $(RF)_s$, we calculated $(RF)_b$ and $(RF)_s$ also for (LL)/(DL) = 0.25 and 2. The calculated $(RF)_b$ and $(RF)_s$ for these (LL)/(DL) ratios were compared with those for (LL)/(DL) = 1.0. Table 6.1 and Table 6.2 summarize the percentages of increase or decrease of $(RF)_b$ and $(RF)_s$ when (LL)/(DL) changes to 0.25 or 2 from 1 for $p_{f,\text{target}} = 10^{-3}$ and 10^{-4}, respectively.

The mean factor of safety $(\text{FS})_{\text{mean}}$ calculated using equation (3.13) is plotted in Figure 6.18, in which they are also compared to the value of 3 for the FS commonly used in driven pile designs . $(\text{FS})_{\text{mean}}$ tends to increase with increasing $Q_{b,ult}^{(n)}/\ Q_{sL}^{(n)}$. This is in agreement with our earlier observation that our shaft resistance estimation tends to be conservative for lower relative densities, when $Q_{b,ult}\ /\ Q_{sL}$ will tend to be lower. For very high $Q_{b,ult}^{(n)}/Q_{sL}^{(n)}$, $(\text{FS})_{\text{mean}}$ values were as high as 3.4 for $p_f = 10^{-3}$ and 5.2 for $p_f = 10^{-4}$. The very

TABLE 6.1
Percentage of increase/decrease of $(RF)_b$ and $(RF)_s$ when (LL)/(DL) =1 changes to 0.25 or 2 for $p_{f,\text{target}} = 10^{-3}$

	(LL)/(DL) = 0.25		(LL)/(DL) = 2	
Profile	$(RF)_b$	$(RF)_s$	$(RF)_b$	$(RF)_s$
(1)	−8.2%	−4.1%	+6.6%	+5.6%
(2)	−6.2%	−4.5%	+8.4%	+5.9%
(3)	−9.5%	−3.3%	+6.3%	−0.2%
(4)	−8.0%	−2.3%	+4.1%	+2.3%
(5)	−6.1%	−3.1%	+5.9%	−0.2%
(6)	−10.1%	−3.9%	+3.4%	−0.7%
Average	−8.0%	−3.5%	+5.8%	+2.1%

TABLE 6.2
Percentage of increase/decrease of $(RF)_b$ and $(RF)_s$ when (LL)/(DL) =1 changes to 0.25 or 2 for $p_{f,\text{target}} = 10^{-4}$

	(LL)/(DL) = 0.25		(LL)/(DL) = 2	
Profile	$(RF)_b$	$(RF)_s$	$(RF)_b$	$(RF)_s$
(1)	−13.0%	−2.2%	+3.5%	+0.7%
(2)	−9.6%	−3.6%	+4.9%	+0.6%
(3)	−9.4%	−1.6%	+9.2%	−0.1%
(4)	−11.3%	−3.2%	+5.3%	+1.1%
(5)	−7.7%	−2.0%	+4.0%	+0.5%
(6)	−10.8%	−4.4%	+9.2%	−3.7%
Average	−10.3%	−2.8%	+6.0%	−0.2%

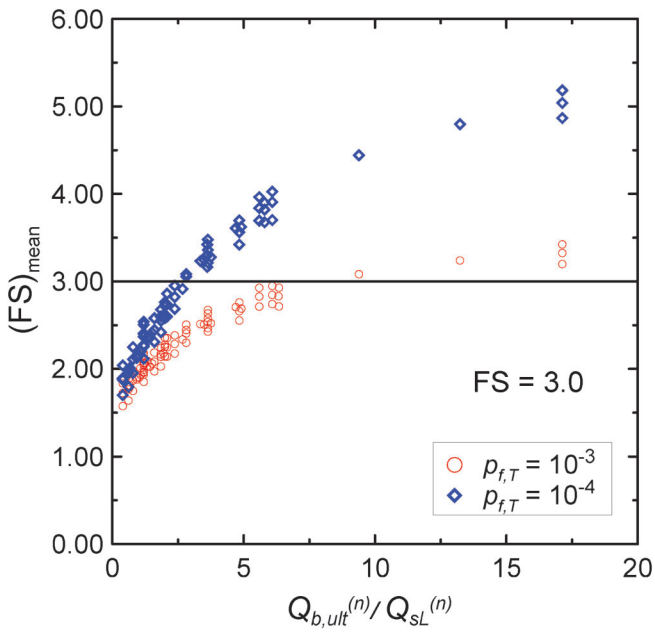

Figure 6.18. $(FS)_{mean}$ calculated using equation (3.13) compared with typical ASD FS value of 3.0 for $p_f = 10^{-3}$ and 10^{-4}.

high $(FS)_{mean}$ values were calculated for exceedingly large (bordering on unrealistic) pile diameters (0.9m), short pile lengths (10m), very low relative density (20%) along the shaft and high relative density (80%) at the base under fully-saturated condition.

Resistance factors $(RF)_b^{code}$ and $(RF)_s^{code}$ for $p_f = 10^{-3}$ that are compatible with the AASHTO load factors are given in Table 6.3. The relatively high shaft resistance factors in part reflect a relatively conservative equation for shaft resistance that we used.

CHAPTER 7. RESISTANCE FACTORS OF DRIVEN PILES IN CLAY

7.1. Introduction

In this chapter, we develop the resistance factors for driven piles in clay for a soil variable-based design method. We first discuss the calculation of the limit unit base and shaft resistance in clay. Systematic probabilistic analyses are then performed with the uncertainties (probability density functions) associated with each of the soil variables appearing in the design equations carefully quantified. The analyses rely on Monte-Carlo (M-C) simulations and a target acceptable risk (i.e., target probability of failure) to identify the corresponding most probable limit state (at which the resistance equals imposed loads with probability equal to the probability of failure). The load and resistance factors are obtained by dividing the limit state values of loads and resistances by the corresponding nominal values.

7.2. Unit Base and Shaft Resistance: Purdue Clay Method for Displacement Piles

To calculate the unit shaft resistance q_{sL} in clay, we used the α method, according to which:

$$q_{sL} = \alpha s_u \tag{7.1}$$

where s_u is the undrained shear strength. To determine α, Basu et al. (2009) performed finite element analysis coupled with an advanced constitutive model to investigate the mechanics of load transfer at the interface of displacement piles in clay. Based on those analyses, they proposed the following equations for α :

$$\alpha_{ST} = 1.03\left[A_1 + (1-A_1)\exp\left\{-\left(\frac{\sigma_v'}{p_A}\right)(\phi_c - \phi_{r,\min})^{A_2}\right\}\right] \tag{7.2}$$

$$\alpha_{LT} = 1.28\left(\frac{s_u}{\sigma_{v0}'}\right)^{-0.05}\left[A_1 + (1-A_1)\exp\left\{-\left(\frac{\sigma_{v0}'}{p_A}\right)(\phi_c - \phi_{r,\min})^{A_3}\right\}\right] \tag{7.3}$$

where α_{ST} is a short-term value of α; α_{LT} is a long-term value of α; σ_v' is the *in situ* vertical effective stress at the depth at which q_{sL} is calculated; ϕ_c is the critical-state friction angle; $\phi_{r,\min}$ is the minimum residual state

TABLE 6.3
Resistance factors calculated for different combinations of $Q_{b,ult}^{(n)}/Q_{sL}^{(n)}$, (LL)/(DL), and $p_{f,target}$ adjusted with the AASHTO load factors [$(LF)_{DL}^{code} = 1.25$ and $(LF)_{LL}^{code} = 1.75$]

		$Q_{b,ult}^{(n)}/Q_{sL}^{(n)}$									
		0.5		1		2		5		10	
$p_{f,target}$	(LL)/(DL)	$(RF)_b^{code}$	$(RF)_s^{code}$	$(RF)_s^{code}$	$(RF)_s^{code}$	$(RF)_s^{code}$	$(RF)_s^{code}$	$(RF)_s^{code}$	$(RF)_s^{code}$	$(RF)_s^{code}$	$(RF)_s^{code}$
10^{-3}	0.25	0.55	0.89	0.45	0.91	0.39	0.94	0.35	1.01	0.34	1.06
	1	0.60	0.93	0.49	0.95	0.43	0.98	0.38	1.05	0.37	1.11
	4	0.63	0.95	0.52	0.97	0.45	1.00	0.40	1.07	0.38	1.13
10^{-4}	0.25	0.44	0.83	0.32	0.88	0.25	0.94	0.21	1.04	0.19	1.09
	1	0.49	0.86	0.36	0.90	0.28	0.97	0.23	1.08	0.22	1.13
	4	0.52	0.85	0.38	0.89	0.30	0.96	0.25	1.07	0.23	1.12

friction angle; p_A is the reference stress value (100kPa); A_1 is a coefficient equal to 0.43 for $\phi_c - \phi_{r,\min} \geq 12$ degrees, 0.75 for $\phi_c - \phi_{r,\min} \leq 5$ degrees and a linearly interpolated value between 0.43 and 0.75 for 5 degrees $\leq \phi_c - \phi_{r,\min} \leq 12$ degrees; A_2 is a coefficient determined by equation $A_2 = 0.55 + 0.43 \ln (s_u / \sigma_v')$; A_3 is a coefficient determined by equation $A_3 = 0.64 + 0.40 \ln (s_u / \sigma_v')$.

Equations (7.2) and (7.3) capture the dependence of shaft resistance on the undrained shear strength, effective normal stress and the difference between critical-state friction angle and minimum residual-state friction angle. Equation (7.3) was proposed to estimate the shaft resistance available after dissipation of pore pressures caused by pile installation, which is what we are interested in when designing a pile.

Salgado et al. (2004) used finite element limit analysis to investigate the upper and lower bound of the ratio of net bearing capacity q_{bL}^{net}, defined as

$$q_{bL}^{\text{net}} = q_{bL} - q_0 \tag{7.4}$$

where q_0 is the surcharge at the pile base level, to undrained shear strength s_u for piles. Based on their analysis, Salgado et al. (2004) found that the lower and upper bound values of N_c $\left(= q_{bL}^{\text{net}} / s_u\right)$ increase with increasing relative depth D/B (the ratio of the length of the pile to the width of the pile), as Figure 7.1 shows. For $D/B = 5.0$, the lower and upper bound values of N_c are 11.0 and 13.7, respectively.

By substituting N_c into equation (7.4), the equation of the limit unit base resistance is:

$$q_{bL} = N_c s_u + q_0 \tag{7.5}$$

Equations (7.1)–(7.5) constitute the basis for the Purdue Clay Method for Displacement Piles (PCM-DP).

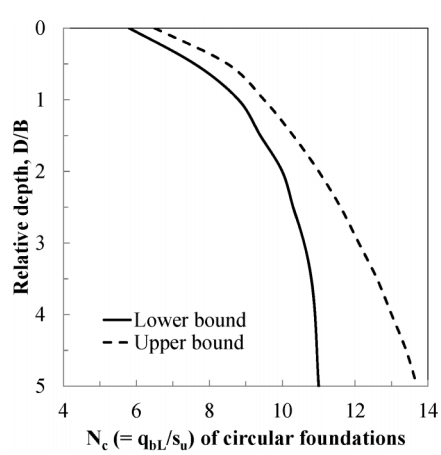

Figure 7.1 Limit unit base resistance of circular foundation versus depth (Salgado et al. 2004)

7.3. Uncertainty Assessment of Design Variables and Model Uncertainty

We assumed that the pile geometry (defined by B_p and L_p) is deterministic. This is because driven piles are typically prefabricated so the uncertainty of pile geometry is negligible. It is necessary to consider the variability of soil variables and model transformations. The soil variables required for pile capacity calculations are ϕ_c, $\phi_{r,\min}$, s_u and soil unit weight γ. We will discuss how we assigned variability parameters to these variables and to the model transformations next.

7.3.1. Uncertainties in Soil Variables

The soil variables required for pile capacity calculations in this analysis are ϕ_c, $\phi_{r,\min}$, s_u and soil unit weight γ (required to calculate the in situ stresses). Based on experimental observations, Bolton (1986) reported a $\pm 1^\circ$ band encompassing all measurements of the critical-state friction angle ϕ_c for sand. It is reasonable to assume that this forms an upper bound to the variability for clay. Thus, the expectation of the maximum error in the estimation of ϕ_c at a particular site is $\pm 1^\circ$. Assuming that ϕ_c follows a normal distribution, the spread of 2° results in a standard deviation of 0.33° for ϕ_c based on the 6σ method (Foye 2005). Because ϕ_c of different clays typically lie within the 15°–30° range (Salgado 2008), the maximum and minimum values of COV of ϕ_c are 0.33°/15° = 0.022 and 0.33°/30° = 0.011 at a particular site. In this study, we conservatively assume the COV of ϕ_c to be equal to 0.03, which is greater than the maximum value of 0.022 estimated in this manner.

We also assume that the maximum error in the estimation of $\phi_{r,\min}$ is $\pm 1^\circ$. For a clay such as Boston Blue Clay, there is no softening towards lower, residual values of friction angle, so $\phi_{r,\min}$ is equal to ϕ_c and is therefore within the 15°–30° range, which is a typical range of ϕ_c in clay. For a clay such as London Clay, however, $\phi_{r,\min}$ is within the 7.5°–9.4° range of much lower friction angles (Bishop et al. 1971). From these previous studies, we assume that the minimum value of $\phi_{r,\min}$ is 7.5°. Assuming that $\phi_{r,\min}$ follows a normal distribution with a standard deviation of 0.33°, the maximum COV of $\phi_{r,\min}$ is 0.33°/7.5° = 0.044. In this study, we conservatively assume the COV of $\phi_{r,\min}$ to be equal to 0.05, which is greater than the maximum value of 0.044 that we calculated.

Many researchers have studied the variability of soil unit weight. Baecher and Christian (2003) reported, based on studies by Lee et al. (1983), Lacasse and Nadim (1996) and Lumb (1974), that the COV of unit weight does not exceed 0.1. Kim (2008) corroborates the finding based on studies by Phoon and Kulhawy (1999), White et al. (2005) and Hammit (1966). In our research, we assumed that γ follows a normal distribution with a COV = 0.1.

Equations (7.1), (7.2), (7.3), and (7.5) show that the limit unit base and shaft resistances are functions of

undrained shear strength s_u. The equation for s_u in terms of cone resistance is:

$$s_u = \frac{q_c - \sigma_v}{N_k} \tag{7.6}$$

where q_c is cone resistance, σ_v is vertical stress and N_k is the cone factor. The minimum value of N_k is 11.0 and the maximum value of N_k is 13.7 (Salgado et al. 2004). In this research, we assume cone resistance q_c for a soil profile as the starting point in design and calculate the PDF of undrained shear strength s_u from the PDF of q_c and from the PDF of the relationship between q_c and s_u given by equation (7.6). According to the research by Foye (2006), the COV of q_c in clay is 0.06 and q_c follows a normal distribution. In this study, we followed the proposed COV and distribution of q_c by Foye (2006).

An alternative way to estimate the undrained shear strength s_u of clay, commonly used by some DOTs, is the unconfined compression (UC) test. Based on experimental observations, Fredlund and Dahlman (1971) reported that the COV of s_u from UC tests lie within the 0.40 to 0.50 range. This range is 0.27 to 0.41 according to Ladd, et al. (1971) (based on data for soft Bangkok clay), 0.11 to 0.45 according to Wolff (1985), and 0.30 to 0.40 according to Shannon and Wilson Inc. and Wolff (1994). Based on these studies, the COV of s_u from UC tests lies in the 0.11 to 0.50 range. In this study, we conservatively assumed the COV of s_u from UC tests to be 0.45. According to the studies by Spry et al. (1988) and Phoon and Kulhawy (1999), a lognormal distribution can be assumed for most soil properties. Using a lognormal distribution for s_u from UC test prevents random realizations of s_u from being negative, which would happen if a normal distribution with a high COV were assumed for possibly low to moderate values of nominal s_u. In these reasons, we assume the undrained shear strength s_u from UC test following lognormal distribution.

7.3.2. Model Uncertainties

If the input data are values of cone resistance q_c, the uncertainties in the $q_c \rightarrow s_u$ relationship must be considered. Equation (7.6) already implies the level of uncertainty in the $q_c \rightarrow s_u$ relationship since the cone factor N_k is expressed as a range. The upper and lower bound values of N_k are 13.7 and 11.0, respectively, with a range for N_k of 2.7. We can assess the standard deviation for a variable that has upper and lower bound values and follows a normal distribution using the 6σ method (Withiam et al. 1997, Foye et al. 2006):

$$\sigma = \frac{\text{Range}}{6} \tag{7.7}$$

where σ is the standard deviation. In this study, we assumed that the mean value of N_k is 12.35, and, assuming that N_k follows normal distribution, the standard deviation of N_k is 0.45, which is equal to the range divided by 6.0.

The relationship $s_u \rightarrow q_{bL}$ for a pile is similar physically to the $s_u \rightarrow q_c$ relationship. If the dimensions of the pile are given, we can obtain the lower and upper bound values of N_c from Figure 7.1. We assumed that the mean value of N_c is equal to the mean value of the lower and upper bound values. The range of N_c is the difference between the lower and upper bound value and we calculated the standard deviation of N_c based on the 6σ method from this range by assuming that N_c follows normal distribution. Typically, the relative depth of a pile is much greater than 5.0, so the maximum and minimum values of N_c are taken as 13.7 and 11.0. From this range, it is reasonable to set the mean and the standard deviation of N_c as 12.35 and 0.45, respectively.

The model uncertainty associated with q_{sL} arises in the estimation of α through the use of equation (7.3). Although equation (7.3) follows from rigorous finite element analysis which themselves introduce essentially no error in the results, there is an error when we compare equation (7.3) with field data. Figure 7.2 shows plots of the long-term α_{LT} from equation (7.3) and from field database.

From Figure 7.2, to quantify the error in the predicted value of α, which we will refer to as $\alpha_{equation}$, with respect to the field value α_{field}, we estimate the distribution of the ratio of $\alpha_{equation}$ to α_{field}. We found that the maximum and minimum value of the ratio of the $\alpha_{equation}$ (which is α_{LT}) from equation (7.3) to α_{field} is approximately 1.6 and 0.6, respectively. Additionally, the distribution of the ratio ($\alpha_{equation}/\alpha_{field}$) suggests that there is no bias. With the assumption that the ratio ($\alpha_{equation}/\alpha_{field}$) follows a normal distribution, the 6σ method leads to an estimate of the standard deviation of this ratio as 0.167 (=1.0/6.0). So, to incorporate the model uncertainty of shaft resistance in our analysis, we introduced a new variable M_α that follows a normal

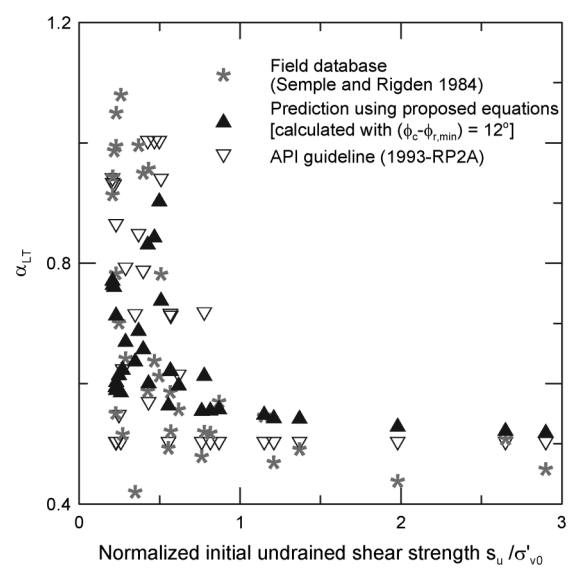

Figure 7.2 Comparison of α values predicted by the proposed equations with those calculated following the API RP-2A criterion and obtained from the field data reported by Sempel and Rigden (1984) (P. Basu et al 2010)

distribution with expectation $E(M_\alpha) = 1.0$ and standard deviation $S_{M\alpha} = 0.2$, which is more conservative than 0.167. The equation used to calculate unit limit shaft resistance in the Monte-Carlo simulation is:

$$q_{sL} = M_\alpha 1.28 \left(\frac{s_u}{\sigma'_{v0}}\right)^{-0.05} \left[A_1 + (1 - A_1)\exp\left\{-\left(\frac{\sigma'_{v0}}{p_A}\right)(\phi_c - \phi_{r,min})^{A_3}\right\}\right] s_u \quad (7.8)$$

7.3.3. Uncertainties in Applied Loads

According to Ellingwood and Tekie (1999), dead load follows a normal distribution with a bias factor of 1.05 and COV equal to 0.1. According to Nowak (1994) and FHWA (2001), the bias factor and COV for dead load are in the range 1.03−1.05 and 0.08−0.1, respectively, depending on the type of structural components. In this analysis, we assumed, that dead load follows a normal distribution with a bias factor = 1.05 and COV = 0.1.

Live load is often assumed to follow a lognormal distribution (Foye et al. 2006a). According to FHWA (2001), live load has a bias factor of 1.1–1.2 and a COV of 0.18. According to Ellingwood and Tekie (1999), however, live load is represented by a Type 1 distribution of largest values with a bias factor = 1.0 and COV = 0.25. We plotted the PDFs of the Type 1 extreme value distribution and the lognormal distribution for identical values of bias factor and COV, and found that the PDFs of both distributions are nearly identical for the range of live load values encountered in practice for piles. This finding is indirectly corroborated by Ghosn and Moses (1998), who separately calculated reliability indices for highway bridge structures with live loads following a lognormal distribution and a Type 1 extreme value distribution, and found that the results of both calculations were sufficiently close. Consequently, we decided to use the widely-used lognormal distribution to describe live loads. For most of the problems analyzed in this research, we conservatively chose a COV = 0.25 and the corresponding bias factor = 1.0, as recommended by Ellingwood and Tekie (1999).

7.4. Analysis

Monte-Carlo (M-C) simulations were performed to obtain the probability distributions of the capacity ($Q_{b,ult}$ + Q_{sL}), the demand (DL + LL) and their difference. We assumed in our analysis that the capacity and the demand are statistically independent. We also assumed that all the random variables — soil properties, loads and the variables representing model uncertainties — are uncorrelated.

We start with a soil profile with known (or assumed) mean values of ϕ_c, $\phi_{r,min}$ and γ. If undrained shear strength s_u is estimated from q_c, we assumed mean trend of CPT profile $q_c(z)$, where z is the depth. If unconfined compression (UC) tests are used to estimate s_u, we assumed mean values of s_u within the soil layers. We also assume a mean value of applied dead load $(DL)^{(mean)}$ and an (LL)/(DL) ratio (which gives the mean live load $(LL)^{(mean)}$). Then, we consider a displacement pile with an assumed length and an assumed mean diameter embedded in the soil profile. With the mean soil profile, applied loads and pile dimensions established, we start the first run of the M-C simulations (Figure 7.3).

We start with shaft resistance calculations at depth $z = 0$ m and move down along the pile shaft. If a mean cone resistance trend is given as input, random values of q_c, γ and N_k are generated for a particular depth to calculate a random value of s_u using equation (7.6). If mean undrained shear strength data from UC tests within the soil layers are given as input, random values of s_u and γ are generated for a particular depth. Subsequently, a random value of M_α is generated to calculate a random value of shaft resistance for that depth using equation (7.8). This shaft capacity calculation is repeated for different depths along the pile shaft with new random values of q_c (typically, soil sub-layers of 1 m thickness with different mean q_c were assumed), s_u and the other variables. By summation of the calculated shaft capacities at the different depths over the entire pile length, we can obtain the random value of the total shaft resistance Q_{sL}. Then, as we reach the pile base, a random value of the base resistance $Q_{b,ult}$ is calculated using the random values of soil variables, a random value of s_u, a random value of B_p and a random value of N_c. Equations (7.5) and (7.8) were used to obtain these random values of $Q_{b,ult}$ and Q_{sL}. After calculating the random $Q_{b,ult}$ and Q_{sL}, random values of (DL) and (LL) are generated and the difference ($Q_{b,ult}$ + Q_{sL}) − (DL + LL) between the random values of capacity C = $Q_{b,ult}$ + Q_{sL} and demand D = (DL + LL) is calculated. The above set of calculations completes one run of the M-C simulations.

The above set of calculations (corresponding to one M-C run) was repeated n_{total} times; the value of n_{total} depends on the target probability of failure. We will call this repeated n_{total} number of calculations one set of M-C simulations. Each set of M-C simulations generated the probability distributions (or histograms) of the capacity and demand. The number of runs n_f for which ($Q_{b,ult}$ + Q_{sL}) − (DL + LL) was less than zero (i.e., the number of times for which demand exceeded capacity) was noted. The ratio n_f / n_{total} approximates the probability of failure p_f. Theoretically, for a continuous probability distribution of (capacity – demand), the area under the PDF curve on the negative side of the (capacity – demand) axis gives p_f.

7.5. Results

The primary goal we have with this chapter is to provide resistance factors that can be useful in design of driven piles in clay deposits. However, before doing that, we will investigate how the optimal resistance and load factors change with different field conditions and

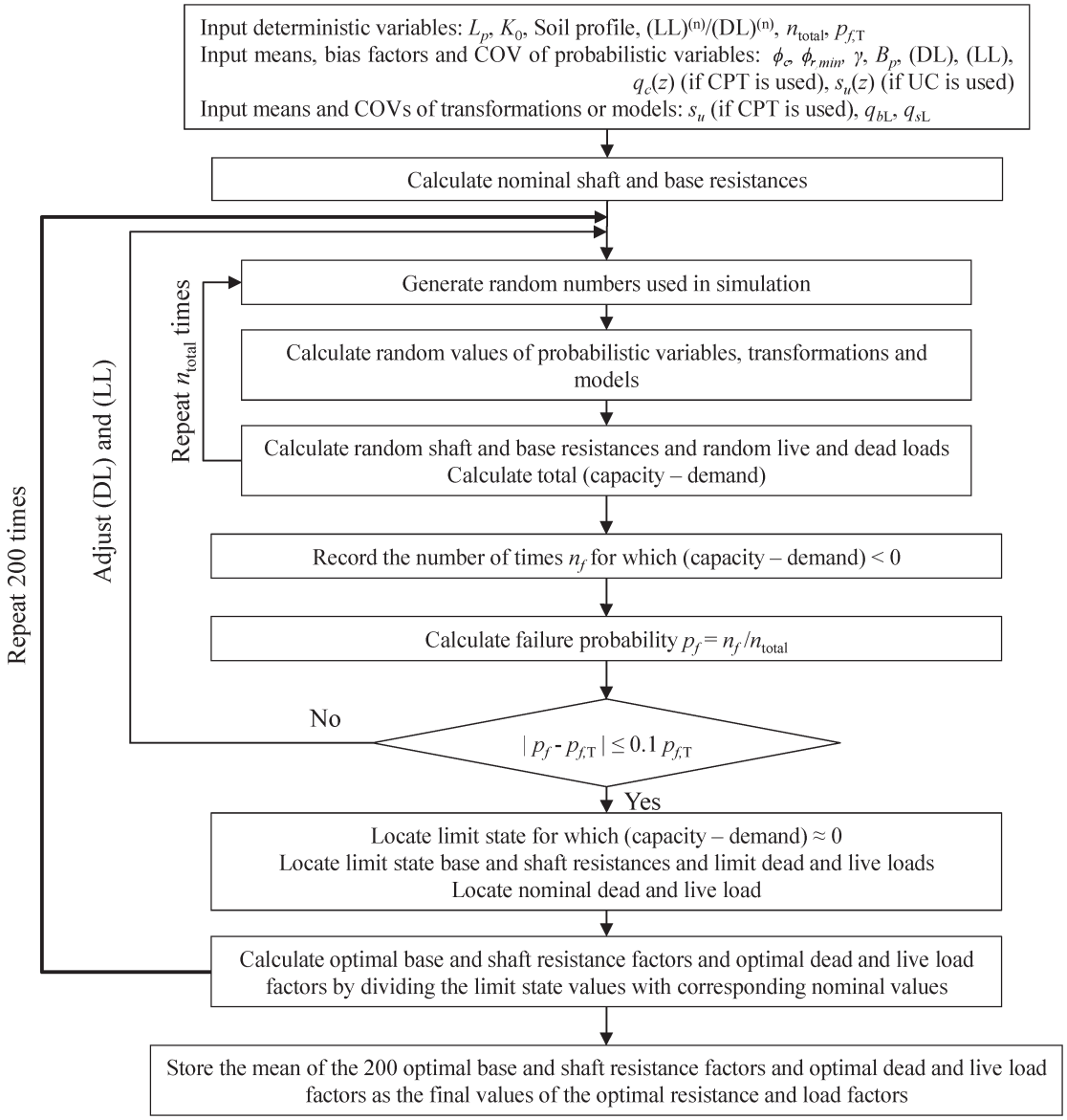

Figure 7.3 Flow chart of Monte-Carlo simulations

variables. We will consider a range of soil properties and pile dimensions that may occur in field conditions.

Figure 7.4 shows the details of a homogeneous, completely saturated deposit of normally consolidated clay with $s_{u,mean} / \sigma'_{v0,mean} = 0.17$ with the water table located at the ground surface. For this deposit, we considered three different clay types. All clay deposits have identical mean critical-state friction angle $\phi_{c,mean} = 21^\circ$. However, we considered three different values of mean minimum residual-state friction angle $\phi_{r,min,mean}$: 21°, 16°, and 9°. We estimated the mean unit weight, the mean void ratio and the mean vertical stress at the desired depth along the pile using the relation between unit weight and void ratio in clay, $\gamma = (G_s + Se)/(1 + e)$ (G_s = specific gravity of clay solid particles = 2.67, S = degree of saturation = 1.0), and the relation between mean effective stress and void ratio, $e = N - \lambda \ln (p'/p'_A)$ (p'_A = reference mean effective stress, N = void ratio at the reference mean effective stress, λ = the slope of normal consolidation line on e-ln(p') plane). If the mean cone resistance profiles $q_{c,mean}(z)$ are given as input, the mean undrained shear strength s_u follows

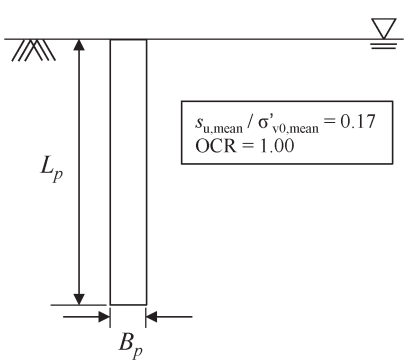

Figure 7.4 Details of soil profile

from equation (7.6). The $q_{c,\text{mean}}(z)$ curves were initially back-calculated from void ratio, stress state and a pre-assumed ratio of undrained shear strength to effective vertical stress (s_u / σ'_{v0}). If the mean undrained shear strength $s_{u,\text{mean}}$ was given as input, the $s_{u,\text{mean}}$ was back-calculated from void ratio, stress state and a pre-assumed ratio of undrained shear strength to effective vertical stress (s_u / σ'_{v0}).

The relative depth or slenderness ratio (D / B = L_p / B_p) and diameter and length of driven piles that we considered in this research ranged from values that would be considered very low to values considered high for real field conditions. We studied the responses of three driven piles with (A) mean diameter $B_{p,\text{mean}}$ = 0.3 m and length L_p = 10 m, (B) mean diameter $B_{p,\text{mean}}$ = 0.6 m and length L_p = 10 m and (C) mean diameter $B_{p,\text{mean}}$ = 0.9 m and length L_p = 10 m. With this, we have covered the complete range expected for driven piles, certainly onshore.

The proportion of live and dead loads acting on a bridge structure depends on the span length (Hansell and Viest 1971). Titi et al. (2004) tabulated the (LL)/(DL) ratios recommended by AASHTO and FHWA for design of bridge structures; the recommended values vary over a wide range of 0.28–1.92. Accordingly, we considered (LL)/(DL) = 0.25, 1.0 and 2.0.

7.5.1. Results for CPT-Based Design

In this section, we describe how the optimal resistance and load factors change with different field conditions for CPT-based design. Subsequently, we will compare the optimal resistance factors with code-adjusted resistance factors. We also propose design values of code-adjusted resistance factors for use with CPT data as input.

Figure 7.5(a) shows the plots of the load and resistance factors with respect to ($\phi_{c,\text{mean}} - \phi_{r,\text{min,mean}}$) for driven pile A with (LL)/(DL) = 0.25 with target failure probability $p_f = 10^{-3}$ when mean cone resistance trend is given as input. Figure 7.5(b) shows the plots of the load and resistance factors with respect to ($\phi_{c,\text{mean}} - \phi_{r,\text{min,mean}}$) for driven pile C with (LL)/(DL) = 2.0 with target failure probability $p_f = 10^{-3}$. In Figure 7.5, it is evident that the optimal load and resistance factors are independent on ($\phi_{c,\text{mean}} - \phi_{r,\text{min,mean}}$). The minor variations in the resistance and load factors observed in Figure 7.5 are typical of all driven piles; the fluctuations in the load and resistance factors were rather random without any particular trend.

Figure 7.6(a) shows the plots of the load and resistance factors with respect to diameter to length ratio for the driven piles considered in our study with (LL)/(DL) = 0.25, $\phi_{c,\text{mean}} - \phi_{r,\text{min,mean}} = 12^\circ$ and target failure probability $p_f = 10^{-3}$ when mean cone resistance trend is given as input. Figure 7.6(b) shows the plots of the load and resistance factors with respect to diameter to length ratio for considered driven piles with (LL)/(DL) = 2.0, $\phi_{c,\text{mean}} - \phi_{r,\text{min,mean}} = 12^\circ$ and target failure probability $p_f = 10^{-3}$. In both Figure 7.6 (a) and (b), as diameter to length ratio B_p/L_p increases, the shaft resistance factor increases slightly and the base resistance factor decreases slightly. Figure 7.6 also shows that the load factors are nearly independent on the diameter to length ratio B_p/L_p. The trends observed in Figure 7.6, are typical of all the other cases. Although there are slight variations in resistance factor with respect to diameter to length ratio, for practical purposes, these variations can be considered negligible.

Soil properties and pile dimensions have practically no effect on the resistance and load factors. The (LL)/(DL) ratio, however, has a non-negligible effect on the

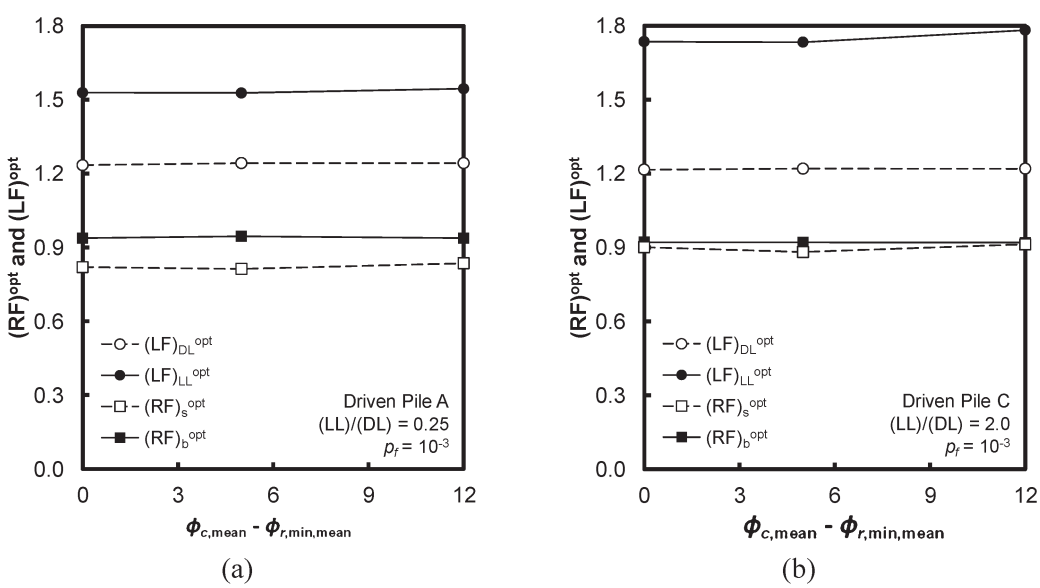

Figure 7.5 Optimal load and resistance factors versus $\phi_{c,\text{mean}} - \phi_{r,\text{min,mean}}$ for (a) driven pile A and (b) driven pile C when $q_{c,\text{mean}}(z)$ is given as input

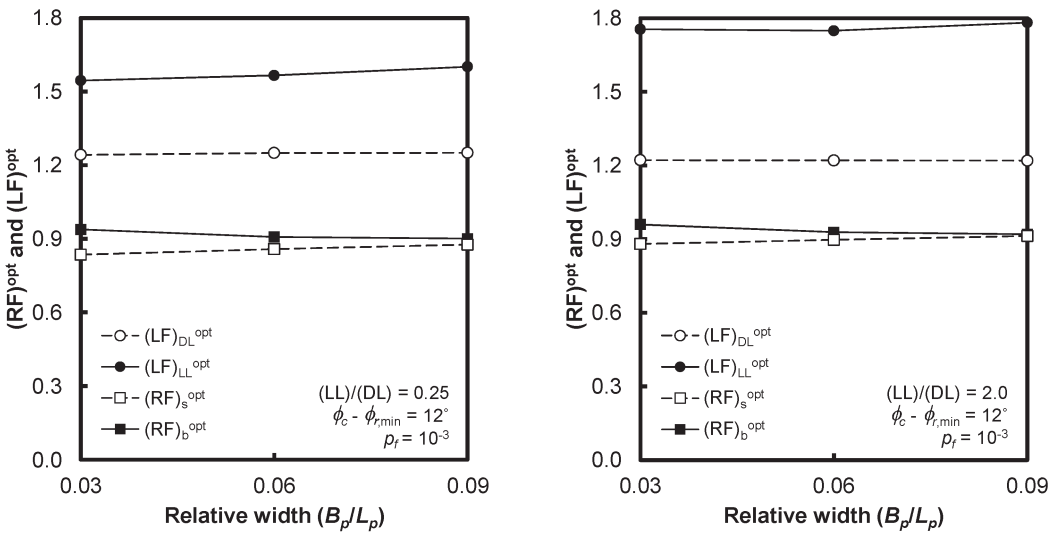

(a) (b)

Figure 7.6 Optimal load and resistance factors versus diameter to length ratio for (a) LL/DL = 0.25 and (b) LL/DL = 2.0 when $q_{c,\text{mean}}(z)$ is given as input

live load factor. Figure 7.7(a) and Figure 7.7(b) show the plots of the load and resistance factors with respect to the (LL)/(DL) ratio for driven pile A and driven pile C, respectively when $\phi_{c,\text{mean}} - \phi_{r,\text{min,mean}} = 12°$, target failure probability $p_f = 10^{-3}$, and mean cone resistance trend is given as input. In both Figure 7.7(a) and Figure 7.7(b), the optimal resistance factors increase slightly and the optimal dead load factor decreases slightly with increase in (LL)/(DL) ratio; however, the optimal live load factor increases significantly with increase in (LL)/(DL) ratio.

Figure 7.7 implies that (LL)/(DL) ratio affects the mean factor of safety $(\text{FS})_{\text{mean}}$ because of a significant change of live load factor. Figure 7.8(a) and Figure 7.8(b) show $(\text{FS})_{\text{mean}}$ versus p_f for driven piles A and C, respectively, when mean cone resistance trend is given as input. To study the effect of p_f, we performed additional M-C simulations with target $p_f = 10^{-2}$. Both Figure 7.8(a) and Figure 7.8(b) shows that $(\text{FS})_{\text{mean}}$ increases with decrease of p_f. Also, the larger the (LL)/(DL) ratio, the higher the $(\text{FS})_{\text{mean}}$ is. This shows that $(\text{FS})_{\text{mean}}$ is not a true indicator of the reliability of a design; for the same mean factor of safety, the probabilities of failure are different for different proportions of applied live to dead load. From another viewpoint, for the same probability, a higher factor of safety is required to account for the higher uncertainty levels of live loads if (LL)/(DL) ratio increases.

Figure 7.9(a) and Figure 7.9(b) plot the optimal resistance and load factors versus the probability of

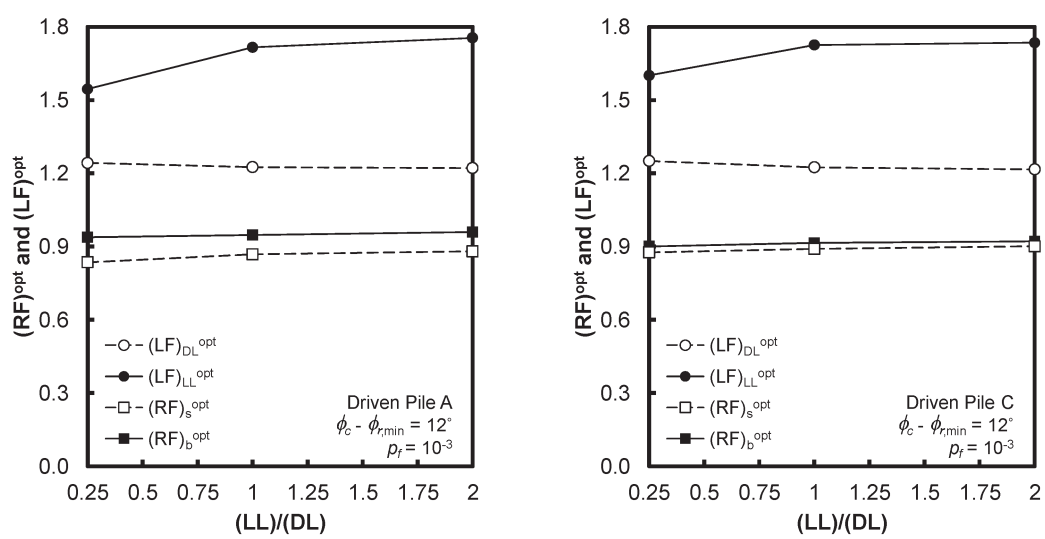

(a) (b)

Figure 7.7 Optimal load and resistance factors versus live load to dead load ratio for (a) driven pile A and (b) driven pile C when $q_{c,\text{mean}}(z)$ is given as input

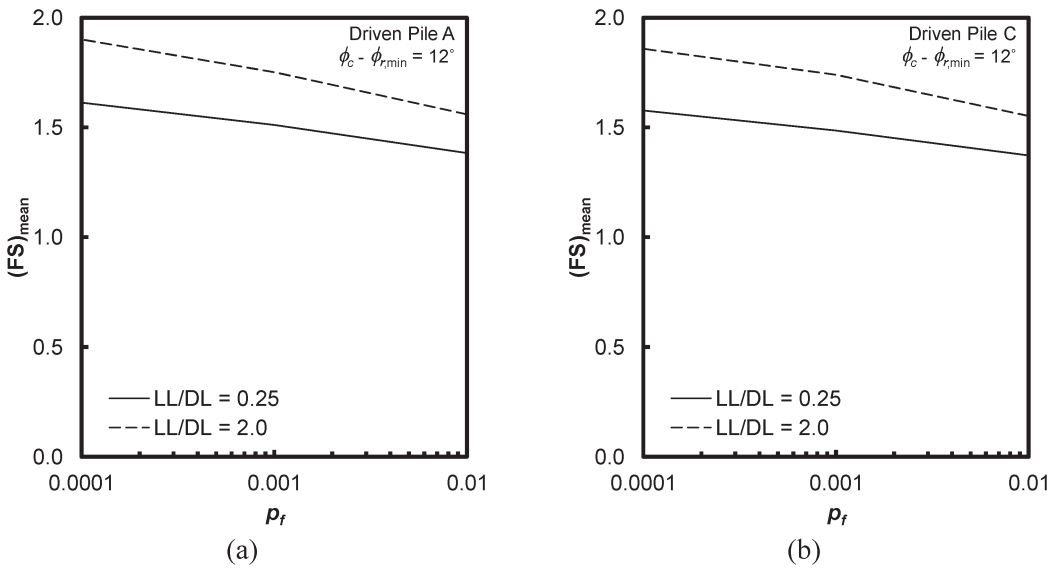

Figure 7.8 Mean factor of safety versus target probability of failure for (a) driven pile A and (b) driven pile C when $q_{c,\text{mean}}(z)$ is given as input

failure p_f for a driven pile A with $\phi_{c,\text{mean}} - \phi_{r,\text{min,mean}} = 12^\circ$ when (LL)/(DL) = 0.25 and (LL)/(DL) = 2.0, respectively. Both figures show the effect of p_f on the optimal resistance and load factors. As p_f increases, the resistance factors increase slightly and the dead load factor decreases slightly. The live load factor, however, significantly deceases with increase of p_f. So, it is evident that the change in $(FS)_{\text{mean}}$ due to change in p_f is mainly influenced by the live load.

Figure 7.10 (a) and Figure 7.10 (b) show the optimal and code-adjusted resistance factors for driven pile A and driven pile C, respectively when $p_f = 10^{-3}$ and mean cone resistance trend is given as input. The code-adjusted resistance factors were obtained from the optimal resistance factors by using equation (3.10). For both driven piles, the code-adjusted resistance factors are slightly more conservative than the optimal resistance factors. Moreover, the code-adjusted resistance factors do not vary as much as the optimal resistance factors with (LL)/(DL) ratio.

Since the code-adjusted resistance factors do not vary significantly for the different driven piles and soil properties, we consolidate the results of the adjusted resistance factors obtained from driven piles A, B and C and the range of soil properties considered. We calculated the mean, standard deviation (SD), maximum and minimum of the resistance factor obtained for the all driven piles. We report these statistics in Table 7.1. We present the data separately for $p_f = 10^{-3}$ and 10^{-4}. Based on the values of means and standard

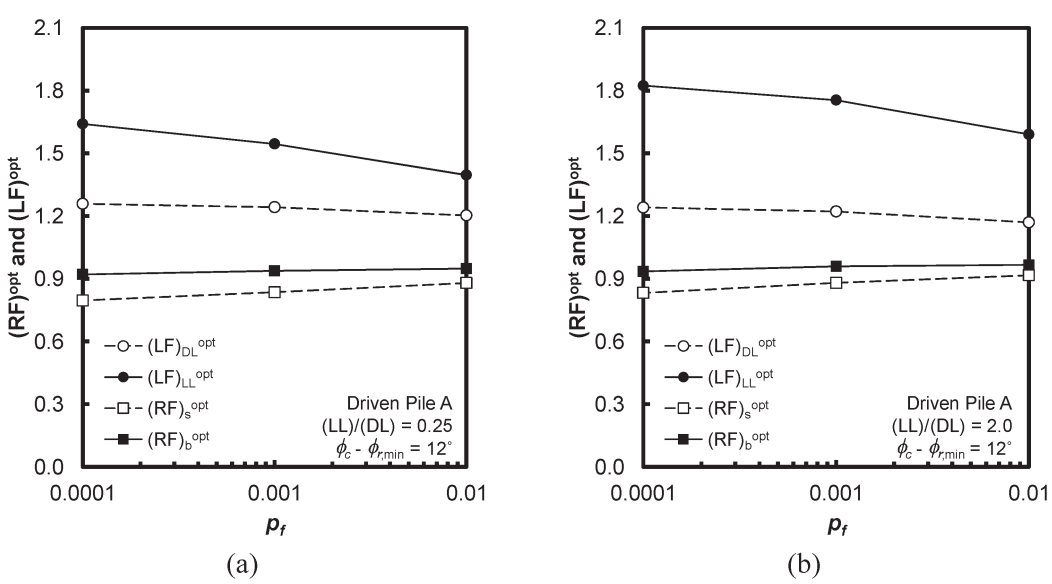

Figure 7.9 Optimal resistance and load factors versus target probability of failure for driven pile A and (a) LL/DL = 0.25 and (b) LL/DL = 2.0 when $q_{c,\text{mean}}(z)$ is given as input

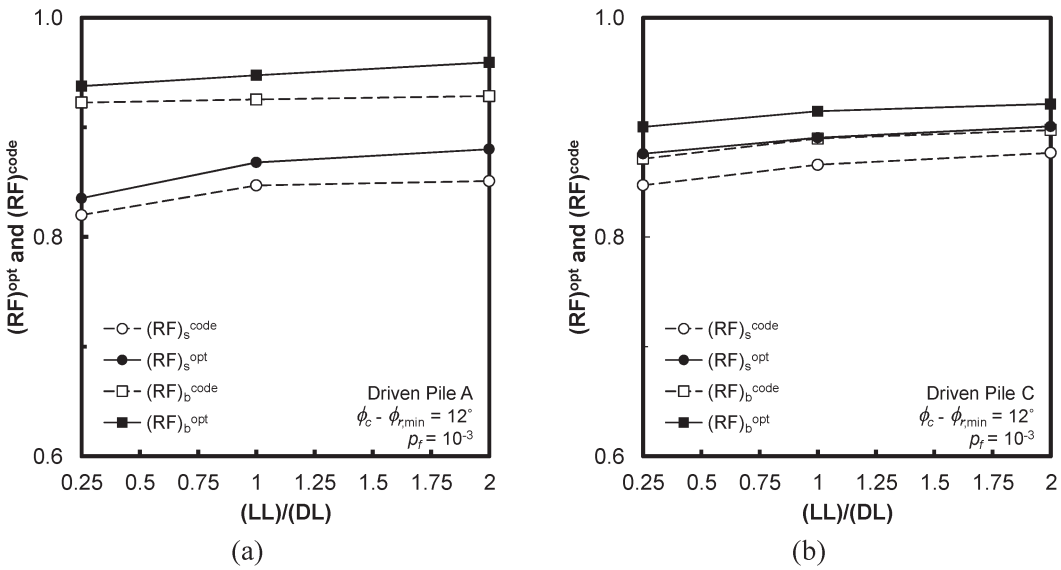

Figure 7.10 Optimal and code-adjusted resistance factors versus live load to dead load ratio for (a) driven pile A and (b) driven pile C when $q_{c,\text{mean}}(z)$ is given as input

deviation of the resistance factors, we calculated the code-adjusted resistance factor with 99% confidence as: $(\text{RF})_b^{\text{code}} = 0.71$ and $(\text{RF})_s^{\text{code}} = 0.68$ for $p_f = 10^{-3}$ and $(\text{RF})_b^{\text{code}} = 0.68$ and $(\text{RF})_s^{\text{code}} = 0.65$ for $p_f = 10^{-4}$.

7.5.2. Results for Design Based on Unconfined Compressive Strength

In this section, we describe how the optimal resistance and load factors change with different field conditions when unconfined compression tests are used to estimate undrained shear strength. Subsequently, we will compare the optimal resistance factors with code-adjusted resistance factors. We also propose design values of code-adjusted resistance factors for use with UC test data as input.

Figure 7.11(a) shows the plots of the load and resistance factors with respect to $(\phi_{c,\text{mean}} - \phi_{r,\text{min,mean}})$ for driven pile A with (LL)/(DL) = 0.25 when with target failure probability $p_f = 10^{-3}$ when mean undrained shear strength data from unconfined compression (UC) test are given as input. Figure 7.11(b) shows the plots of the load and resistance factors with respect to $(\phi_{c,\text{mean}} - \phi_{r,\text{min,mean}})$ for driven pile C with (LL)/(DL) = 2.0 with target failure probability $p_f = 10^{-3}$. In Figure 7.11 (a) and (b), it is evident that the optimal load and resistance factors are independent on $(\phi_{c,\text{mean}} - \phi_{r,\text{min,mean}})$. The minor variations in the resistance and load factors observed in Figure 7.11 are typical of all other driven piles; the fluctuations in the load and resistance factors were rather random without any particular trend.

Figure 7.12(a) shows the plots of the load and resistance factors with respect to diameter to length ratio (B_p/L_p) for the driven piles considered in this study with (LL)/(DL) = 0.25, $\phi_{c,\text{mean}} - \phi_{r,\text{min,mean}} = 12°$ and target failure probability $p_f = 10^{-3}$ when mean undrained shear strength data are given as input. Figure 7.12(b) shows the plots of the load and resistance factors with respect to diameter to length ratio for the driven piles with (LL)/(DL) = 2.0, $\phi_{c,\text{mean}} - \phi_{r,\text{min,mean}} = 12°$ and target failure probability $p_f = 10^{-3}$. In both Figure 7.12 (a) and (b), as diameter to length ratio B_p/L_p increases, the shaft resistance factor

TABLE 7.1
Resistance factors for different driven piles and adjusted with $(\text{LF})_{\text{DL}}^{\text{code}} = 1.25$ and $(\text{LF})_{\text{LL}}^{\text{code}} = 1.75$ when $q_{c,\text{mean}}(z)$ is given as input

		Diameter to Length Ratio			
		B_p / L_p = 0.3		B_p / L_p = 0.9	
Probability of failure	Statistics	$(\text{RF})_b^{\text{code}}$	$(\text{RF})_s^{\text{code}}$	$(\text{RF})_b^{\text{code}}$	$(\text{RF})_s^{\text{code}}$
10^{-3}	Mean	0.927	0.825	0.888	0.865
	SD	0.086	0.058	0.077	0.081
	Maximum	1.263	0.994	1.106	1.117
	Minimum	0.638	0.650	0.624	0.624
10^{-4}	Mean	0.887	0.776	0.838	0.811
	SD	0.084	0.052	0.067	0.068
	Maximum	1.093	0.892	1.012	0.988
	Minimum	0.643	0.615	0.633	0.620

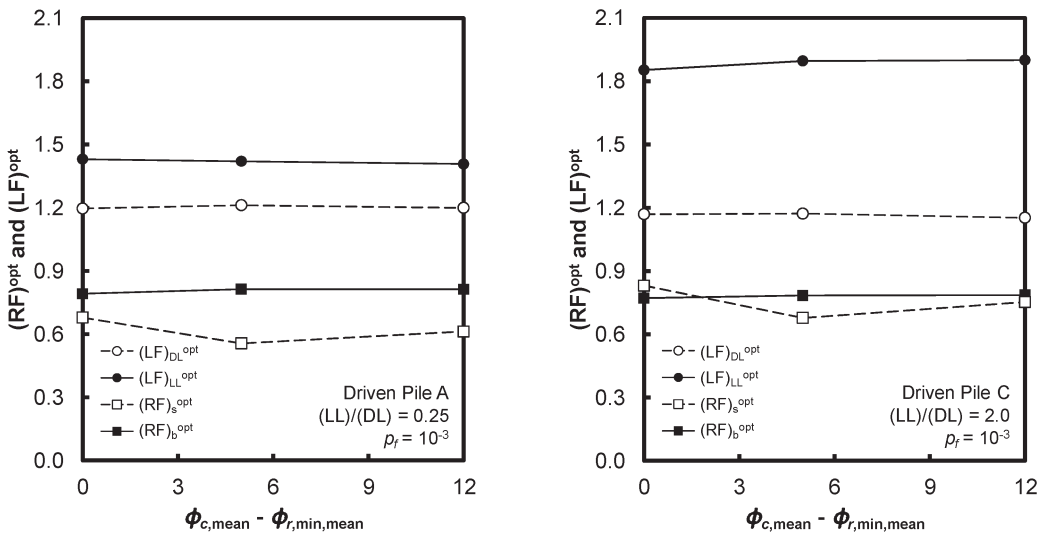

(a) (b)

Figure 7.11 Optimal load and resistance factors versus $\phi_{c,\text{mean}} - \phi_{r,\text{min,mean}}$ for (a) driven pile A and (b) driven pile C when $s_{u,\text{mean}}$ from UC testing is given as input

increases slightly and the base resistance factor decreases slightly. Figure 7.12 also shows that the load factors are nearly independent on the diameter to length ratio B_p/L_p. The trends observed in Figure 7.12, are typical of all the other cases. Although there are slight variations in resistance factor with respect to diameter to length ratio, for practical purposes, these variations can be considered negligible.

Soil properties and pile dimensions have practically no effect on the resistance and load factors. The (LL)/(DL) ratio, however, has a non-negligible effect on the live load factor. Figure 7.13 (a) and (b) show the plots of the load and resistance factors with respect to the (LL)/(DL) ratio for driven piles A and driven pile C, respectively when $\phi_{c,\text{mean}} - \phi_{r,\text{min,mean}} = 12^\circ$, target failure probability $p_f = 10^{-3}$, and mean undrained shear strength data are given as input. In both Figure 7.13 (a) and (b), the optimal resistance factors increase slightly and the optimal dead load factor decreases slightly with increase in (LL)/(DL) ratio; however, the optimal live load factor increases significantly with increase in (LL)/(DL) ratio.

Figure 7.13 implies that (LL)/(DL) ratio affects the mean factor of safety $(\text{FS})_{\text{mean}}$ because of a significant change of live load factor. Figure 7.14(a) and Figure 7.14(b) show $(\text{FS})_{\text{mean}}$ versus p_f for driven piles A and C, respectively, when mean undrained shear strength data are given as input. To study the effect of

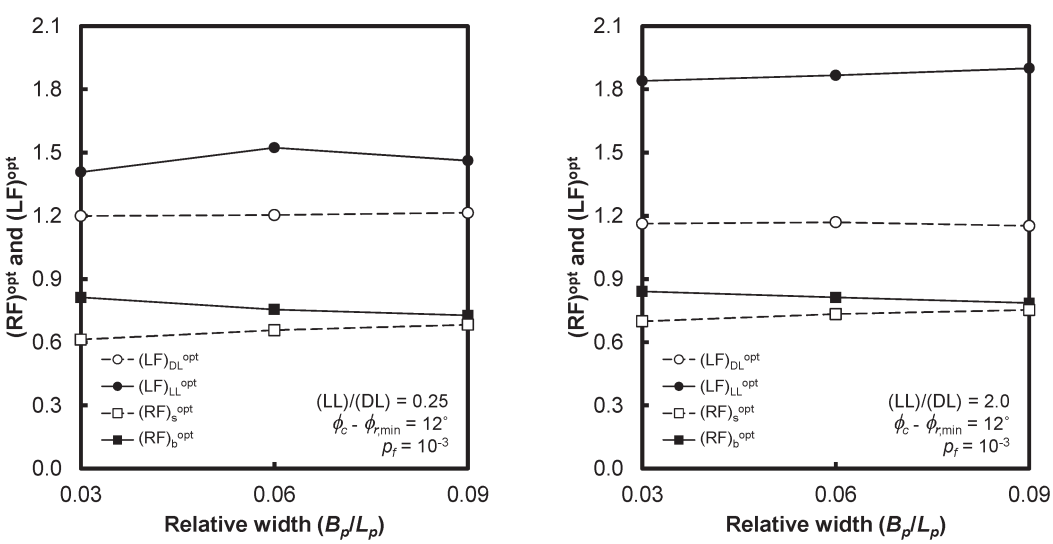

(a) (b)

Figure 7.12 Optimal load and resistance factors versus diameter to length ratio for (a) LL/DL = 0.25 and (b) LL/DL = 2.0 when $s_{u,\text{mean}}$ from UC testing is given as input

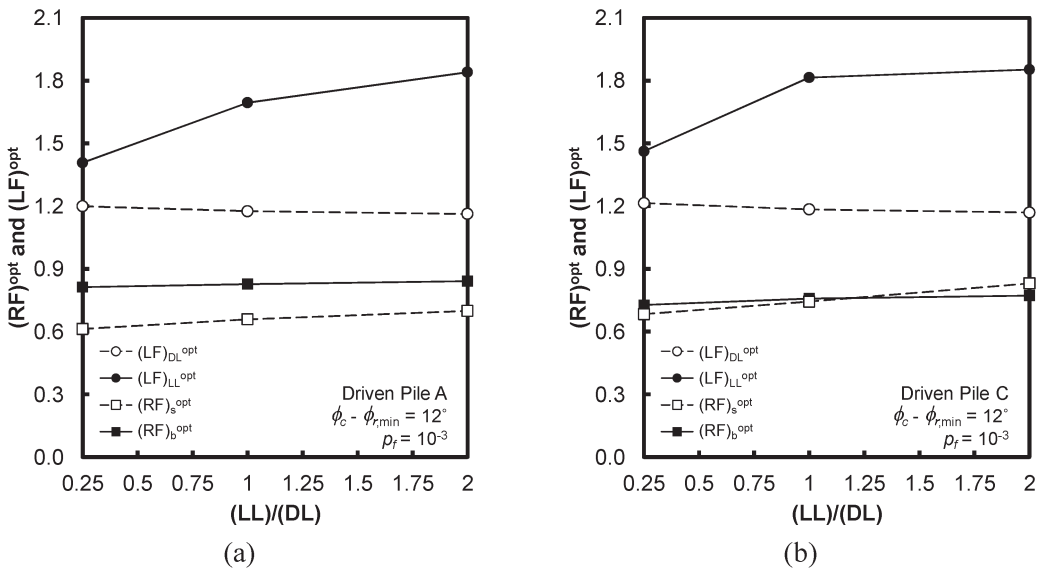

Figure 7.13 Optimal load and resistance factors versus live load to dead load ratio for (a) driven pile A and (b) driven pile C when $s_{u,\text{mean}}$ from UC testing is given as input

p_f, we performed additional M-C simulations with target $p_f = 10^{-2}$. Both Figure 7.14 (a) and (b) show that $(\text{FS})_{\text{mean}}$ increases with decrease of p_f. Also, the larger the (LL)/(DL) ratio, the higher the $(\text{FS})_{\text{mean}}$ is. This shows that $(\text{FS})_{\text{mean}}$ is not a true indicator of the reliability of a design; for the same mean factor of safety, the probabilities of failure are different for different proportions of applied live to dead load. From another viewpoint, for the same probability, a higher factor of safety is required to account for the higher uncertainty levels of live loads if (LL)/(DL) ratio increases.

Figure 7.15(a) and Figure 7.15(b) plot the optimal resistance and load factors versus the probability of failure p_f for driven pile A with $\phi_{c,\text{mean}} - \phi_{r,\text{min,mean}} = 12^\circ$ when (LL)/(DL) = 0.25 and (LL)/(DL) = 2.0, respectively. Both figures show the effect of p_f on the optimal resistance and load factors. As p_f increases, the resistance factors increase slightly and the dead load factor decreases slightly. The live load factor, however, significantly decreases with increase of p_f. So, it is evident that the change in $(\text{FS})_{\text{mean}}$ due to change in p_f is mainly influenced by the live load.

Figure 7.16(a) and Figure 7.16(b) show the optimal and code-adjusted resistance factors for driven pile A and driven pile A, respectively when $p_f = 10^{-3}$ and mean undrained shear strength data are given as input. The code-adjusted resistance factors were obtained from the optimal resistance factors by using equation (3.10). For both driven piles, the code-adjusted resistance factors are slightly more conservative than

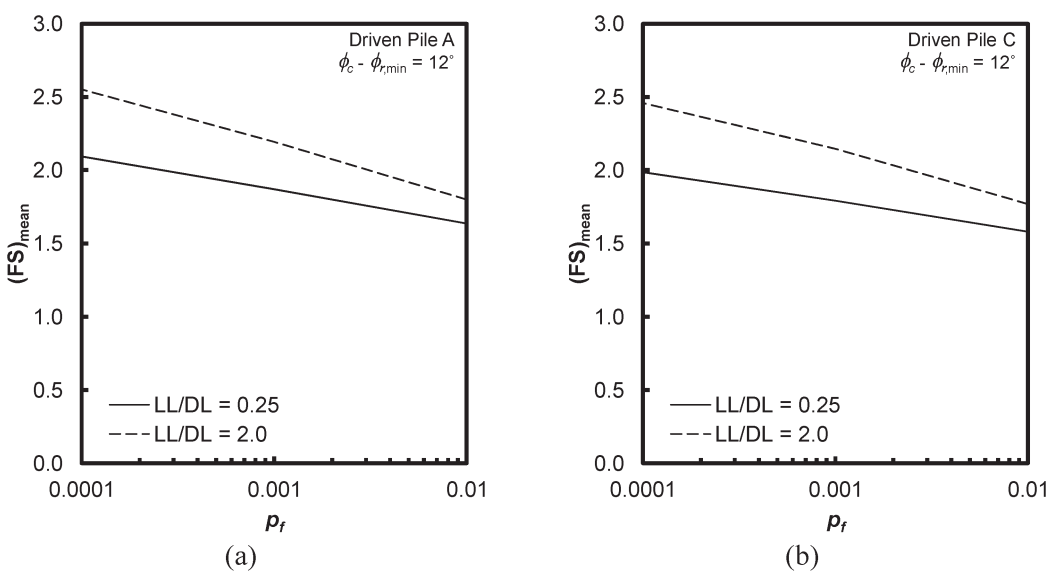

Figure 7.14 Mean factor of safety versus target probability of failure for (a) driven pile A and (b) driven pile C when $s_{u,\text{mean}}$ from UC testing is given as input

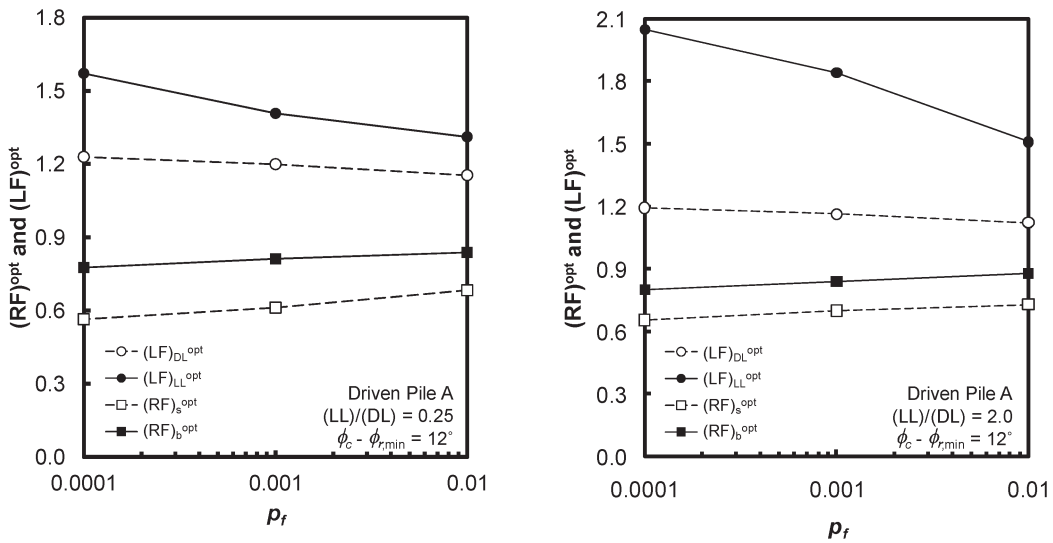

(a) (b)

Figure 7.15 Optimal resistance and load factors versus target probability of failure for driven pile A and (a) LL/DL = 0.25 and (b) LL/DL = 2.0 when $s_{u,\text{mean}}$ from UC testing is given as input

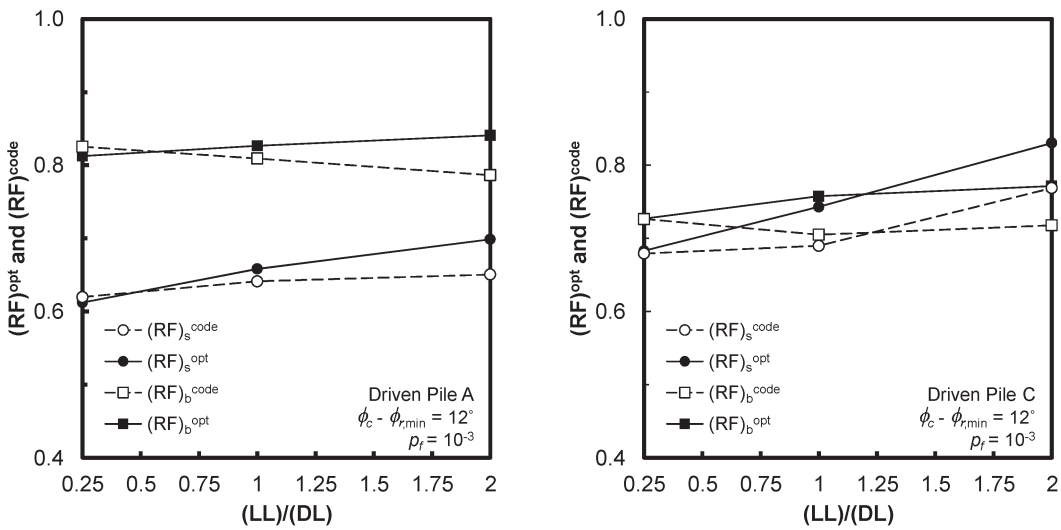

(a) (b)

Figure 7.16 Optimal and code-adjusted resistance factors versus live load to dead load ratio for (a) driven pile A and (b) driven pile C when $s_{u,\text{mean}}$ from UC test is given as input

TABLE 7.2
Resistance factors for different driven piles and adjusted with $(\text{LF})_{\text{DL}}^{\text{code}} = 1.25$ and $(\text{LF})_{\text{LL}}^{\text{code}} = 1.75$ when $s_{u,\text{mean}}$ from UC test is given as input

		Diameter to Length Ratio			
		B_p / L_p = 0.3		B_p / L_p = 0.9	
Probability of failure	Statistics	$(\text{RF})_b^{\text{code}}$	$(\text{RF})_s^{\text{code}}$	$(\text{RF})_b^{\text{code}}$	$(\text{RF})_s^{\text{code}}$
10^{-3}	Mean	0.807	0.630	0.717	0.688
	SD	0.125	0.074	0.093	0.106
	Maximum	1.210	0.838	1.025	1.119
	Minimum	0.474	0.430	0.411	0.402
10^{-4}	Mean	0.721	0.551	0.644	0.601
	SD	0.126	0.056	0.076	0.078
	Maximum	1.137	0.710	0.852	0.855
	Minimum	0.383	0.388	0.401	0.380

the optimal resistance factors. Moreover, the code-adjusted resistance factors do not vary as much as the optimal resistance factors with (LL)/(DL) ratio.

Since the code-adjusted resistance factors do not vary significantly for the different driven piles and soil properties, we consolidate the results of the adjusted resistance factors obtained from the driven piles A, B and C and soil properties considered. We calculated the mean, standard deviation (SD), maximum and minimum of the resistance factor obtained for the all driven piles. We report these statistics in Table 7.2. We present the data separately for $p_f = 10^{-3}$ and 10^{-4}. Based on the values of means and standard deviation of the resistance factors, we calculated the code-adjusted resistance factor with 99% confidence as: $(\mathrm{RF})_b^{\mathrm{code}} = 0.48$ and $(\mathrm{RF})_s^{\mathrm{code}} = 0.44$ for $p_f = 10^{-3}$ and $(\mathrm{RF})_b^{\mathrm{code}} = 0.43$ and $(\mathrm{RF})_s^{\mathrm{code}} = 0.41$ for $p_f = 10^{-4}$.

7.6. Conclusions

We performed a systematic probabilistic analysis to develop the resistance factors for driven piles in normally consolidated clay for a soil variable-based design method. The analysis involved identification of a robust design method, the Purdue Clay method for Displacement Piles, quantification of the uncertainties (probability distributions) associated with the design variables and the design equations and subsequent performance of Monte-Carlo simulations to generate the probability distributions of the pile capacities and applied loads. The limit state loads and shaft and base capacities can be identified from these distributions based on a target probability of failure. From the calculated limit state and nominal values of shaft and base capacities and dead and live loads, the optimal resistance and load factors are obtained. The optimal resistance factors are then adjusted to make them compatible with the dead and live load factors recommended by AASHTO (2007).

In the course of the study, performed with different soil properties and for three different dimensions of driven piles, we found that the resistance and load factors did not vary to any significant extent between the different soil properties and driven piles considered. The ratio of live to dead load was identified as the only variable that affected the results; however, it affected mostly the live load factor, with minimal effect on the resistance and dead load factors. The mean factor of safety was found, reasonably, to increase with decrease in the target probability of failure. The change in the mean factor of safety with the target probability of failure was a function of the live load to dead load ratio.

Based on the study, we recommended base and shaft resistance factors that can be used in design together with the dead load and live load factors of 1.25 and 1.75, respectively, recommended by AASHTO (2007). In CPT-based design, the recommended base and shaft resistance values are 0.71 and 0.68 for a probability of failure of 10^{-3} and 0.68 and 0.65 for a probability of failure of 10^{-4}. These could be rounded to 0.70 and 0.70 and 0.70 and 0.65. When unconfined compression test is used in the estimation of undrained shear strength, the recommended base and shaft resistance values are 0.48 and 0.44 for a probability of failure of 10^{-3} and 0.43 and 0.41 for probability of failure of 10^{-4}. These could be rounded to 0.50 and 0.45 and 0.45 and 0.40.

CHAPTER 8. SUMMARY AND CONCLUSIONS

8.1. General

In the present study, we performed a systematic probabilistic analysis to develop the resistance factors for piles in sands and clays for soil variable-based and *in situ*-based design methods. The analysis involved identification of robust design methods, quantification of the uncertainties (probability distributions) associated with the design variables and the design equations and subsequent performance of Monte-Carlo simulations to generate the probability distributions of the pile capacities and applied loads. The loads and shaft and base capacities of a pile at the most probable limit state are obtained from these distributions for a given target probability of failure. From the calculated limit state and nominal values of shaft and base capacities and dead and live loads, the optimal resistance and load factors are then obtained. The optimal resistance factors are finally adjusted to make them compatible with the dead and live load factors recommended by AASHTO (2007).

The analyses do not take into account site variability, so we recommend that designers cautiously select CPT or N_{SPT} logs, or s_u values, as the case may be, to perform their designs. We have not accounted for any benefits from quality control, such as dynamic pile testing during driving or integrity tests or various concrete quality tests performed during construction. Until a methodology is firmly in place to account for any possible reductions in resistance factors, caution is recommended in any reduction.

The present study can be used as a basis for recommending base and shaft resistance factors that can be used in design with the AASHTO (2007) recommended dead load and live load factors of 1.25 and 1.75. We summarize next the main conclusions and values of resistance factors to use in connection with AASHTO load factors for the four cases we have examined. The recommendations apply to design methods covered in this report.

8.2. Drilled Shafts in Sand

In the course of the study, performed for six different soil profiles with different soil properties and for five different dimensions of drilled shafts, we found that the resistance and load factors did not vary to any significant extent between the different soil profiles and drilled shafts considered. The ratio of live to dead load was identified as the only variable that affected the results; however, it affected mostly the live load factor,

with minimal effect on the resistance and dead load factors. The mean factor of safety was found, reasonably, to increase with decrease in the target probability of failure. The change in the mean factor of safety with the target probability of failure was a function of the live load to dead load ratio.

In CPT-based designs, , the recommended base and shaft resistance values are 0.80 and 0.75 for a probability of failure of 10^{-3} and 0.65 and 0.60 for a probability of failure of 10^{-4}. In SPT-based designs, the recommended base and shaft resistance values are 0.45 and 0.60 for a probability of failure of 10^{-3} and 0.35 and 0.5 for a probability of failure of 10^{-4} considering COV of N_{60} as 0.3. If a more conservative value of COV(N_{60}) = 0.5 is assumed for the SPT, the recommended base and shaft resistance values are 0.40 and 0.60 for a probability of failure of 10^{-3} and 0.35 and 0.50 for a probability of failure of 10^{-4}.

8.3. Drilled Shafts in Clay

In the course of the study, performed with different soil properties and for three different dimensions of drilled shafts, we found that the resistance and load factors did not vary to any significant extent between the different soil profiles and drilled shafts considered. The ratio of live to dead load was identified as the only variable that affected the results; however, it affected mostly the live load factor, with minimal effect on the resistance and dead load factors (of course, after adjustment of the factors to code-proposed load factors, there is an effect on all resistance and load factors). The mean factor of safety was found, reasonably, to increase with decreasing target probability of failure. The change in the mean factor of safety with the target probability of failure was found to be a function of the live load to dead load ratio.

In CPT-based designs, the recommended base and shaft resistance values are 0.70 and 0.75 for a probability of failure of 10^{-3} and 0.65 and 0.70 for a probability of failure of 10^{-4}. When unconfined compression tests are the basis for estimation of undrained shear strength, the recommended base and shaft resistance values are 0.50 and 0.45 for a probability of failure of 10^{-3} and 0.40 and 0.40 for probability of failure of 10^{-4}.

8.4. Driven Piles in Sand

The case of driven piles in sand is the only of the four studied for which theory-based design methods are not available. This case should be reanalyzed when more rigorous design methods become available. Two ratios, (LL)/(DL) and $Q_{b,ult}{}^{(n)}/Q_{sL}{}^{(n)}$, were found to affect the values of resistance factors. The recommended resistance factors compatible with the AASHTO load factors are given in Table 6–3. The recommended base and shaft resistance factors are in the 0.34 – 0.63 and 0.89 – 1.13 ranges for a probability of failure of 10^{-3} and 0.19 – 0.52 and 0.83 – 1.13 ranges for a probability of failure of 10^{-4}, depending on (LL)/(DL) and $Q_{b,ult}{}^{(n)}/Q_{sL}{}^{(n)}$. These dependencies are likely a result of the empirical nature of the design methods.

8.5. Driven Piles in Clay

In the course of the study, performed with different soil properties and for three different dimensions of driven piles, we found that the resistance and load factors did not vary to any significant extent between the different soil profiles and driven piles considered. The ratio of live to dead load was identified as the only variable that affected the results; however, it affected mostly the live load factor, with minimal effect on the resistance and dead load factors. The mean factor of safety was found, reasonably, to increase with decrease in the target probability of failure. The change in the mean factor of safety with the target probability of failure was a function of the live load to dead load ratio.

When CPT is used in site investigation, the recommended base and shaft resistance values are 0.70 and 0.70 for a probability of failure of 10^{-3} and 0.70 and 0.65 for a probability of failure of 10^{-4}. When unconfined compression tests are used in the estimation of undrained shear strength, the recommended base and shaft resistance values are 0.50 and 0.45 for a probability of failure of 10^{-3} and 0.45 and 0.40 for probability of failure of 10^{-4}.

REFERENCES

AASHTO (2007). AASHTO LRFD Bridge Design Specifications, AASHTO.

Allen, T. M. (2005). *Development of Geotechnical Resistance Factors and Downdrag Load Factors for LRFD Foundation Strength Limit State Design*, Publication No. FHWA-NHI-05-052, Federal Highway Administration, U.S. Department of Transportation.

Altaee, A., Fellenius, B. H., and Evgin, E. (1992). "Axial load transfer for piles in sand. I. Tests on an instrumented precast pile." *Canadian Geotechnical Journal*, 29, 11–20.

Altaee, A., Fellenius, B. H., and Evgin, E. (1993). "Load transfer for piles in sand and the critical depth." *Canadian Geotechnical Journal*, 30, 455–463.

Baecher, G. B. and Christian, J. T. (2003). *Reliability and Statistics in Geotechnical Engineering*. John Wiley & Sons Ltd.

Basu, P., Salgado, R., Prezzi, M. And Chakraborty, T. (2009). "A method for accounting for pile set up and relaxation in pile design and quality assurance." *Joint Transportation Research Program*, SPR-2930.

Basu, D. and Salgado, R. (2011) "Load and Resistance Factor Design of Drilled Shaft in Sand." Working paper.

BCP Committee. (1971). "Field tests on piles in sand." *Soils and Foundations*,11(2), 29–49.

Beringen, F. L., Windle, D., and Van Hooydonk, W. R. (1979). "Results of loading tests on driven piles in sand." *Proc., Conf. on Recent Developments in the Design and Construction of Piles*, ICE, London, 213–225.

Bolton, M. D. (1986). "The strength and dilatancy of sands." *Geotechnique*, 36, 65–78.

Briaud, J.-L., Tucker, L. M., and Ng, E. (1989). "Axially loaded 5 pile group and a single pile in sand." *Proc., 12th Int. Conf. on Soil Mechanics and Foundation Engineering*, 2, 1121–1124.

Chakraborty, T., Salgado, R; and Loukidis, D. (2011) "A two-surface plasticity model for clay." Working paper.

Chakraborty, T., Salgado, R., Basu, P., and Prezzi, M. (2011) "The shaft resistance of drilled shafts in clay." Working paper.

Ching, J.J. and Lin, H.D. (2010). "Calibrating Resistance Factors of Single Bored Piles Based on Incomplete Load Test Information." *Proceedings of the GeoFlorida 2010 Conference, Advances in Analysis, Modeling, & Design*.

Colombi, A. (2005). Physical Modelling of an Isolated Pile in Coarse Grained Soils. Ph.D. Thesis, Univ. of Ferrara.

Ellingwood, B., MacGregor, J. G., Galambos, T. V. and Cornell, C. A. (1980). "Probability based load criteria: load factors and load combinations." *Journal of Structural. Engineering Division*. 108(ST5), 978–997.

Ellingwood, B. R. and Tekie, P. B. (1999). "Wind load statistics for probability-based structural design." *Journal of Structural. Engineering*, 125(4), 453–463.

Fang, Y.S., Chen, J.M. and Chen, C.Y. (1997). "Earth pressures with sloping backfill," *Journal of Geotechnical and Geoenvironmental Engineering*, 123(3), 250–259.

Fenton, G. A. and Griffiths, D. V. (2008). *Risk Assessment in Geotechnical Engineering*. John Wiley & Sons.

FHWA (2001). Load and Resistance Factor Design (LRFD) for Highway Bridge Substructures. FHWA HI-98-032, FHWA.

Fioravante, V. (2002). "On the shaft friction modelling of non-displacement piles in sand." *Soils and Foundations*. 42(2), 23–33.

Fisher, J. W., Galambos, T. V., Kulak, G. L., Ravindra, M. K. (1978). "Load and resistance factor design criteria for connectors." *Journal of Structural Engineering Division*. 104(9), 1427–1441.

Foye, K. C. (2005). A rational probabilistic method for the development of geotechnical load and resistance factor design. Ph. D. Thesis, Purdue University.

Foye, K. C., Salgado, R. and Scott, B. (2006a). "Assessment of variable uncertainties for reliability-based design of foundations." *Journal of Geotechnical and Geoenvironmental Engineering*. 135(1), 1–13.

Foye, K. C., Abou-Jaoude, G., Prezzi, M., and Salgado, R. (2009). "Resistance factors for use in load and resistance factor design of driven pipe piles in sands." *Journal of Geotechnical and Geoenvironmental Engineering*. 132(9), 1208–1218.

Foye, K. C., Salgado, R. and Scott, B. (2006b). "Resistance factors for use in shallow foundation LRFD." *Journal of Geotechnical and Geoenvironmental Engineering*. 132(9), 1208–1218.

Fredlund, D. G. and Dahlman A. E. (1971). "Statistical Geotechnical Properties of Glacial Lake Edmonton Sediments." Proceedings of the First International Conference on Applications of Statistics and Probability to Soil and Structural Enginnering, 203–228.

Ghionna, V. N., Jamiolkowski, M., Pedroni, D. And Salgado, R. (1994). "The tip resistance of drilled shafts in sands.". *Vertical and Horizontal Deformations of Foundations and Embankments, Proc Settlement '94* ASCE 2, 1039–1057.

Ghosn, M. and Moses, F. (1998). *Redundancy in Highway Bridge Superstructures*. NCHRP Report 406, TRB.

Gregersen, O. S., Aas, G., and Dibiagio, E. (1973). "Load tests on friction piles in loose sand." *Proc., 8th Int. Conf. on Soil Mechanics and Foundation Engineering*, 2, 109–117.

Hammitt, G.M. (1966). Statistical Analysis of Data from Comparative Laboratory Test Program Sponsored by ACIL. U.S. Army Waterways Experiment Station, Vicksburg, MS.

Hansell, W. C. and Viest, I. M. (1971). "Load factor design for steel highway bridges." *AISC Engineering Journal*. 8(4), 113–123.

Hendron, A.J. (1963). A Typical relationship between the coefficient of earth pressure at rest and the initial void ratio, Ph.D thesis.

Honjo, Y., Suzuki, M., Shirato, M. And Fukui, J. (2002). "Determination of partial factors for a vertically loaded pile based on reliability analysis." *Soils and Foundations*, 42(5), 91–109.

Jardine, R.J., Chow, F.C., Overy, R.F., and Standing, J.R., (2005). *ICP design methods for driven piles in sand and clays*, Thomas Telford, London.

JCSS (2000). *Probabilistic Model Code*. JCSS-OSTL/DIA/VROU-10-11-2000, Joint Committee on Structural Safety.

Kim, D. W. (2008). Load and resistance factor design of slopes and MSE walls. Ph.D. Thesis, Purdue University.

Kim, K.J., Rahman, M.S., Gabr, M.A., Sarica, R.Z., and Hossain, M.S. (2005). "Reliability based calibration of resistance factors for axial capacity of driven piles." *Advances in Deep Foundations 2005 (GSP132)*, 1–12.

Kwak, K., Park, J. H., Kim, K. J., Choi, Y. K. and Huh, J. (2007). "Evaluation of resistance bias factors for load and resistance factor design of driven pipe piles." *Contemporary Issues in Deep Foundations*, GSP 158, ASCE.

Kulhawy, Fred H., Trautmann, Charles H. (1996). "Estimation of In-site Test Uncertainty." *Proceedings of Uncertainty in the Geologic Environment: from Theory to Practice*, Geotechnical Special Publication No. 58, ASCE, Vol. 1, 269–286.

Lacasse, S. and Nadim, F. (1996). "Uncertainties in characterising soil properties." *Uncertainty in the Geologic Environment, Proc. Uncertainty 96*, 49–73.

Ladd, Charles C., Moh, Za-Chieh, and Gifford, Douglas G. (1971). "Statistical Analysis of Undrained Strength of Soft Bangkok Clay." *Proceedings of the First International Conference on Applications of Statistics and Probability to Soil and Structural Enginnering*, 313–328.

Lee, J., Salgado, R., and Paik, K. (2003). "Estimation of load capacity of pipe piles in sand based on cone penetration test results." *Journal of Geotechnical and Geoenvironmental Engineering*, 129(6), 391–403.

Lee, J. H. and Salgado, R. (1999). "Determination of pile base resistance in sands." *Journal of Geotechnical and Geoenvironmental Engineering*, 125(8), 673–683.

Lee, I. K., White, W. and Ingles, O. G. (1983). *Geotechnical Engineering*. Pitman.

Lehane, B. M., Jardine, R. J., Bond, A. J., and Frank, R. (1993). "Mechanisms of shaft friction in sand from instrumented pile tests." *Journal of Geotechnical Engineering*, 119(1), 19–35.

Loukidis, D. and Salgado, R. (2008). "Analysis of shaft resistance of non-displacement piles in sand." *Géotechnique* 58(4), 283–296.

Loukidis, D., Salgado, R. and Abou-Jaoude, G. (2008). Assessment of Axially-Loaded Pile Dynamic Design Methods and Review of INDOT Axially-Loaded Pile Design Procedure. FHWA/IN/JTRP-2008/6, Purdue Univ.

Lumb, P. (1974). "Application of statistics in soil mechanics." *Soil Mechanics – New Horizons, Ed. Lee, I. K.*, American Elsevier Publishing Company.

Malkawi, A.I.H., Hassan, W.F., and Abdulla, F.A. (2000). "Uncertainty and reliability analysis applied to slope stability." *Structural Safety*, 22, pp 161–187.

McVay, M., Ellis, R., Birgisson, B., Consolazio, G., Putcha, S. And Lee, S. M. (2003). "Use of LRFD, cost and risk to design a drilled shaft load test program in Florida limestone." *TRB 2003 Annual Meeting*, CD ROM.

Meyerhof, G. G. (1957). "Discussion for Session I." Proceedings of the forth International Conference of Soil Mechanics and Foundation Engineering, London, Vol. 3(10).

Misra, A. and Roberts, L. A. (2006). "Probabilistic analysis of drilled shaft service limit state using the "t-z" method." *Canadian Geotechnical Journal*, 43, 1324–1332.

Misra, A. and Roberts, L. A. (2009). "Service limit state resistance factors for drilled shafts", *Géotechnique*, 59(1), 53–61.

Misra, A., Roberts, L. A. and Levorson, S. M. (2007). "Reliability of drilled shaft behavior using finite difference method and Monte Carlo simulation." *Geotech. Geol. Engng*. 25, 65–77.

Negussey, D., Wijewickreme, W. K. D. and Vaid, Y. P. (1987). "Constant-volume friction angle of granular materials," *Canadian Geotechnical Journal*, 25, pp50–55.

Nowak, A. S. (1994). "Load model for bridge design code." *Canadian Geotechnical Journal*, 21, 36–49.

Ochiai, H., Otani, J. And Matsui, K. (1994). "Performance factor for bearing resistance of bored friction piles." *Structural Safety*, 14, 103–130.

Okochi, Y. and Tatsuoka, F. (1984). "Some factors affecting K0-values of sand measured in triaxial cell," *Soils and Foundations*, 24(3), 52–68.

O'Neill, M. W. and Hassan, K. M. (1994). "Drilled shafts: effects of construction on performance and design criteria." *Proc. Int. Conf. Design Constr. Deep Fdns*, Orlando, Florida. 137–187.

O'Neill, M. W. and Resse, L. C. (1999). *Drilled shafts: Construction procedures and design methods*. Report No. FHWA-IF-99-025, FHWA.

Paik, K., Salgado, R., Lee, J., and Kim, B. (2003). "Behavior of open and closed-ended piles driven into sands." *Journal of Geotechnical and Geoenvironmental Engineering*, 129(4), 296–306.

Paikowsky, S. G. (2004). *Load and resistance factor design (LRFD) for deep foundations*. NCHRP Report 507, Transportation Research Board.

Park, J.H., Lee, J.H., Chung, M., Kwak, K., and Huh, J. (2009). " Resistance factor calibration based on FORM for driven steel pipe piles in Korea." *Proceedings of the 2nd International Symposium on Geotechnical Risk and Safety*, pp173–176.

Phoon, K. K. and Kulhawy, F. H. (1999). "Characterization of geotechnical variability." *Canadian Geotechnical Journal*, 36(4), 612–624.

Phoon, K. K. and Kulhawy, F. H. (1999). "Evaluation of Geotechnical Property Variability." *Canadian Geotechnical Journal*, 36(4), 625–639

Randolph, M. F. (2003). "Science and Empiricism in Pile Foundation Design." *Geotechnique*, 53(10), 847–875.

Rao, K. S., Allam, M. M., and Robinson, R. G. (1998). "Interfacial friction between sands and solid surfaces." *Proc., ICE, Geotechnical Engineering*, 131, 75–82.

Reese, L. C., Touma, F. J. and O'Neill, M. W. (1976). "Behavior of drilled piers under axial loading." *Journal of Geotechnical. Engineering Division,* 102(5), 493–510.

Salgado, R. (1993). *Analysis of Penetration Resistance in Sands*. Ph.D. Thesis. Univ. of California, Berkeley.

Salgado, R. (2008). *The Engineering of Foundations*. McGraw Hill.

Salgado, R. and Prezzi, M. (2007). "Computation of cavity expansion pressure and penetration resistance in sands." *International Journal of Geomechanics*. 7(4), 251–265.

Salgado, R. and Randolph, M. F. (2001). "Analysis of cavity expansion in sand." *Int. J. Geomech*. 1(2), 175–192.

Salgado, R., Lyamin, A. V., Sloan, S. W., and Yu, H. S. (2004). "Two- and three-dimensional bearing capacity of foundations in clay." *Géotechnique*, 54(5), 297–306.

Shannon and Wilson, Inc., and Wolff, T. F. (1994). "Probability Model for Geotechnical Aspects of Navigation Structures." *Report to the St. Louis District*, U. S. Army Corps of Engineers.

Skempton, A. W. (1986) "Standard Penetration Test Procedures and the Effects in Sands of Overburden Pressure, Relative Density, Particle Size, Ageing and Overconsolidation." *Geotechnique*, 36(3), 425–447.

Spry, M. J., Kulhawy, F. H., and Grigoriu, M. D. (1988). "Reliability-based Foundation Design for Transmission Line Structures: Geotechnical Site Characterization Strategy." *Rep. No. EL-5507(1)*, Electric Power Research Institute, Palo Alto, CA.

Stas, C. V. and Kulhawy, F. H. (1984). *Critical evaluation of design methods for foundations under axial uplift and compression loading*. EPRI Report EL-3771, Research Project 1493-1, Electric Power Research Institute, Palo Alto, California.

Titi, H. H., Mahamid, M., Abu-Farsakh, M. Y. and Elias, M. (2004). "Evaluation of CPT methods for load and resistance factor design of driven piles." *GeoTrans 2004*, ASCE.

Verdugo, R. and Ishihara, K. (1996). "The steady state of sandy soils." *Soils and Foundations*. 36(2), 81–91.

Vesic, A. S. (1970). "Tests on instrumented piles, Ogeechee river site." *Journal of Soil Mechanics and Foundations Division*, 96(2), 561–584.

White, D. J., Schaefer, V. R., Yang, H., and Thompson, M. J., (2005). *Innovative Solutions for Slope Stability Reinforcement and Characterization: Vol. I*. Final report CTRE Project 03-127. Center for Transportation Research and Education, Iowa State University.

Wolff, T. F. (1985) "Analysis and Design of Embankment Dam Slopes: A Probabilistic Approach." *Ph. D. Dissertation*, Purdue University, West Lafayette, IN.

Yang, L. (2006). Reliability-based design and quality control of driven piles, Ph.D thesis, University of Akron.

Yang, X., Han, J., Parsons, R. L. and Henthorne, R. W. (2008). "Resistance factors for drilled shafts in weak rock based on O-cell test data." *J. TRB* 2045, 62–67.

Yoon, G. L. and O'Neil, M. W. (1996). "Design model bias factors for driven piles from experiments at NGES-UH." *Uncertainty in Geologic Environment*, GSP ASCE 58(2), 759–773.

Yoon, S., Abu-Farsakh, M.Y., Tsai, C., Zhang, Z. (2008) "Calibration of Resistance Factors for Axially Loaded Concrete Piles Driven into Soft Soils." *Journal of the Transportation Research Board*, 39–50.

Zhang, L. M., Li, D. Q. And Tang, W. H. (2005). "Reliability of bored pile foundations considering bias in failure criteria." *Canadian Geotechnical Journal*, 42, 1086–1093.